The Chemistry of Transition Metal Complexes related to Solar Energy Storage : H_2 Production and Small Molecule (CO_2 and HX; X = Cl, Br) Chemistry

by

Changhoon Lee

B.S. Chemistry, Korea Advanced Institute of Science and Technology, 1998

M.S. Chemistry, Korea Advanced Institute of Science and Technology, 2000

SUBMITTED TO THE DEPARTMENT OF CHEMISTRY IN PARTIAL FULFILLMENT OF THE REQUIREMENTS FOR THE DEGREE OF

DOCTOR OF PHILOSOPHY IN INORGANIC CHEMISTRY

AT THE

MASSACHUSETTS INSTITUTE OF TECHNOLOGY

September 2011

Signature of Author _____

Department of Chemistry
July 5 2011

Certified By _____

Daniel G. Nocera
The Henry Dreyfus Professor of Energy and Professor of Chemistry
Thesis Supervisor

Accepted by _____

Robert W. Field
Haslam and Dewey Professor of Chemistry
Chairman, Departmental Committee on Graduate Students

This doctoral thesis has been examined by a Committee of the Department of Chemistry as follows:

Professor Christopher C. Cummins

Professor of Chemistry
Chairman

Professor Daniel G. Nocera

Henry Dreyfus Professor of Energy and Professor of Chemistry
Thesis Supervisor

Professor Richard R. Schrock

Frederick G. Keyes Professor of Chemistry

The Chemistry of Transition Metal Complexes related to Solar Energy Storage : H_2 Production and Small Molecule (CO_2 and HX; X = Cl, Br) Chemistry

by

Changhoon Lee

Submitted to the Department of Chemistry on July 5, 2011, in partial fulfillment of the requirements for the degree of Doctor of Philosophy.

Abstract

The studies in this thesis have focused on the chemistry of transition metal complexes related to solar energy storage: electrochemical H_2 production, HX splitting and CO_2 activation mediated by transition metal complexes. Transition metal complexes, for example with macrocyclic ligands, can catalyze electrochemical proton reduction, a half reaction of water splitting to H_2/O_2 by electricity generated by sunlight. The strategy for designing efficient molecular catalysts were explored by introducing a Hangman scaffold into metallomacrocyles. The study exhibits synthesis and electrochemistry of metallomacrocyles, and an example of Hangman effect for electrochemical H_2 production. Thermodynamically demanding HX splitting to H_2/X_2 by sunlight can be a promising method for solar energy storage. To date, most HX splitting chemistry was studied with metal complexes based on 2^{nd} or 3^{rd} row transition metals. Hence, the usage of cheaper first row metals is an imperative to discover economically viable catalytic systems. HX chemistry of Ni complexes and photoelimination of H_2 from Ni hydride complexes, and photoactivation of Ni–Cl bonds were studied. CO_2 can be utilized as a carrier of H_2 by the syntheses of liquid fuels from CO_2 and H_2. The challenge of using CO_2 as a precursor for organic molecules is the activation of strong O=CO bonds. The reaction with metal complexes is one of the methods to break or weaken the bonds. The CO_2 chemistry of Ni complexes was explored, and generation of a new binding mode of CO_2 and activation of CO_2 to CO were studied.

Thesis Supervisor : Daniel G. Nocera

Title : The Henry Dreyfus Professor of Energy and Professor of Chemistry

Table of contents

List of Figures

Chapter 1:

Chapter 2:

Chapter 3:

List of Tables

Chapter 1:

Chapter 2:

Chapter 3:

List of Schemes and Charts

Chapter 1:

Chapter 2:

Chapter 3:

List of Abbreviations

br	broad	LD-MS	laser desorption mass spectrometry
calcd.	calculated	LUMO	lowest unoccupied molecular orbital
cm^{-1}	wavenumber	Lut	lutidine
CV	cyclic voltammogram	m	multiplet
d	doublet	MALDI	matrix-assisted laser desorption/ionization
DFT	density functional theory	mg	milligram
e	electron	mL	milliliter
EDX	energy dispersive X-ray analysis	min	minutes
ESI	electrospray ionization	NHC	N-heterocyclic carbene
Et	ethyl	NMR	nuclear magnetic resonance
equiv	equivalent	OAc	acetate
Fc	ferrocene	OTf	trifluoromethylsulfonate
g	gram	s	singlet
h	hour	SEM	scanning electron microscopy
HER	hydrogen evolution reaction	t	triplet
HOMO	highest occupied molecular orbital	tert	tertiary
HRMS	high resolution mass spectrometry	tosic	*p*-toluenesulfonic
Hz	hertz	vis	visible
IR	infra red	δ	chemical shift
J	coupling constant	ε	extinction coefficient

Chapter 1. Electrochemical H_2 Production on Metallomacrocylces

Portions of this have been published:

(1) Lee, C. H.; Dogutan, D. K.; Nocera, D. G. *J. Am. Chem. Soc*, **2011**, *133*, 8775–8777. Reproduced with permission. Copyright 2011 American Chemical Society

1.1 Introduction

The worldwide energy consumption rate in 2007 was 16.2 TW and, because of economic growth and rising standards of living of a growing world population, the energy demand is expected to double by 2050 and triple by 2100.[1,2] Currently, our energy supplies mostly rely on burning fossil fuels and it is suggested that the amount of oil, natural gas and coal in the reserves will meet this energy need.[1] However, the combustion of fossil fuels has been contributing to accumulation of green house gases in the atmosphere by emitting CO_2. Moreover, because there are no natural pathways for CO_2 decomposition, the emitted CO_2 will remain in the atmosphere for a long period of time. The current CO_2 concentration of 380 ppm in the atmosphere is significantly higher than those in last 0.65 million years. Hence, staying reliant on burning fossil fuels at current rate might cause a significant global climate issues such as global warming, sea level rises and permafrost loss.

To suppress the increase of CO_2 level in the atmosphere, the development of CO_2 capturing and sequestration technologies is needed and, more importantly, drastic change in energy supply from fossil fuels to carbon neutral energy sources is urgent. Nuclear fission and biomass are the ways of avoiding additional CO_2 emission. However, those methods are limited due to slow rate of construction of nuclear power plants and low energy efficiency of photosynthesis,[3] and not sufficient enough to keep up the growing energy demand. Among the other energy sources, the sun is the largest renewable carbon neutral energy source. The energy from the sun provided per 1 hr is more than the energy consumption on the world in 1 yr.[1]

To harness energy from the sun, technologies converting solar energy to utilizable forms are needed and, because we need continuous energy supply to support our everyday life, viable means of storing the energy for dark hour usage is also very important. Sunlight can be captured and converted to electricity by photovoltaics, though electricity produced through photovoltaics is still not as cost-effective as that derived from fossil fuels and the developments for decrease of manufacturing cost is required. Even if we have the technology to produce electricity from sunlight cost-effectively, however, without the technologies to store that electricity, continuous energy supply cannot be achieved, because sunlight is not available 24 hours a day.

Solar energy could be stored in compressed air, flywheels, super capacitors, pumped water or batteries.[3] In considering energy densities, they are, however, impractical for large amounts of energy storage due to low energy densities in those storage forms.[3,4] The other

method of storing solar energy is the production of fuels possessing high energy chemical bonds through thermodynamically uphill reactions driven by sunlight, analogous to how nature captures and stores solar energy through photosynthesis. This method will enable very dense energy storage in chemical bonds.[4,5] For example, by splitting water to H_2 and O_2, an energy of 140 MJ can be stored in 1 kg of H_2.[4]

The storage of solar energy for dark hour usage could be realized by electrolyzing water to produce H_2 and O_2 using electricity generated by photovoltaics. The H_2 could be used in fuel cells to release the stored solar energy when the sunlight is not available.[1,3] An electrochemical cell designed by Turner et al. exhibits such a system with photoelectrochemical-photovoltaic design harvesting solar energy through electrolysis of water with high efficiency.[6] In the cell, oxygen and protons are generated at platinum electrode and protons are reduced to hydrogen at a photoactive semiconductor. However, the usage of expensive electrode materials like platinum, of which reservoirs are not enough for world wide application of the cell design, is the problem of this system. Thus, it has been the imperative to discover cheap catalytic system for practical applications. A catalytic system composed of cobalt and phosphate, which splits water into oxygen and protons at neutral pH with low overpotential, has been discovered recently by our group[7] and the next step will be to couple such a system with cheap and economically viable proton reduction catalysts.

Interest in cost-effective proton reduction catalysts replacing precious metal electrodes has led to the studies of hydrogen evolution reaction (HER) with metal electrodes. However, the research indicated that precious metals, particularly platinum, are the most active in hydrogen evolution reaction.[3] Nature has enzymes called hydrogenases, operating near the thermodynamic potential for H_2 activation and generation. They usually contain iron or nickel as metal components. Inspired by nature's enzymes, metal complexes based on earth abundant first row transition metals including model complexes of hydrogenase[8–10] and macrocycles have been studied for hydrogen evolution reaction.[11–23]

Complexes with macrocyclic or chelating ligands are attracting attention due to stability of the complexes imparted by the chelate effect. For example, first row metal based metalloporphyrins (e.g. chart 1.1 **A**)[20–23], metallo-diglyoximes(e.g. **B**)[15–19] and complexes with chelating ligand (e.g. **C**)[11,13,14] were studied and are now well known to catalyze proton reduction. Cobalt diglyoximes catalyze proton reduction at promisingly low overpotential (e.g.

$Co(dmgBF_2)(CH_3CN)_2$ ($dmgBF_2$ = difluoroboryldimethlyglyoxime)).[16] The complex C has the design of incorporating internal bases taking advantage of proton relay by pendant base group.[11] Porphyrins with iron[22], cobalt[20,21] and rhodium[23] as central metal atoms are also known to catalyze proton reduction.

Chart 1.1

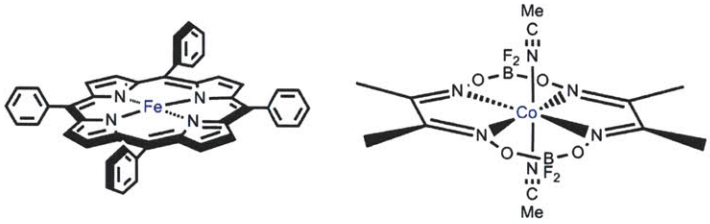

A **B**

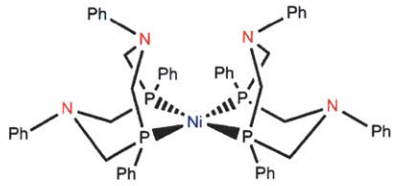

C

1.2 Hydrogen Generation by Hangman Metalloporphyrins

A particularly fascinating design element of emergent catalysts is the incorporation of a proton relay from a pendant acid-base group proximate to the metal center where H_2 production occurs.[11–13,24–27] These catalysts are akin to the active sites of hydrogenases, which feature pendant bases positioned near the metal centers that are postulated to play a role in enzyme catalysis.[28] The benefits of a pendant proton relay are consistent with the early proposal of H_2 generation via the pathway shown in Scheme 1.1A: reduction of a Co^{II} center to Co^{I} followed by H^+ attack to yield a hydridic $Co^{III}H$ species that yields H_2 upon protonolysis or bimetallic reaction. However, this mechanism has been recently re-considered in view of the contention that $Co^{III}H$ centers are not sufficiently basic to drive protonolysis. Accordingly, the suggestion has been made that more reduced cobalt species must be attained before protonolysis can occur (Scheme 1.1B).[29,30] The inability to control proton stoichiometry in most catalytic cycles has made it difficult to distinguish mechanisms and thus discern which intermediate is involved in catalysis. On this count, we realized the utility of hangman active sites for providing insight into the mechanism of H_2 evolution by stoichiometric generation of a key intermediate as a result of the hangman effect. In the hangman construction, an acid-base functionality is positioned from a xanthene or furan spacer over the face of a redox-active macrocycle such as porphyrin,[31,32] salen[33,34] or corrole.[35] The acid-base hanging group permits the facile transfer of a single proton to or from a substrate bound to metal macrocycle. With the ability to control proton stoichiometry from the hanging group, we undertook studies to examine H_2 generation at **CoHPX-CO_2H (1-Co)** shown in Chart 1.2. Comparison of the electrochemistry of **1-Co** to a macrocyclic analog in which the hanging group has been removed **CoHPX-Br (2-Co,** Chart 1.2) establishes the hangman effect (via a reduced overpotential) and that the Co center produces H_2 only beyond reduction potentials exceeding the Co^{I} oxidation state. Our results are consistent with the generation of $Co^{II}H$ as a key intermediate in H_2 electrocatalysis at the hangman cobalt porphyrin active sites.

Synthesis and Electrochemistry

We recently published an efficient synthesis for hangman porphyrins bearing a pendant carboxylic acid group under microwave irradiation.[36] The new procedure allows us to obtain hangman porphyrins in multimilligram quantities, in shorter synthesis time, and with much better

Scheme 1.1

$$Co(II) + e^- \longrightarrow Co(I)$$
$$Co(I) + H^+ \longrightarrow Co(III)H$$

(A)

$$Co(III)H + H^+ \longrightarrow Co(III) + H_2$$
$$2Co(III)H \longrightarrow 2Co(II) + H_2$$

or

(B)

$$Co(III)H + e^- \longrightarrow Co(II)H$$
$$Co(II)H + H^+ \longrightarrow Co(II) + H_2$$

yields. The new hagman library was synthesized with various substituents on the 5, 10, 15 meso positions. Cobalt (II) complexes of hangman porphyrins bearing electron withdrawing (pentafluorophenyl, 3,5-bis-trifluoromethylphenyl), electron releasing (4-methoxyphenyl, 4-*tert*-butylphenyl), bulky (2,4,6-trimethylphenyl) and alkyl (pentyl) substituents were delivered in workable amounts. The good yields in the porphyrin forming reaction and easy purification of the crude reaction mixture allowed us to structurally characterize the new hangman porphyrin library.[36,37] In this study we synthesized a new A_3B type of hangman porphyrin bearing a bromine (**CoHPX-Br, 2–Co**) instead of carboxylic acid to emphasize the key advantage of

Chart 1.2

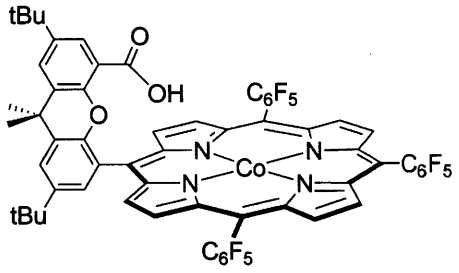

CoHPX-CO_2H (1-Co)

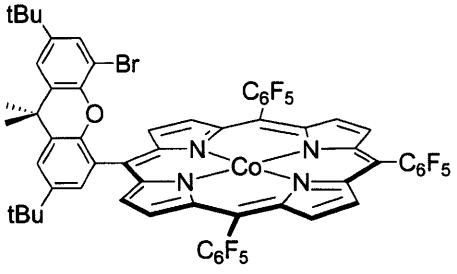

CoHPX-Br (2-Co)

having proton donating group for electrochemical H^+ reduction.

The synthesis of **2-Co** was accomplished with two different routes. In route 1, statistical Lindsey porphyrin synthesis[38] was performed by condensing pentafluorobenzaldeyhde with xanthene aldehyde (**3**)[39] and excess pyrrrole in the presence of BF_3•EOt_2. The reaction afforded the corresponding A_3B (A = pentafluorophenyl, B = xanthene backbone) porphyrinogen *in situ*. The 6 H^+, 6 e^- oxidation of the latter with 2,3-dichloro-5,6-dicyanobenzoquinone (DDQ)

Scheme 1.2A

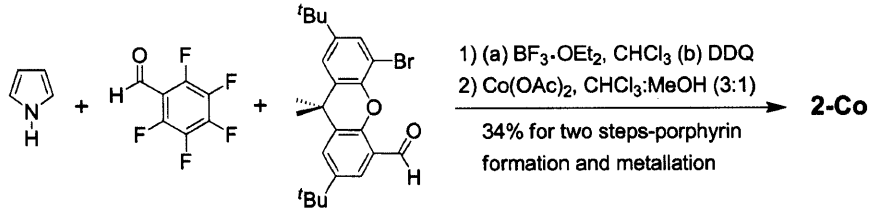

Scheme 1.2B

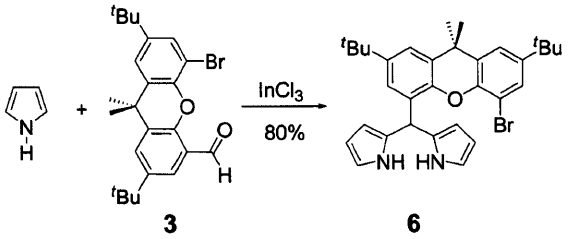

Scheme 1.2C

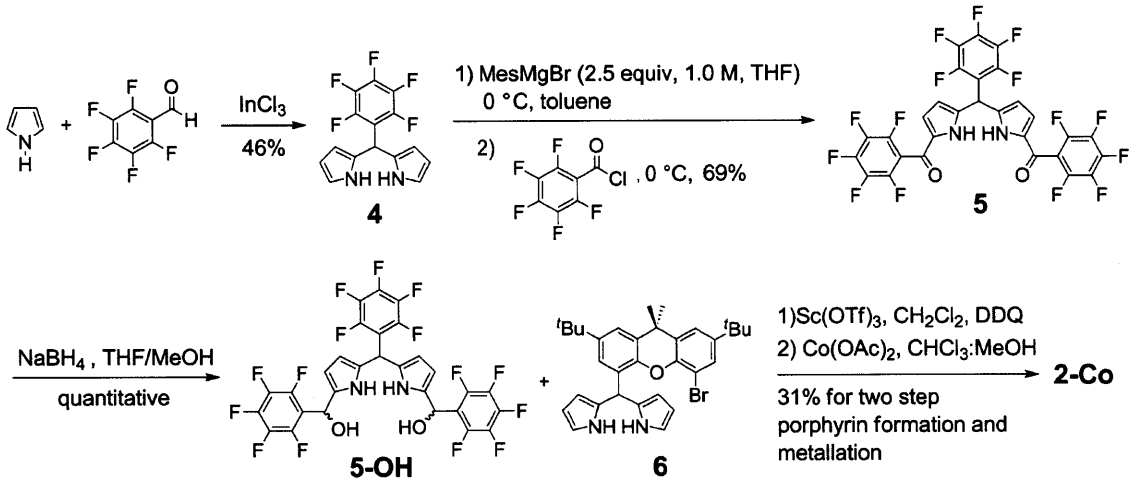

delivered the free-base **HPX-Br (2)** in 38% isolated yield. Metallation of **2** with $Co(OAc)_2$ under microwave irradiation gave **2-Co** in 34% overall chemical yield (Scheme 1.2A).

The lengthy purification of the **2** with flash column chromatography (3 days, see experimental section) encouraged us to try the synthesis of the target porphyrin in stepwise fashion. In route 2, the 1,9-diacyldipyrromethane (**5**) and a new dipyrromethane (**6**) (Scheme 1.2B) were synthesized by modifying the published procedures.[36,40] *In situ* reduction of **5** with excess $NaBH_4$ afforded the corresponding 1,9-diacyldipyrromethane dicarbinol, **5-OH** in quantitative yield. Lewis acid catalyzed condensation of the latter with the second dipyrromethane **6** was followed with *in situ* DDQ oxidation. The fast filtration of the crude

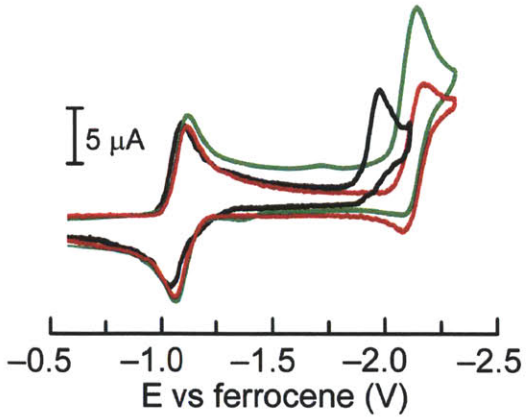

Figure 1.1. CVs of 0.5 mM of **1-Co** (—), **2-Co** (—), and **2-Co** in the presence of 0.5 mM benzoic acid (—). Scan rate, 100 mV/s; 0.1 M NBu_4PF_6 in acetonitrile. Glassy carbon working electrode, $Ag/AgNO_3$ reference electrode and Pt wire counter electrode.

reaction mixture through a pad of silica afforded free-base porphyrin **2** in 32% isolated yield. Final metallation of the title compound with $Co(OAc)_2$ under microwave irradiation afforded **2-Co** in 31% over all yield (Scheme 1.2C). Although the stepwise synthesis of **2−Co** has three additional steps (synthesis of compounds **4**, **5**, and **6**) versus statistical synthesis, easy purification of the free-base porphyrin **2** (2h versus 3 days) makes this route more attractive.

As shown in Figure 1.1, **1-Co** and **2-Co** exhibit reversible waves for the $Co^{II/I}$ couple at almost the same potentials (−1.08 V vs the ferrocene/ferrocenium couple for **1-Co** and −1.10 V for **2-Co**). The cyclic voltammogram (CV) of **2-Zn** shows redox waves at −1.52 and −1.92 V (Figure 1.2), and confirms that each electrochemical feature of **1-Co** and **2-Co** has significant cobalt character. For simplicity, the reduction potentials will be formally ascribed to Co, though we believe that there is significant electron density on the porphyrin ring at very reducing potentials.

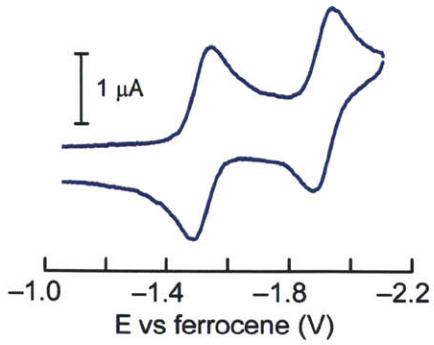

Figure 1.2. CV of **2-Zn**. Scan rate, 25 mV/s; 0.1 M NBu_4PF_6 in acetonitrile. Glassy carbon working electrode, $Ag/AgNO_3$ reference electrode and Pt wire counter electrode.

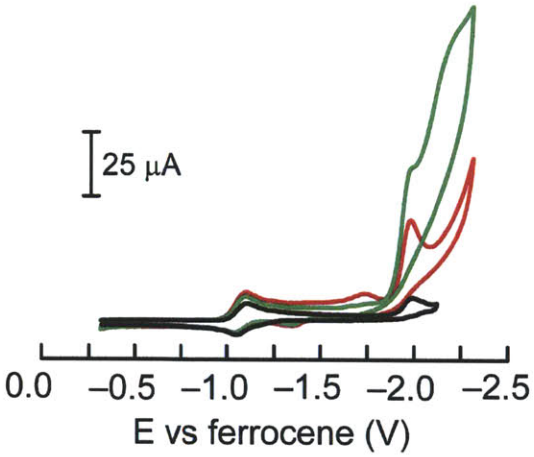

Figure 1.3. CV of 0.5 mM **1-Co** in the presence of 0 (—), 7.0 (—) and 14.6 mM (—) benzoic acid.

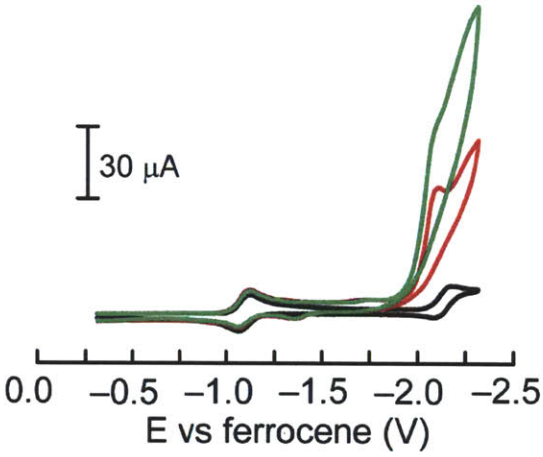

Figure 1.4. CV of 0.5 mM **2-Co** in the presence of 0 (—), 7.5 (—) and 15 mM (—) benzoic acid.

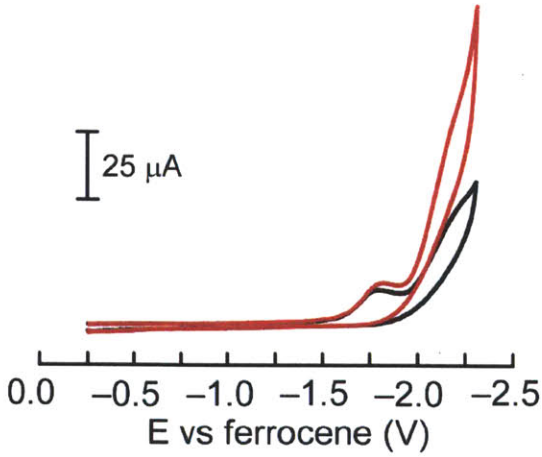

Figure 1.5. CV of 7.5 (—) and 15.0 mM (—) benzoic acid.

Whereas **2-Co** shows a reversible wave for $Co^{I/0}$ at −2.14 V, interestingly, **1-Co** produces an irreversible wave for the reduction of Co^{I} and the wave is positively shifted by ~200 mV. The only structural difference between **1-Co** and **2-Co** is the hanging carboxylic acid group and accordingly the irreversible process of **1-Co** is ascribed to the hangman effect where the reduction of Co^{I} to Co^{0} is followed by immediate proton transfer from the hanging group to produce $Co^{II}H$. The second wave in the CV of **2-Co** also becomes irreversible upon the addition of external benzoic acid. At 1 equiv of benzoic acid, the wave begins to exhibit irreversibility, also indicating protonation of the Co^{0} species. Complete irreversibility of the wave is observed only upon addition of >1 equiv of benzoic acid; this observation is also consistent with the hangman effect in **1-Co**.

In the presence of excess benzoic acid (pK_a = 20.7 in acetonitrile),[41] **1-Co** and **2-Co** exhibit catalytic cathodic waves (Figures 1.3, 1.4 and 1.7a). Although the overpotential for catalysis is large (~800 mV), the catalysis performance is not our interest; the CV features of the electrocatalysis uncover essential mechanistic details of HER at cobalt porphyrins and the effect of dangling acid group. The $Co^{II/I}$ reduction feature is not affected much by the presence of acid (Figure 1.3, 1.4 and 1.6) but the second reduction wave exhibits pronounced catalytic activity. These results indicate that benzoic acid is too weak an acid to protonate the Co^{I} center, and hence catalytic H_2 production is observed only upon further reduction to Co^{0} (Scheme 1.3). The overpotential for proton reduction of **1-Co** is ~120 mV lower potential than that of **2-Co** at 3 mM acid concentration. Moreover, the potential of the second reduction wave of **1-Co** is the same in the presence and absence of acid (Figure 1.3). This is not the case for **2-Co**; with increasing acid concentration the wave shifts to higher potential by 80 mV (Figure 1.4). These results are also

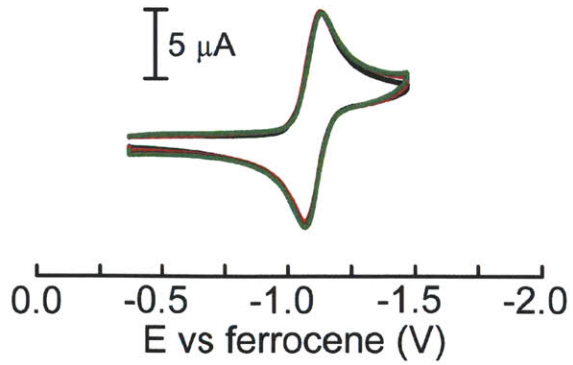

Figure 1.6. CV of 0.5 mM **2-Co** in the presence of 0 (—), 7.5 (—) and 15.0 mM (—) benzoic acid.

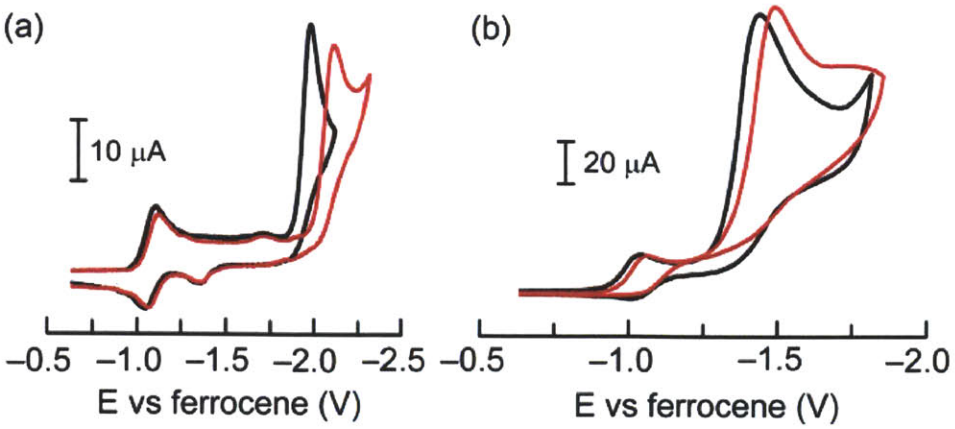

Figure 1.7. (a) CV of 0.5 mM of **1-Co** in the presence of 2.5 mM benzoic acid (—) and 0.5 mM of **2-Co** in the presence of 3.0 mM benzoic acid (—). (b) CV of 0.8 mM of **1-Co** (—) and **2-Co** (—) in the presence of 10 mM tosic acid. Scan rate, 100 mV/s; 0.1 M NBu_4PF_6 in acetonitrile. Glassy carbon working electrode, $Ag/AgNO_3$ reference electrode and Pt wire counter electrode.

Scheme 1.3

$$\begin{aligned} Co(II) + e^- &\longrightarrow Co(I) \\ Co(I) + e^- &\longrightarrow Co(0) \\ Co(0) + H^+ &\longrightarrow Co(II)H \\ Co(II)H + H^+ &\longrightarrow Co(II) + H_2 \end{aligned}$$

indicative of the hangman effect since in **1-Co**, proton transfer is not rate-determining for catalysis (hence the insensitivity of the reduction wave to proton concentration) whereas in **2-Co**, the proton transfer is a determinant of the mechanism (hence the shift to more positive potential with increasing acid). For either case, H_2 catalysis is initiated from the $Co^{II}H$.

Bulk electrolysis was performed in acetonitrile solutions of 0.4 mM **1-Co** at −2.05 V and of 0.5 mM **2-Co** at −2.20 V in the presence of 15 mM benzoic acid. The amount of H_2 gas produced during the electrolysis was determined by gas chromatography after 15 C of charges had passed. Faradaic efficiencies for H_2 production were *ca.* 80% and 85% for **1-Co** and **2-Co**, respectively; no other gaseous product is detected in the experimental condition. On the basis of TLC, mass spectra and UV-vis measurements, the decomposed product in bulk electrolysis in the presence of **2-Co** does not correspond to a demetallated porphyrin or other porphyrin product.

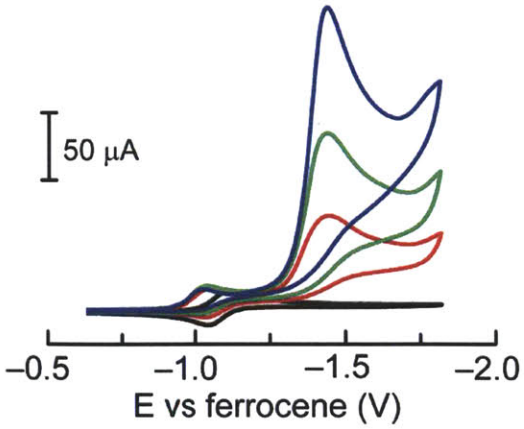

Figure 1.8. CV of 0.8 mM **1-Co** in the presence of 0 (—), 5.0 (—), 10 (—), 20 (—) mM tosic acid.

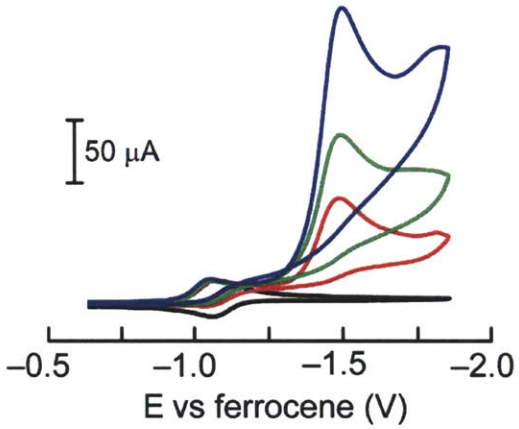

Figure 1.9. CV of 0.8 mM **2-Co** in the presence of 0 (—), 5.0 (—), 10 (—), 20 (—) mM tosic acid.

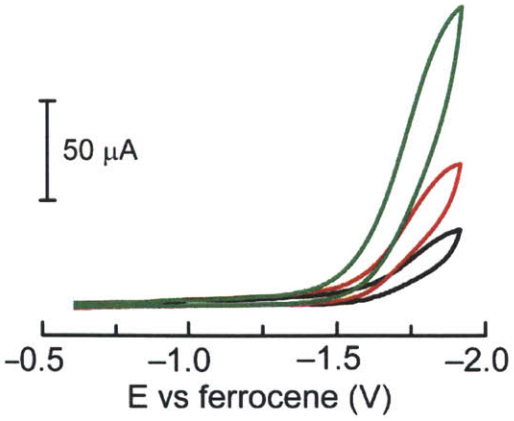

Figure 1.10. CV of 5.0 (—), 10 (—), 20 (—) mM tosic acid.

In the presence of the stronger tosic acid (*p*-toluenesulfonic acid, pK_a = 8.3 in acetonitrile),[41] both **1-Co** and **2-Co** exhibit catalytic cathodic waves at ~ −1.5 V (Figures 1.7b, 1.8 and 1.9). The similarity of the CVs with regard to current and the onset of electrocatalysis suggest that the stronger acid overwhelms the chemistry of the system and the hangman effect is diminished. As observed for benzoic acid, electrocatalysis for **1-Co** and **2-Co** occurs at potentials negative of the $Co^{II/I}$ couple. However, there is one significant difference between the benzoic acid and tosic acid data; unlike the situation for benzoic acid, the $Co^{II/I}$ wave becomes irreversible in the stronger tosic acid for both **1-Co** and **2-Co** (Figures 1.7b, 1.8 and 1.9). This indicates that Co^{I} is protonated by the tosic acid. But the observation that catalysis occurs well past the $Co^{II/I}$ reduction event indicates that a $Co^{III}H$ species, when formed, needs to be further reduced to $Co^{II}H$ for H_2 generation to occur. One determinant of the metal basicity is the presence of meso groups on macrocycle periphery. The electron withdrawing C_6F_5 groups will attenuate the metal center basicity and make the metal less reactive to protons, as has previously been observed.[16,42]

In summary, the hangman porphyrin provides mechanistic insight into H^+ reduction owing to the ability to control proton equivalency precisely via the hanging group. The irreversibility and positive shift of the reduction of Co^{I} in **1−Co** together with a lowered overpotential for H_2 production are a result of the hangman effect. For the case of weak acids, H_2 is produced upon reduction to Co^{0} followed by protonation (Scheme 1.3). For stronger acids, Co^{I} is first protonated and electron reduction follows it (Scheme 1.1B). Regardless of the strength of the acid, these results are consistent with H_2 production being mediated by $Co^{II}H$. Further reduction of the metal is needed for the effective protonation of the hydride to produce H_2.

1.3 Synthesis of Modified Tetraazamacrocycles and Hydrogen Generation by the Tetraazamacrocycles.

Modification on macrocyclic ligand framework aiming at tuning the properties of complexes has been one of the main topics in inorganic chemistry. Our group has invented the Hangman concept to faithfully capture the distal function of the enzymes such as hydrogenases and oxygenases.[31–35] Also, our group has reported cofacial bisporphyrins providing the Pacman effect in a single framework.[43] Inspired by our previous results, we decided to prepare analogues of modified porphyrins with different macrocyclic ligand, bpda (2,12–dimethyl–3,7,11,17–tetraazabicyclo[11.3.1]heptadeca–1(17),2,11,13,15-pentane, bisiminopyridylamine) and utilize some of the Co macrocyclic complexes for electrochemical H_2 production in order to understand the effect of functionalities introduced into the macrocycle on the ability of H_2 production. Among reported synthetic macrocyclic ligands, bpda ligand is one of the most extensively studied ligands since Busch et al. reported synthesis of $Ni(bpda)Br_2$.[44] Also, $Co(bpda)Br_2$ catalyzes the electro- and photoelectrochemical reduction of CO_2 in the presence of H^+ to produce CO with H_2 as side product.[45] In this work, we report derivatives of diacetylpyridine, **7** and **8** along with **9** which were prepared by Suzuki coupling following borylation reaction, and

Chart 1.3

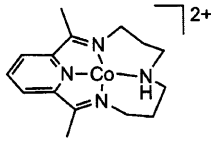

10

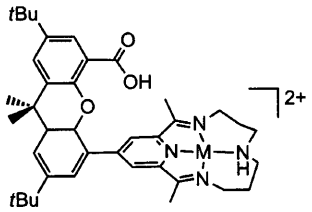

11 : M = Zn
14 : M = Co

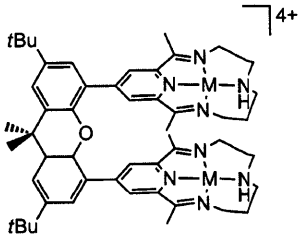

12 : M = Zn
15 : M = Co

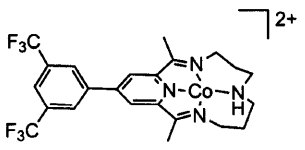

13

macrocyclic compounds with modified ligand framework, **11–15**, which were prepared by template reaction of the derivatives and 3,3′-diaminodipropylamine in the presence of Zn^{2+} or Co^{2+} (Scheme 1.4 and 1.5).

It turned out that the Co complex **10** is a stable electrocatalyst for H_2 generation. The $Co^{II/I}$ reduction potential can be positively shifted with the addition of electron withdrawing groups on the **13.** However, this electronic perturbation given by an electron-withdrawing group hinders proton reduction. The electrochemistry of Hangman complex **14** was complicated by putative palladium impurities from coupling reaction reagents.

Synthesis and Electrochemistry

Derivatives of diacetylpyridine were obtained according to Scheme 1.4 and 1.5 by Suzuki coupling reactions following iridium catalyzed borylation of the 4-position of the pyridine moiety. The methods of borylation of heteroarenes based on iridium catalysts have been developed by Ishiyama, Miyaura and Hartwig et. al.,[46,47] and we utilized $[Ir(OMe)(COD)]_2$ (COD = cyclooctadiene) as a precatalyst for the borylation of diacetylpyridine in the presence of dtbpy (4,4'-Di-tert-butyl-bipyridyl). After the borylation reaction, volatile materials were removed from the reaction mixture and the reagents for Suzuki coupling reaction were added to

Scheme 1.4

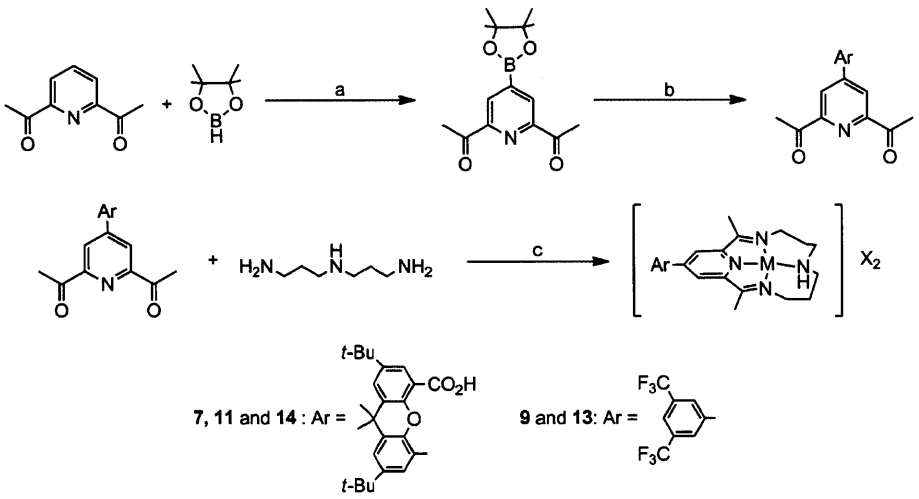

a $[Ir(OMe)(COD)]_2$, 2dtbpy, cyclohexane, 100 °C. b Ar-Br, $Pd(PPh_3)_4$, Na_2CO_3, H_2O, DMF, 90 °C. c **11** : $ZnBr_2$, **7**, methanol, 1,2-dichloroethane and 60 °C , **13** : $Co(NO_3)_2 \cdot 6H_2O$, **9**, ethanol, H_2O, acetic acid and 70 °C, **14** : $Co(NO_3)_2 \cdot 6H_2O$, **7**, ethanol, and 60 °C.

Scheme 1.5

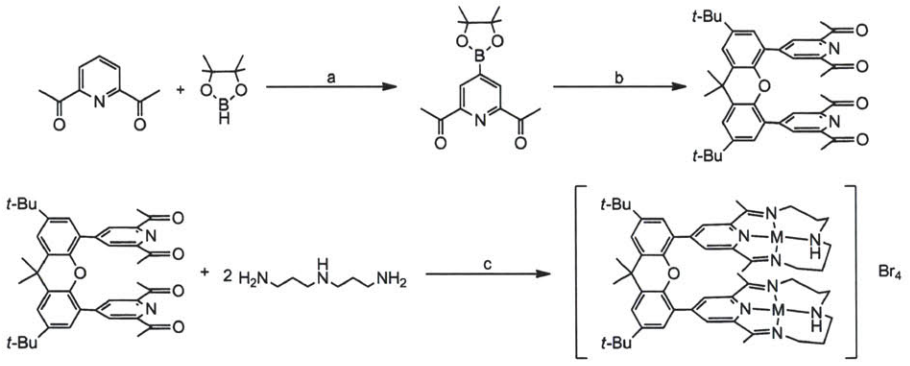

a $[Ir(OMe)(COD)]_2$, 2dtbpy, cyclohexane, 100 °C. b 4,5-dibromo-2,7-di-tert-butyl-9,9-dimethylxanthene, $Pd(PPh_3)_4$, Na_2CO_3, H_2O, DMF, 90 °C. c **12** : $ZnBr_2$, **8**, methanol, 1,2-dichloroethane and 60 °C , **15** : $CoBr_2$, **8**, ethanol, 1,2-dichloroethane and 70 °C.

the flask without isolation of the borylated product. Each compound was purified by column chromatography and characterized by NMR spectroscopy, mass spectrometry and elemental analysis. Compound **7** and **8** were structurally characterized by X-ray crystallography, and functionalization of 4-position diacetylpyridine was confirmed (Figure 1.11 and 1.12).

Metal complexes were prepared by metal templated reactions of the derivatized diacetylpyridines and 3,3′-diaminodipropylamine in the presence of metal salts and purified by

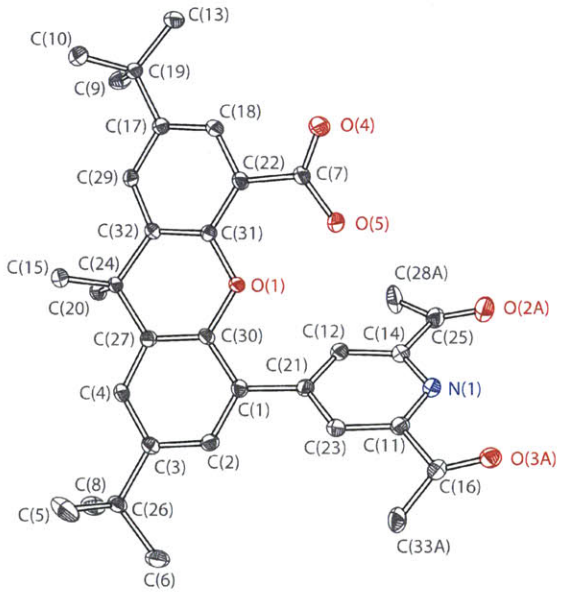

Figure 1.11. Crystal structure of **7** showing thermal ellipsoids at 50% probability. Disordered atoms and hydrogen atoms are omitted for clarity.

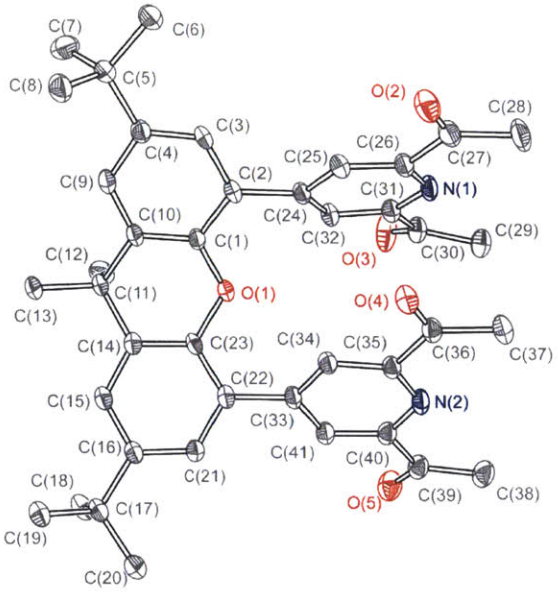

Figure 1.12. Crystal structure of **8** showing thermal ellipsoids at 50% probability. Disordered atoms and hydrogen atoms are omitted for clarity

recrystallization (Scheme 1.4 and 1.5). The macrocyclic complex **10** prepared this way according to the literature[48] was purified by recrystallization from acetonitrile solution. It was characterized by X-ray crystallography (Figure 1.13) and elemental analysis. In the literature, the complex was crystallized upon the cooling of concentrated reaction mixutre and hydrated crystals were formed.[48]

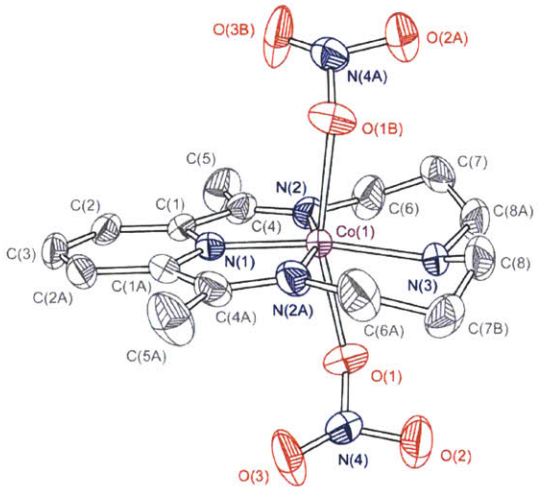

Figure 1.13. Crystal structure of **10** showing thermal ellipsoids at 50% probability. Disordered components and hydrogen atoms are omitted for clarity.

The ^{1}H NMR spectrum of **11** shows singlets at 1.36, 1.43 ppm for *tert*-butyl protons and 1.75 ppm for methyl protons on xanthene spacer, and two overlapped singlets at 2.66 ppm for protons of methyl groups on the imine carbons. The protons on aromatic rings of xanthene spacer shows doublets at 7.52 – 7.76 ppm and the protons on the pyridine ring shows singlet at 8.57 ppm. The protons on dipropylamine linker show multiplets at 1.83 – 4.26 ppm. The MALDI mass analysis agrees with the structure with hangman scaffold and it is confirmed that the complex is isolated as hydrated form by elemental analysis.

Single crystal of **12** was obtained by slow diffusion of Et_2O into methanol solution of crude product. As shown in Figure 1.14, the crystal structure of **12** confirms cofacial nature of two macrocycles containing Zn atoms. Contrary to **10** which has the metal center in octahedral geometry where 4 nitrogen atoms form rather square planar structure (Figure 1.13), each metal center in **12** has distorted square pyramidal geometry with one bromide coordinated to the metal. The distance between two Zn metals is 6.259 Å. The ^{1}H NMR spectrum of **12** shows singlets at 1.38 ppm for *tert*-butyl protons, 1.81 ppm for methyl protons on xanthene spacer and 2.23 ppm for protons of methyl group on the imine carbons. The protons on aromatic rings of xanthene spacer are found as two doublets at 7.34 and 7.68 ppm and the protons on the pyridine ring are

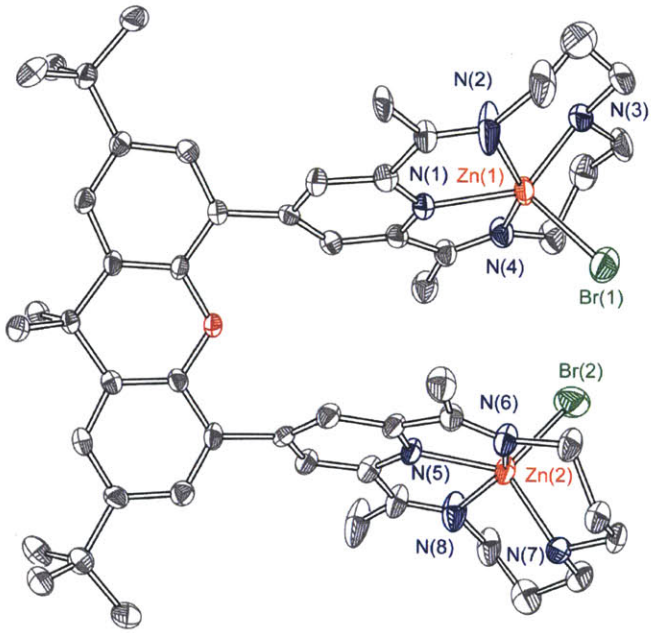

Figure 1.14. Crystal structure of **12** showing thermal ellipsoids at 50% probability. Solvents, hydrogen atoms and two bromide anions are omitted for clarity.

found as singlet at 8.10 ppm. The protons on dipropylamine linker are found as multiplets at 2.05 – 4.31 ppm. The spectrum shows some small signals besides the major signals corresponding to the structure. However, the sample was pure by elemental analysis, therefore these signals seem to be originated from small amount of conformers generated by rotation of macrocycles or flipping of dipropylamine linker.

The complex **13**, **14**, and **15** were prepared in a similar way and characterized by mass spectrometry. ESI mass analyses agree with the expected macrocyclic structure of the complexes. Complex **13** was isolated as analytically pure crystals from acetonitrile solution by layering diethyl ether.

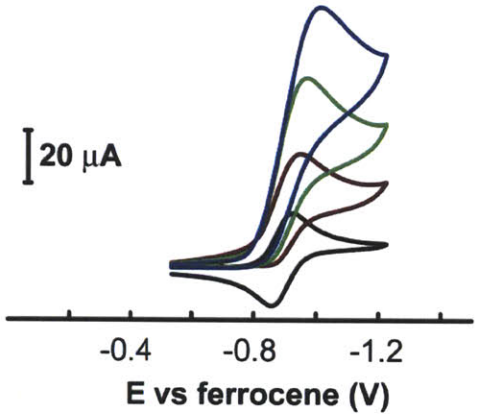

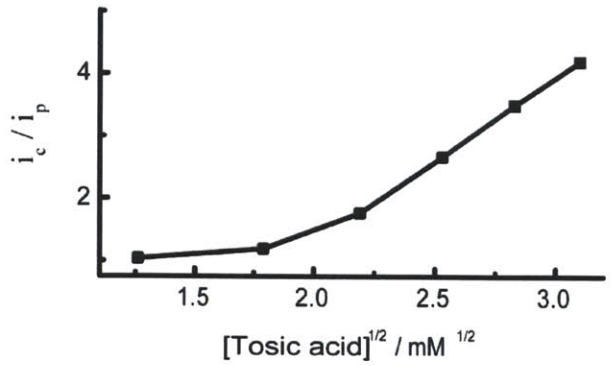

Figure 1.15. Cyclic voltammograms of 1 mM of **10** in 0.1 M NBu_4PF_6 acetonitrile solution at 0 (—), 4.8 (—), 8.0 (—), 12.0 (—) mM of tosic acid. (Top) The plot of i_c/i_p vs [tosic acid]$^{1/2}$. (Bottom) Scan rate: 100 mV/s. Glassy carbon working electrode (0.07 cm^2) and $Ag/AgNO_3$ reference electrodes.

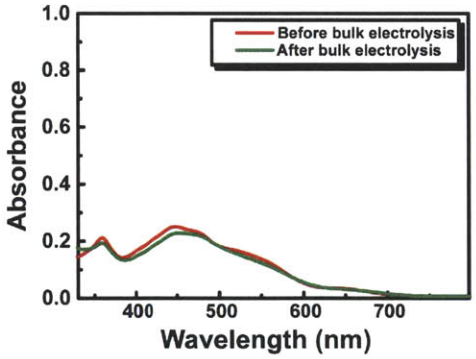

Figure 1.16. UV-vis spectra of the sample containing **10** obtained before and after bulk electrolysis in the presence of tosic acid.

Complex **10,** $Co(bpda)(NO_3)_2$, exhibits a reversible wave for the $Co^{II/I}$ potential at −0.89 V vs the ferrocene/ferrocenium (Fc/Fc^+) couple. In the presence of *p*-toluenesulfonic acid hydrate (tosic acid, pK_a = 8.3 in acetonitrile),[41] **10** produces catalytic cathodic waves near the $Co^{II/I}$ redox couple (Figure 1.15). Overpotential for H_2 production is ~430 mV as thermodynamic potential for H_2 production of 10 mM tosic acid in acetonitrile is −0.48 V.[41] Control experiments performed in the absence of the complexes show that the working glassy carbon electrode is almost inert under the same experimental conditions. Bulk electrolysis was performed at *ca.* −1.2 V in a gas-tight electrochemical cell until 20 C of charges were consumed. The atmosphere in the headspace of the cell was analyzed with a GC to confirm H_2 production. The current efficiency for H_2 production of **10** was found to be ~100%. By comparing UV-vis spectra of the solution containing the complexes before and after bulk electrolysis, the complexes appear to be quite stable during electrolysis (Figure 1.16).

In Figure 1.15, the plot of i_c/i_p vs [tosic acid]$^{1/2}$, where i_c is catalytic peak current and i_p is peak current in the absence of acid, exhibits linear relationship at high acid concentration. Figure 1.17 shows that the catalytic current is almost linearly proportional to concentration of **10** and CV has plateau shape at 0.25 mM of **10** and 20 mM of tosic acid. Considering relationships shown in Figure 1.15 and 1.17, the approximate rate constants for the overall H_2 production reaction can be calculated from plateau current which is given by by $i = nFAC_o^*(D\,k_f)^{1/2}$ (A = the surface area of electrode, C_o^* = the bulk concentration of catalyst, D = the diffusion coefficient, $k_f = kC_z$, C_z = concentration of substrate) and is estimated to be 1.37×10^3 M^{-1} s^{-1}.[49–52]

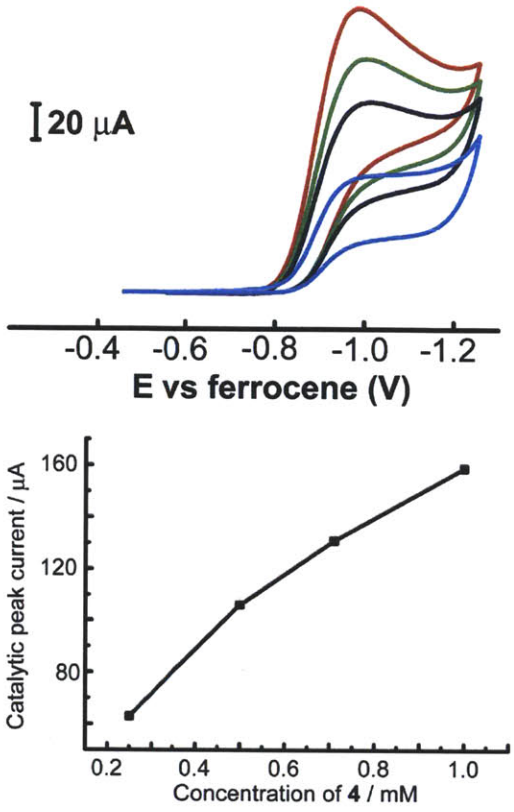

Figure 1.17. Cyclic voltammograms of **10** in 0.1 M NBu_4PF_6 and 20 mM tosic acid acetonitrile solution at 0.25 (—), 0.5 (—), 0.71 (—), 1.0 (—) mM of **10**. The plot of i_c vs catalyst concentrations. Scan rate: 100 mV/s. Glassy carbon working electrode and $Ag/AgNO_3$ reference electrode.

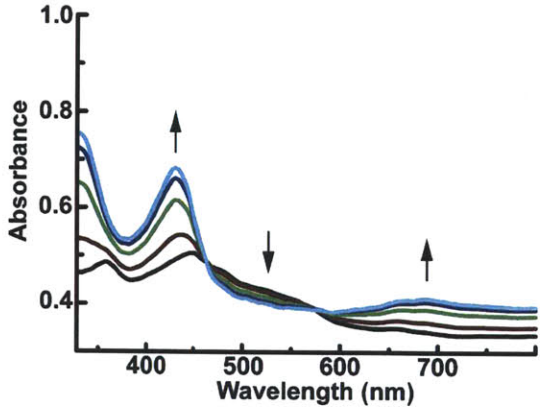

Figure 1.18. UV-vis spectra of 1mM **10** in 0.1 M NBu_4PF_6 during bulk electrolysis. 0 (—), 25 (—), 50 (—), 75 (—), 100 s (—) from the initiation. Pt working and $Ag/AgNO_3$ reference electrodes.

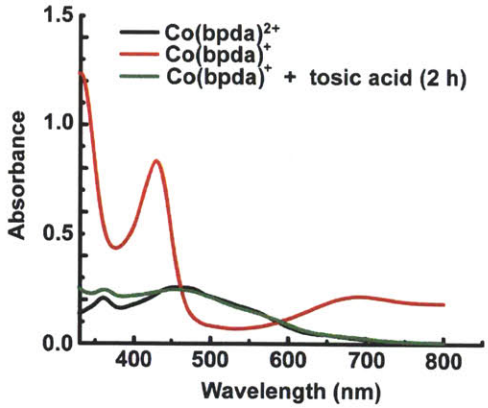

Figure 1.19. UV-vis spectra of $Co^{I}(bpda)^{+}$, $Co^{II}(bpda)^{2+}$ (**10**) and reaction mixture of $Co^{I}(bpda)^{+}$ and tosic acid.

Figure 1.18 is UV-vis spectrum changes of **10** during bulk electrolysis in the absence of acid and the spectra show the generation of a new species, Co^{I}. The same species can be produced chemically by the treatment with cobaltocene and the addition of tosic acid to Co^{I} results in the absorption features of Co^{II}. This suggests the electrocatalytic H_2 production is mediated by Co^{I}.

As expected from the two added trifluoromethyl groups, complex **13** exhibits a $Co^{II/I}$ redox couple at more positive reduction potential (–0.80 V) than **10**. However, the complex does not produce pronounced catalytic waves upon addition of tosic acid. We believe that the tosic acid is not acidic enough to be reduced efficiently by Co^{I} in **13**. This is consistent with other

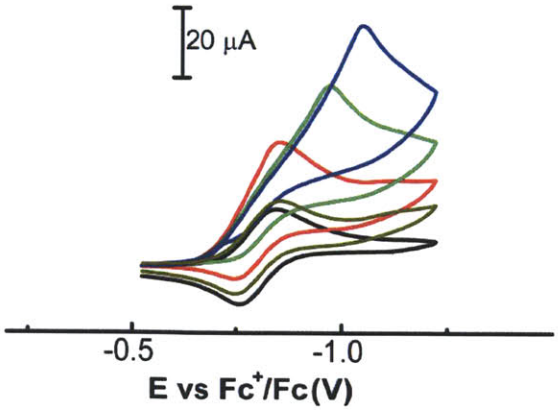

Figure 1.20. Cyclic voltammograms of 1 mM of **13** in 0.1 M NBu_4PF_6 acetonitrile solution at 0 (—), 3.0 (—), 4.0 (—), 5.0 (—), 6.0 (—) mM of triflic acid. Scan rate: 100 mV/s. Glassy carbon working electrode (0.07 cm^2) and $Ag/AgNO_3$ reference electrodes.

reports concerning structural perturbation of reduction potential; compounds with more positive reduction potentials owing to small structural changes are less nucleophilic and consequently less active for proton reduction.[16,42] Pronounced catalytic waves can be observed when triflic acid (p*K*a = 2.6 in acetonitrile)[41] is used as an acid source (Figure 1.20). The complex, however, was not stable enough in high acid concentration for bulk electrolysis.

Like **10**, complex **14** also produces catalytic wave in the presence of tosic acid at almost the same potential as that for **10** (−0.90 V vs Fc/Fc^+) (Figure 1.21) and chemically reduced species results in Co^{II} upon treatment with tosic acid (Figure 1.22). The complex generates hydrogen quanitatively and appears to be quite stable upon bulk electrolysis (Figure 1.23). However, it seems some impurities adsorbed onto the electrode contribute to the catalytic current and complicate the electrochemistry. Washed electrode after electrochemical measurements produces catalytic wave (peak around −1.0 V) in acid solution without the complex, even though the washed electrode does not show electrochemical activity in the absence of acid. We speculate that the adsorbed species could be small amount of residual palladium species from coupling reaction for preparation of **7** which was not completely removed during the purification steps. SEM images of glassy carbon plate used for bulkelectrolysis of **14** in the presence of tosic acid showed small particles on the surface and EDX analysis of the surface revealed that some parts of the surface contained palladium (Figure 1.24). This indicates study of catalyst prepared through metal catalyzed reaction should be carried out with extreme care. The hangman complex **14** itself does not show any enhancement from structural modification and this is possibly

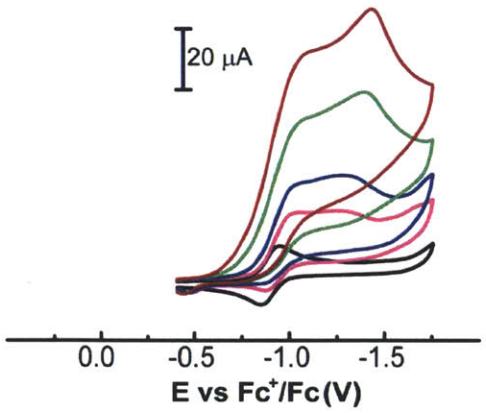

Figure 1.21. Cyclic voltammograms of 1 mM of **14** in 0.1 M NBu_4PF_6 acetonitrile solution at 0 (—), 2.0 (—), 3.2 (—), 6.4 (—), 9.6 (—) mM of tosic acid. Scan rate: 100 mV/s. Glassy carbon working electrode (0.07 cm^2) and $Ag/AgNO_3$ reference electrodes.

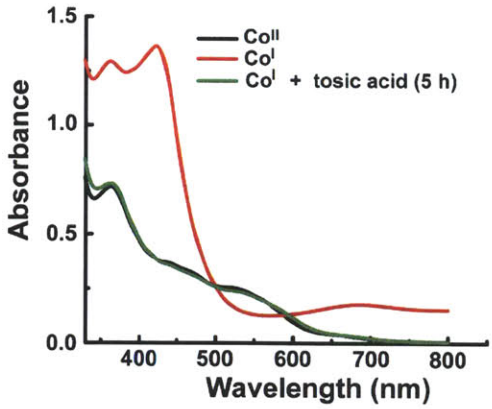

Figure 1.22. UV-vis spectra of Hangman Co^{I}, Hangman Co^{II} (**14**) and reaction mixture of Co^{I} and tosic acid.

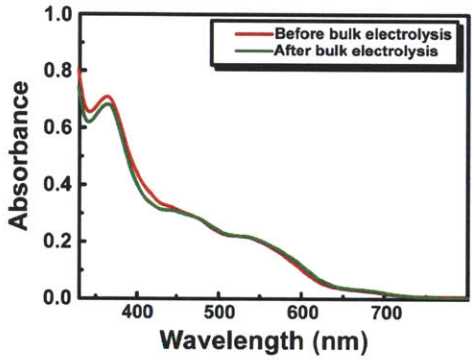

Figure 1.23. UV-vis spectra of the sample containing **14** obtained before and after bulk electrolysis in the presence of tosic acid.

because the $Co^{II/I}$ couple is at too positive potential to reduce the hanging carboxylic acid group. The thermodynamic reduction potential of 1mM benzoic acid is –1.20 V in acetonitrile[41] and we found that chemically reduced species of **14** did not react with benzoic acid.

In conclusion, we have prepared derivatives of diacetylpyridine, **7**-**9** through Suzuki coupling reaction following borylation of 4-position of diacetylpyridine. These derivatives were used as a precursor to derivatized macrocyclic complexes, **11**-**15**, by metal mediated template synthesis. Complex **11** and **14** have a hanging carboxylic group over the metal center. Complex **12** and **15** have cofacial bimetallic structure. We showed the macrocyclic complex **10** is a stable catalyst for electrochemical hydrogen production. The electron withdrawing groups on **13** shifts reduction potential of the complex toward positive. However, the complex shows less activity in hydrogen generation.

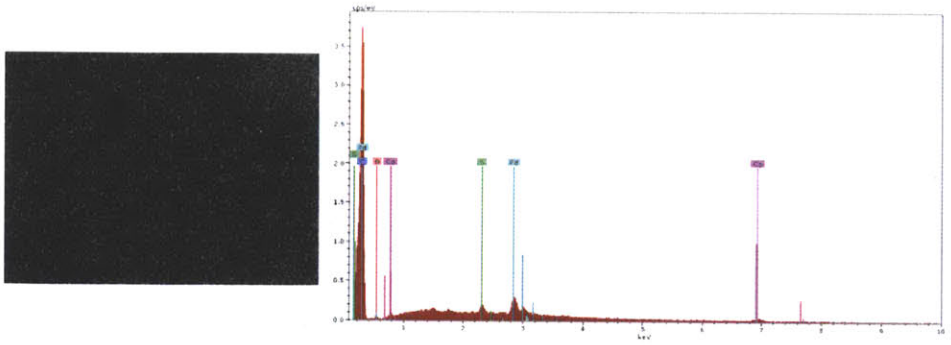

Figure 1.24. SEM and EDX analyses of glassy carbon plate after bulkelectrolysis of **14** in the presence of tosic acid (Pd (▬); Co (▬)).

1.4 Experimental Section

1.4.1 Hydrogen Generation by Hangman Metalloporphyrins

^{1}H NMR spectra (500 MHz) were recorded on samples in $CDCl_3$ at room temperature unless noted otherwise. Silica gel (60 μm average particle size) was used for column chromatography. 4-Formyl-5-bromo-2,7-di-*tert*-butyl-9,9-dimethylxanthene (**3**)[39] 5-pentafluorophenyldipyrromethane (**4**),[40] 1,9-bis(pentafluorobenzoyl)-5-(pentafluorophenyl)dipyrromethane (**5**),[36] 1,9-bis(pentafluorobenzoyl)-5-(pentafluorophenyl)dipyrromethane dicarbinol (**5-OH**),[36] 5-(4-(5-hydroxycarbonyl-2,7-di-*tert*-butyl-9,9-dimethyl-xanthene))-10,15,20-tris(pentafluorophenyl)-porphyrinatocobalt(II) (**1-Co**)[36] were prepared as described in the literature. THF (anhydrous), methanol (anhydrous) and CH_2Cl_2 (anhydrous) and all other chemicals were reagent grade and were used as received. LD-MS data was measured on porphyrins in the absence of matrix.

The microwave-assisted reactions were performed inside the cavity of a CEM Discover microwave synthesis system equipped with infrared, pressure and temperature sensors for monitoring the synthesis. The reaction vessels were 10 mL crimp-sealed thick-wall glass tubes. The contents of each vessel were stirred with a magnetic stirrer.

UV-vis spectra were recorded at room temperature in quartz cuvettes in anhydrous CH_2Cl_2 on a Varian Cary 5000 UV-vis-NIR spectrophotometer. Steady state emission spectra were recorded on an automated Photon Technology International (PTI) QM 4 fluorimeter equipped with a 150-W Xe arc lamp and a Hamamatsu R928 photomultiplier tube. Excitation light was wavelength selected with glass filters. Solution samples were prepared under ambient atmosphere in anhydrous CH_2Cl_2 and contained in screw-cap quartz fluorescence cells.

Syntheses

5-(4-(5-bromo-2,7-di-tert-butyl-9,9-dimethylxanthene))dipyrromethane (6).

A mixture of 4-formyl-5-bromo-2,7-di-*tert*-butyl-9,9-dimethylxanthene **3**, (1.00 g, 2.33 mmol) and pyrrole (15.6 mL, 233 mmol) in a 50-mL flask was degassed with a stream of argon for 10 min at room temperature. The mixture was heated to 75 °C to obtain a clear solution. $InCl_3$ (50.0 mg, 0.226 mmol) was then added, and the mixture was stirred at 75 °C for 2 h. A

sample of NaOH (0.280 g, 7.00 mmol) was added and the mixture was stirred at 75 °C for 1.5 h. The mixture was filtered. The filtrate was concentrated and resulting crude product was chromatographed [silica, hexanes:CH_2Cl_2 (3:2)] to afford a light yellow foam solid (1.01 g, 80%). ^{1}H NMR (500 MHz, $CDCl_3$) δ / ppm: 1.27 (s, 9H), 1.32 (s, 9H), 1.63 (s, 6H), 6.02 (br. s, 2H), 6.14-6.16 (m, 3H), 6.69-6.70 (m, 2H), 7.18 (d, J = 2.5 Hz, 1H), 7.28 (d, J = 2.5 Hz, 1H), 7.35 (d, J = 2.5 Hz, 1H), 7.43 (d, J = 2.5 Hz, 1H), 8.24-8.44 (br. s, 2H). Anal. Calcd. for (M + H^+), M = $C_{32}H_{37}BrN_2O$, Calcd. 545.2162, Found for HR(ESI)-MS: 545.2162. Anal. Calcd. for $C_{32}H_{37}BrN_2O$: C, 70.45; H, 6.84; N, 5.13. Found: C, 70.95; H, 6.90; N, 5.09.

5-(4-(5-Bromo-2,7-di-tert-butyl-9,9-dimethylxanthene))-10,15,20- tris(pentafluorophe nyl)-porphyrin (HPX-Br, 2). (Scheme 1.2A)

By following the statistical Lindsey porphyrin forming reaction,[38] $CHCl_3$ (425 mL) was placed in an oven dried round bottom flask (1000 mL) and purged with high flow of argon for 1 h. Pyrrole (0.275 mL, 4.00 mmol) was added via syringe to the reaction flask, which was covered with aluminum foil and the solution was purged with argon for 45 min. The pentafluorobenzaldehyde (0.735 g, 3.75 mmol) and 4-formyl-5-bromo-2,7-di-*tert*-butyl-9,9-dimethylxanthene **3** (0.107 g, 0.25 mmol) were then added to the round bottom. The resulting mixture was purged with argon in the dark for an additional 45 min. A sample of BF_3•OEt_2 (0.168 mL, 1.32 mmol) was added to the reaction mixture dropwise via syringe, the solution stirred under argon in the dark for 1 h, DDQ (0.68 g, 3.0 mmol) was added, and resulting mixture was stirred for an additional 1 h. A sample of triethylamine (13.2 mmol, 10 mol equiv versus BF_3•OEt_2) was added and the reaction mixture was stirred for 10 more min. The resulting crude reaction mixture was concentrated to dryness and chromatographed [silica, hexanes:CH_2Cl_2:$CHCl_3$ (30:1:1), 3 days slow elution, column was not pressurized] to afford purple solid (114 mg, 38%, yield is based on aldehyde **3**). ^{1}H NMR (500 MHz, $CDCl_3$) δ / ppm: –2.75 (s, 2H), 1.24 (s, 9H), 1.56 (s, 9H), 1.91 (s, 6H), 7.03 (d, J = 2.5 Hz, 1H), 7.4 (d, J = 2.5 Hz, 1H), 7.92 (d, J = 2.5 Hz, 1H), 8.05 (d, J = 2.5 Hz, 1H), 8.79 (d, J = 4.5 Hz, 2H), 8.91 (s, 4H), 8.97 (d, J = 4.5 Hz, 2H);. Anal. Calcd. for (M + H^+), M = $C_{61}H_{38}BrF_{15}N_4O$: Calcd. 1207.2062. Found for HR(ESI)-MS: 1207.2108; LD-MS, 1205.42. $\lambda_{max,abs}$/nm (CH_2Cl_2) = 416, 510, 544, 587, 639. $\lambda_{max,em}$(416 exc)/nm = 642, 707.

5-(4-(5-Bromo-2,7-di-*tert*-butyl-9,9-dimethyl-xanthene))-10,15,20- tris(pentafluorophe nyl)-porphyrin (HPX-Br, 2). (Scheme 1.2C)

Following reported procedures,[53] a solution of **5** (0.350 g, 0.500 mmol) in dry THF/methanol (40 mL, 3:1) under argon at room temperature was treated with $NaBH_4$ (0.945 g, 12.5 mmol, 25 mol equiv versus **5**) in small portions with rapid stirring. The progress of the reaction was monitored by silica thin layer chromatography (TLC) analysis using a hexanes/CH_2Cl_2 (1:1) mixture as the eluent. On the basis of TLC, the reaction was found to be completed in ~30 min. The reaction mixture was poured into a solution of saturated aqueous NH_4Cl (100 mL) and ethyl acetate (100 mL). The organic phase was separated, washed with water and brine, dried over Na_2SO_4, and concentrated under reduced pressure at ambient temperature to yield the corresponding 1,9-diacyldipyrromethanedicarbinol (**5-OH**) as a yellow-orange foam-like solid. A sample of a dipyrromethane **6** (0.272 g, 0.500 mmol) was added into the flask containing the **5-OH**. The flask was fitted with a septum and it was then purged with argon for ~10 min. Anhydrous CH_2Cl_2 (20 mL, 25 mM for each reactant) was added under a slow argon flow. The resulting reaction mixture was stirred for 1 min to produce a homogenous solution. $Sc(OTf)_3$ (0.003 g, 0.0650 mmol, 3.25 mM) was slowly added to this solution and the mixture was stirred for 30 min under argon. 2,3-Dichloro-5,6-dicyano-benzoquinone (DDQ) (0.340 g, 1.50 mmol) was added. After stirring at room temperature for 1 h, the flask was charged with triethylamine (0.175 mL, 1.28 mmol). The reaction was stirred for 10 min and concentrated to dryness. The resulting crude product was dissolved in CH_2Cl_2 (100 mL), washed with water and brine, dried over Na_2SO_4 and concentrated to dryness. The crude product was subject to silica chromatography [hexanes:CH_2Cl_2 (4:1)] to afford purple solid (192 mg, 32%). The characterization data are consistent with the batch obtained by statistical synthesis.

5-(4-(5-Bromo-2,7-di-*tert*-butyl-9,9-dimethylxanthene))-10,15,20-tris(pentafluorophenyl)-porphyrinatocobalt (2-Co).

By modifying the published procedure,[36,37] a microwave glass tube (10 mL) containing a magnetic stir bar was charged with 7 mL of $CHCl_3$:MeOH (3:1) and **2** (0.0650 g, 0.0540 mmol). The solution was stirred at room temperature for 10 min to obtain a homogenous mixture. A sample of $Co(OAc)_2$ was added (0.0500 g, 0.270 mmol, 10 mol equiv versus **2**). The resulting mixture was stirred at room temperature for 5 min. The reaction vessel was sealed with a septum and subjected to microwave irradiation at 65 °C. The protocol was as follows: (1) heat the reaction vessel from room temperature to 65 °C, (2) hold at 65 °C and irradiate for 20 min (temperature overshoots of 67–70 °C were permitted; temperature was re-established at 65 °C by

using open flow valve option), (3) allow the reaction mixture to cool to room temperature, (4) check the reaction mixture by silica TLC analysis, (5) repeat steps 1−4 until all of the free base **2** starting material was consumed (9−12h). Upon complete reaction, triethylamine (10 mol equiv to metal salt) was added to the solution, which was washed with water and brine, dried over Na_2SO_4, and concentrated to dryness. The resulting crude product was chromatographed [silica, hexanes : CH_2Cl_2: $CHCl_3$ (8:1:1)] to afford dark red-orange solid (65 mg, 96%). ^{1}H NMR (500 MHz, $CDCl_3$) δ / ppm: 0.99 (s, 9H), 2.47 (s, 9H), 2.94 (s, 6H), 5.77 (s, 1H), 7.83 (s, 1H), 9.58 (s, 1H), 12.2-12.4 (br.s, 1H), 14.54-15.58 (br. s. 8H);. Anal. Calcd. for (M^+), M = $C_{61}H_{36}BrCoF_{15}N_4O$: Calcd. 1263.1159. Found for HR(ESI)-MS: 1263.1144; LD-MS. 1264.03. Anal. Calcd. for $C_{61}H_{36}BrCoF_{15}N_4O$: C, 57.93; H, 2.87; N, 4.43. Found: C, 58.17; H, 3.06; N, 4.26. $\lambda_{max,abs}$/nm (CH_2Cl_2) = 407, 526.

5-(4-(5-Bromo-2,7-di-*tert*-butyl-9,9-dimethyl-xanthene))-10,15,20- tris(pentafluorophenyl)-porphyrintozinc (ZnHPX-Br, 2-Zn).

By modifying the published procedure,[54] a sample of **2** (0.0650 g, 0.0540 mmol) in $CHCl_3$:MeOH (15 mL, 4:1) was treated with $Zn(OAc)_2$•$2H_2O$ (0.295 g, 1.35 mmol, 25 mol equiv vs **2**) at room temperature. The reaction mixture was stirred overnight. The reaction mixture was washed with water, brine, dried with Na_2SO_4 and concentrated to dryness. The resulting crude product chromatographed [silica, hexanes: CH_2Cl_2 (1:3)] afforded a purple solid. (67 mg, 97%). ^{1}H NMR (500 MHz, $CDCl_3$) δ / ppm: 1.21 (s, 9H), 1.55 (s, 9H), 1.89 (s, 6H), 6.98 (d, J = 2.5 Hz, 1H), 7.38 (d, J = 2.5 Hz, 1H), 7.89 (d, J = 2.5 Hz, 1H), 8.08 (d, J = 2.5 Hz, 1H), 8.87 (d, J = 4.5 Hz, 2H), 8.98 (s, 4H), 9.06 (d, J = 4.5 Hz, 2H);. Anal. Calcd. for (M + H^+), M = $C_{61}H_{36}BrF_{15}N_4OZn$: Cald. 1271.1195. Found for HR(ESI)-MS: 1271.1180. $\lambda_{max,abs}$/nm (CH_2Cl_2) = 417, 546. $\lambda_{max,em}$(417 exc)/nm = 589, 642.

Electrochemistry

Electrochemical experiments were performed with a BASi CV50W in a glove box. Cyclic voltammetry experiments were performed using a glassy carbon working electrode (0.07 cm^2), a platinum wire auxiliary electrode and a $Ag/AgNO_3$ (0.1 M) reference electrode in 0.1 M NBu_4PF_6 acetonitrile solution at room temperature. NBu_4PF_6 (Fluka) was dried at 120 °C under vacuum and acetonitrile was purified by passing them under an argon forcing pressure through

columns of neutral alumina. Tosic acid monohydrate (Aldrich) and benzoic acid (Aldrich) were used as received. A polished electrode was used for each cyclic voltammogram. The potentials were referenced to ferrocene/ferrocenium couple by recording the cyclic voltammogram of the complexes in the presence of a small amount of ferrocene.

Bulk electrolysis was performed using a glassy carbon rod (7 mm × 5 cm) working electrode and a platinum mesh auxiliary electrode in a gas-tight electrochemical cell. The amount of H_2 gas produced in the headspace was analyzed by an Agilent 7890A GC. The potentials for the electrolyses (−2.05 V for **1-Co** and −2.20 V vs Fc/Fc^+ for **2-Co**) were referenced with $Co^{II/I}$ redox couples in cyclic voltammogram obtained before adding acid solution.

1.4.2 Synthesis of Modified Tetraazamacrocycles and Hydrogen Generation by the Tetraazamacrocycles.

All synthetic manipulations were executed using standard Schlenk techniques under a N_2 atmosphere, or in a glovebox under a N_2 atmosphere. Reactions were performed in oven-dried glassware. Tetrahydrofuran, hexanes and diethyl ether were purified by passing them under an argon forcing pressure through columns of neutral alumina and stored over molecular sieves. Anhydrous acetonitrile, cyclohexane and DMF were purchased from Aldrich and stored in a glovebox over molecular sieves. Anhydrous ethanol, methanol and 1,2-dichloroethane were purchased from Aldrich and used as received. Dichloromethane and diethyl ether from Aldrich were used as received for handling products in the air. 4-Hydroxycarbonyl-5-bromo-2,7-di-tert-butyl-9,9-dimethylxanthene was synthesized as previously described.[55] 2,6-Diacetylpyridine (Aldrich), pinacolborane (Aldrich), 4,4′-di-tert-butyl-bipyridyl (Aldrich), $[Ir(OMe)(COD)]_2$ (Strem), $Pd(PPh_3)_4$ (Strem), Na_2CO_3 (Aldrich), 4,5-dibromo-2,7-di-tert-butyl-9,9-dimethyl xanthene (Aldrich), 3,5-bis(trifluoromethyl)bromobenzene (Aldrich), glacial acetic acid (Aldrich), 3,3′-diaminodipropylamine (Aldrich), 99.999% $ZnBr_2$ (Strem), 99.999% cobalt(II) nitrate hexahydrate (Aldrich), $CoBr_2$ (Aldrich) and cobaltocene (Strem) were used as received. NBu_4PF_6 (Fluka) was dried at 120 °C under vacuum for a day and stored in a glovebox.

^1H NMR and ^{19}F NMR spectra were recorded on a Varian 300 MHz instrument. High resolution mass spectral analyses were carried out at the MIT Department of Chemistry Instrumentation Facility. Elemental analyses were performed by Midwest Microlab, LLC.

Syntheses

4-hydroxycarbonyl-5-(4-(2,6-diacetylpyridyl))-2,7-di-tert-butyl-9,9-dimethyl xanthene (7)

4,4′-Di-tert-butyl-bipyridyl (11.8 mg, 0.0440 mmole) was added to a 3-neck flask equipped with a condenser and the flask was transferred to a glovebox. $[Ir(OMe)(COD)]_2$ (14.6 mg, 0.0220 mmole) was dispersed in 40 mL of cyclohexane and the mixture was added to the flask. Pinacolborane (192.0 mg, 1.500 mmole) was added to the mixture via syringe. After ~15 min of stirring, diacetylpyridine (245.0 mg, 1.501 mmole) was added to the mixture, the flask was removed from the glovebox and the mixture was stirred at 100 °C for 3 h under a N_2 atmosphere. The mixture was cooled to 30 °C and dried *in vacuo*. The flask was transferred to a glovebox and to it was added $Pd(PPh_3)_4$ (130.0 mg, 0.1125 mmole), Na_2CO_3 (237.0 mg, 2.236 mmole), 4-hydroxycarbonyl-5-bromo-2,7-di-tert-butyl-9,9-dimethylxanthene (500.0 mg, 1.124 mmole) and DMF (5 mL). The flask was again removed from the glovebox and 2 mL of water was added to it via syringe. The mixture was stirred at 90 °C for a day under a N_2 atmosphere. Dichloromethane was added to the mixture after cooling to room temperature. The mixture was transferred into a separatory funnel and washed with water. The aqueous layer was extracted with dichloromethane (3 × 5 mL). The collected organic layer was dried on a rotary evaporator. The crude product was separated by using silica gel column chromatography (dichloromethane:diethyl ether = 6 : 1). After removing the eluent, the resulting oily product was dissolved in diethyl ether and dried slowly in the fume hood. The solid product was dried *in vacuo* to yield 225 mg (38.0%). Further purification of the product can be achieved by recrystallization from the evaporation of a diethyl ether solution of the compound. X-ray diffraction quality crystals were obtained by slow evaporation of diethyl ether solution. ^{1}H NMR ($CDCl_3$): δ 8.45 (s, 2H), 7.80 (d, J = 2.5 Hz, 1 H), 7.63 (d, J = 2.4 Hz, 1 H), 7.57 (d, J = 2.4 Hz, 1 H), 7.28 (d, J = 2.2 Hz, 1 H), 2.88 (s, 6 H), 1.73 (s, 6 H), 1.38 (s, 9 H), 1.34 (s, 9 H). HRMS (ESI) Calcd. $C_{33}H_{37}NO_5$: $[M + Na]^+$, 550.2564. Found: 550.2569. Anal. Calcd. $C_{33}H_{37}NO_5$: C, 75.12; H, 7.07; N, 2.65. Found: C, 74.94; H, 7.10; N, 2.71.

4,5-(bis(4-(2,6-diacetylpyridyl))-2,7-di-tert-butyl-9,9-dimethyl xanthene (8).

4,4′-Di-tert-butyl-bipyridyl (48.0 mg, 0.1788 mmole) was added to a 3-neck flask equipped with a condenser and the flask was transferred to a glovebox. $[Ir(OMe)(COD)]_2$ (60.0

mg, 0.0905 mmole) was dispersed in 40 mL of cyclohexane and the mixture was added to the flask. Pinacolborane (784.0 mg, 6.126 mmole) was added to the mixture via syringe. After ~15 min of stirring, diacetylpyridine (1.0 g, 6.129 mmole) was added to the mixture, the flask was removed from the glovebox and the mixture was stirred at 100 °C for 3 h under a N_2 atmosphere. The mixture was cooled to 30 °C and dried *in vacuo*. The flask was transferred to a glovebox and to it was added $Pd(PPh_3)_4$ (177.0 mg, 0.1532 mmole), Na_2CO_3 (324.0 mg, 3.0569 mmole), 4,5-dibromo-2,7-di-tert-butyl-9,9-dimethylxanthene (736.0 mg, 1.532 mmole) and DMF (20 mL). The flask was again removed from the glovebox and 3 mL of water was added to it via syringe. The mixture was stirred at 90 °C for two days under a N_2 atmosphere. Dichloromethane was added to the mixture after cooling to room temperature. The mixture was transferred into a separatory funnel and washed with water. The aqueous layer was extracted with dichloromethane (2 × 10 mL). The collected organic layer was dried on a rotary evaporator. The residual DMF was removed under vacuum. The crude product was separated by using silica gel column chromatography (dichloromethane). After removing the eluent, the product was dried *in vacuo* to yield 630 mg (63.8% yield). Further purification of the product can be achieved by recrystallization from the evaporation of a diethyl ether solution of the compound. X-ray diffraction quality crystals were obtained by slow evaporation of diethyl ether solution. ^1H NMR ($CDCl_3$): δ 8.05 (s, 4H), 7.53 (d, J = 2.1 Hz, 2 H), 7.18 (d, J = 2.3 Hz, 2 H), 2.76 (s, 12 H), 1.76 (s, 6 H), 1.36 (s, 18 H). HRMS (ESI) Calcd. $C_{41}H_{44}N_2O_5$: $[M + H]^+$, 645.33. Found: 645.33. Anal. Calcd. $C_{41}H_{44}N_2O_5$: C, 76.37; H, 6.88; N., 4.34. Found: C, 76.37; H, 6.75; N, 4.43.

4-(3,5-bis(trifluoromethyl)phenyl)-2,6-diacetylpyridine (9).

4,4′-Di-tert-butyl-bipyridyl (24.0 mg, 0.0894 mmole) was added to a 3-neck flask equipped with a condenser and the flask was transferred to a glovebox. $[Ir(OMe)(COD)]_2$ (30.0 mg, 0.0453 mmole) was dispersed in 40 mL of cyclohexane and the mixture was added to the flask. Pinacolborane (392.0 mg, 3.063 mmole) was added to the mixture via syringe. After ~15 min of stirring, diacetylpyridine (500.0 mg, 3.064 mmole) was added to the mixture, the flask was removed from the glovebox and the mixture was stirred at 100 °C for 3 h under a N_2 atmosphere. The mixture was cooled to 30 °C and dried *in vacuo*. The flask was transferred to the glovebox and to it was added $Pd(PPh_3)_4$ (177.0 mg, 0.1532 mmole), Na_2CO_3 (324.0 mg, 3.057 mmole), 3,5-bis(trifluoromethyl)bromobenzene (897.8 mg, 3.064 mmole) and DMF (5 mL). The flask was removed from the glovebox and 2 mL of water was added to it via syringe.

The mixture was stirred at 90 °C for 12 h under a N_2 atmosphere. Dichloromethane was added to mixture after cooling to room temperature. The mixture was transferred into a separatory funnel and washed with water. The aqueous layer was extracted with dichloromethane (3 × 5 mL). The collected organic layer was dried on a rotary evaporator. The crude product was separated by using silica gel column chromatography (dichloromethane). The product was dried *in vacuo* to yield 352 mg (30.6% yield). ^{1}H NMR ($CDCl_3$): δ 8.48 (s, 2H), 8.16 (s, 2 H), 8.02 (s, 1 H), 2.87 (s, 6 H). ^{19}F NMR ($CDCl_3$): −63.24. HRMS (ESI) Calcd. $C_{17}H_{11}F_6NO_2$: $[M + Na]^+$, 398.0586. Found: 398.0588. Anal. Calcd. $C_{17}H_{11}F_6NO_2$: C, 54.41; H, 2.95; N, 3.73. Found: C, 54.65; H, 3.01; N, 3.58.

Co(bpda)$(NO_3)_2$ (bpda = 2,12-dimethyl-3,7,11,17-tetraazabicyclo[11.3.1]-heptadeca-1(17),2,11,13,15-pentaene) (10).

The complex was prepared as described in the published procedure except for the purification step.[48] The crude product was dispersed in acetonitrile and the mixture was filtered through glass fiber in a pipet. The resulting solution was layered with diethyl ether, cooled and maintained at −40 °C for 4 days. The supernatant was decanted to remove small particles and the resulting solid was washed with diethyl ether. This process was repeated until the supernatant was clear. The product was dried *in vacuo*. The sample for crystallography was obtained by slow diffusion of diethyl ether into acetonitrile solution. Anal. Calcd. $CoC_{15}H_{22}N_6O_6$: C, 40.83; H, 5.02; N, 19.04. Found: C, 40.59; H, 4.91; N, 19.09. (Busch et al. reported the formation of Co(bpda)$(NO_3)_2 \cdot 0.5H_2O$ by elemental analysis on the cooling of a concentrated reaction mixture.)

Hangman Zn(bpda)$Br_2 \cdot H_2O$ (11).

In the glovebox, $ZnBr_2$ (21.3 mg, 0.0946 mmole) were added to a 3-neck flask. The flask was removed from the glovebox and equipped with a condenser. Compound **7** (50.0 mg, 0.0947 mmole) was added and the flask was purged with nitrogen. Anhydrous methanol (6 mL) and 1,2-dichloroethane (2 mL) were added to the flask via syringe and the mixture was stirred at 60 °C for ~30 min. 3,3′-Diaminodipropylamine (12.4 mg, 0.0945 mmole) was added to the flask via syringe. The resulting solution was stirred at 60 °C for 21 hrs. Volatile materials were removed *in vacuo* and the resulting solid was dispersed in methanol and the solution was filtered through glass fiber in a pipet. After the slow diffusion of diethyl ether into this solution for 5 days, the supernatant was decanted and the resulting yellowish solid was washed with diethyl ether several

times. The product was dried *in vacuo* giving 45 mg (56% yield). ^{1}H NMR (CD_3OD): δ 8.57 (s, 2H), 7.76 (d, J = 2.3 Hz, 1 H), 7.71 (d, J = 2.5 Hz, 1 H), 7.66 (d, J = 2.4 Hz, 1 H), 7.52 (d, J = 2.4 Hz, 1 H), 4.26 (m, 2 H + 1H), 3.95 (m, 2 H), 3.40 (m), 3.10 (m), 2.66 (d, 6 H), 2.26 (m, 2H), 1.83 (m, 2H), 1.75 (s, 6 H), 1.43 (s, 9 H), 1.36 (s, 9 H). HRMS (MALDI) Calcd. $ZnC_{39}H_{50}N_4O_3Br_2$: $[M - Br]^+$, 767.23. Found: 767.03. Anal. Calcd. $ZnC_{39}H_{50}N_4O_3Br_2 \cdot H_2O$: C, 54.09; H, 6.05; N., 6.47. Found: C, 53.69; H, 5.89; N, 6.61.

Pacman Zn(bpda)Br_2 (12).

In the glovebox, $ZnBr_2$ (17.5 mg, 0.0777 mmole) were added to a 3-neck flask equipped with a condenser. The flask was removed from the glovebox and **8** (25.0 mg, 0.0388 mmole) was added. The flask was purged with nitrogen. Anhydrous methanol (3 mL) and 1,2-dichloroethane (1 mL) were added to the flask via syringe and the mixture was stirred at 60 °C for ~30 min. 3,3′-Diaminodipropylamine (10.2 mg, 0.0777 mmole) was added to the flask via syringe. The resulting solution was stirred at 60 °C for 20 hrs. Volatile materials were removed *in vacuo*. The resulting solid was dispersed in methanol and the solution was filtered through glass fiber in a pipet. After the slow diffusion of diethyl ether into this solution for 5 days, the supernatant was decanted and the resulting yellowish crystals were washed with diethyl ether several times. The product was dried *in vacuo* giving 15 mg (30% yield). The sample for crystallography was obtained in the same way in the refrigerator. ^{1}H NMR (CD_2Cl_2): δ 8.10 (s, 4H), 7.68 (d, J = 2.4 Hz, 2 H), 7.34 (d, J = 2.4 Hz, 2 H), 2.23 (s, 12 H), 1.81 (s, 6 H), 1.38 (s, 18 H). HRMS (ESI) Calcd. $Zn_2C_{53}H_{70}N_8OBr_4$: $[M - 2Br]^{2+}$, 562.13. Found: 562.13. Anal. Calcd. $Zn_2C_{53}H_{70}N_8OBr_4$: C, 49.52; H, 5.49; N., 8.72. Found: C, 49.21; H, 5.51; N, 8.61.

Co(15-(3,5-bis(trifluoromethyl)phenyl)-bpda)$(NO_3)_2$ (13).

Compound **9** (100.0 mg, 0.2665 mmole) and cobalt(II) nitrate hexahydrate (77.5 mg, 0.2663 mmole) were added to a 3-neck flask equipped with a condenser, and the flask was purged with nitrogen. Anhydrous ethanol was added to the flask via syringe and the mixture was stirred at 70 °C for ~30 min. 3,3′-Diaminodipropylamine (35.00 mg, 0.2667 mmole) was added to the flask via syringe followed by the addition of acetic acid (0.05 mL) via syringe to produce a turbid mixture. Water (1 mL) addition caused the solution to become clear. The resulting solution was stirred at 70 °C for 6 h. Volatile materials were removed *in vacuo* and the flask was transferred to a glovebox. The solid was dispersed in acetonitrile and the solution was filtered through glass fiber in a pipet. The solution was layered with diethyl ether and cooled at −40 °C

for 3 days. The supernatant was decanted to remove small particles and the resulting crystals were washed with diethyl ether. This process was repeated until the supernatant was clear. The product was dried *in vacuo* giving 77 mg (44% yield). ^{19}F NMR (CD_3CN): –62.6. HRMS (ESI) Calcd. $CoC_{23}H_{24}F_6N_6O_6$: $[M - NO_3]^+$, 591.1110. Found: 591.1120. Anal. Calcd. $CoC_{23}H_{24}F_6N_6O_6$: C, 42.28; H, 3.7; N, 12.86. Found: C, 42.46; H, 3.73; 12.88.

Hangman Co(bpda)$(NO_3)_2$ (14).

Compound **7** (50.0 mg, 0.0948 mmole) and cobalt(II) nitrate hexahydrate (27.6 mg, 0.0948 mmole) were added to a 3-neck flask equipped with a condenser, and the flask was purged with nitrogen. Anhydrous ethanol was added to the flask via syringe and the mixture was stirred at 60 °C for ~ 30 min after which 3,3′-diaminodipropylamine (12.4 mg, 0.0945 mmole) was added via syringe and the mixture was stirred at 60 °C for a day. Volatile materials were removed *in vacuo* and the flask was transferred to a glovebox. The solid was dispersed in THF and the mixture was filtered through glass fiber in a pipet. The resulting solution was layered with hexanes and cooled to −40 °C and the temperature was maintained for 3 days. The product was collected on a frit and washed with diethyl ether. The product was dried *in vacuo* to yield 60 mg of **3** (79 % yield). HRMS (ESI) Calcd. $CoC_{39}H_{50}N_6O_9$: $[M - NO_3]^+$, 743.3088. Found: 743.3096.

Pacman Co(bpda)Br_2 (15).

In the glovebox, $CoBr_2$ (34.0 mg, 0.1554 mmole) were added to a 3-neck flask equipped with a condenser. The flask was removed from the glovebox and **8** (50.0 mg, 0.0775 mmole) was added. The flask was purged with nitrogen. Anhydrous ethanol (6 mL) and 1,2-dichloroethane (2 mL) were added to the flask via syringe and the mixture was stirred at 70 °C for ~30 min. 3,3′-Diaminodipropylamine (20.0 mg, 0.1524 mmole) was added to the flask via syringe. The resulting solution was stirred at 70 °C for a day. Volatile materials were removed *in vacuo* and the flask was transferred to a glovebox. The solid was dispersed in acetonitrile and the mixture was filtered through glass fiber in a pipet. The resulting solution was layered with diethyl ether and cooled to −40 °C and the temperature was maintained for 4 days. The product was collected on a frit and washed with diethyl ether. The product was dried *in vacuo* to yield 41 mg (42 % yield). HRMS (ESI) Calcd. $Co_2C_{53}H_{70}N_8OBr_4$: $[M - Br]^+$, 1193.19. Found: 1193.21.

Electrochemistry

Electrochemical experiments were performed with a BASi CV50W or CHI730C or CHI760C potentiostat. Cyclic voltammetry experiments were performed using a glassy carbon working electrode (0.07 cm^2), a platinum mesh auxiliary electrode and a $Ag/AgNO_3$ (0.1 M) reference electrode at room temperature. Aliquots of acid solution were added to 1 mM complexes in 0.1 M NBu_4PF_6 acetonitrile solution. The solutions were stirred before recording cyclic voltammograms in a quiescent state. The potentials for $Co^{II/I}$ redox couples were referenced to ferrocene/ferrocenium couple, which was obtained by recording the cyclic voltammogram of the complexes in the presence of a small amount of ferrocene.

Bulk electrolysis was performed using a glassy carbon rod (7 mm × 5 cm) working electrode and a platinum mesh auxiliary electrode in a gas-tight electrochemical cell. The amount of H_2 gas produced in the headspace was analyzed by a GC. The potentials for the electrolyses (−1.2 V vs Fc/Fc^+) were referenced with $Co^{II/I}$ redox couples in cyclic voltammogram obtained before adding acid solution.

The stability of **10** and **14** upon bulk electrolysis was evaluated by UV-vis spectroscopy. Bulk electrolysis (BE) was carried out for 1.5 hours with a glassy carbon working electrode (0.07 cm^2) and a platinum mesh auxiliary electrode in an H-type cell in the glovebox. One compartment contained a 5 mL of 1 mM complexes and 20 mM tosic acid in 0.1 M NBu_4PF_6 acetonitrile solution. An aliquot of the solution containing complexes was taken for UV-vis measurement before and after completion of the BE experiment. The spectra shown in Figure 1.16 and 1.22 reveal that the compounds are stable to the electrolytic conditions.

X-ray Crystallographic Details

Single crystals were immersed in a drop of Paratone N oil on a clean microscope slide, affixed to a loop and then cooled to 100 K. The crystals were mounted on a Bruker three circle goniometer platform equipped with an APEX detector. A graphic monochromator was employed for wavelength selection of the Mo K_α radiation (λ = 0.71073 Å). The data were processed and refined using the program SAINT supplied by Siemens Industrial Automation Inc. Structures were solved by a Patterson heavy atom map and refined by standard difference Fourier techniques in the SHELXTL program suite (6.10 v., Sheldrick G. M., and Siemens Industrial Automation, Inc., 2000). Hydrogen atoms were placed in calculated positions using the standard riding model and refined isotropically; all other atoms were refined anisotropically. For **7**

structure, a positional disorder of the acetyl groups was modeled. This disorder arose from a rotation about the carbonyl carbon which allowed the carbonyl oxygen and methyl group of the acetyl to sit in similar positions. The 1-2 and 1-3 distances of the disordered parts were restrained to be similar using the SAME command. Anisotropic parameter (SIMU) and rigid bond (DELU) restraints were then applied to the structure. An EADP restraint was used on the disordered carbon and oxygen atoms which approximated the anisotropy of the minor component to match that of the major component. For **10**, a positional disorder of the ligand backbone was modeled. The 1-2 and 1-3 distances of the disordered parts were restrained to be similar using the SAME command. SIMU and DELU restraints were then applied to the structure. A positional disorder of the nitrate counterion was modeled in the same way. Structure validation alerts are explained by the existence of these disordered sites. For **12**, positional disorders of the MeOH solvents of crystallization were modeled and restrained using SIMU, DELU and EADP restraints. A positional disorder of the C28 methyl group was modeled in two parts whose 1-2 and 1-3 distances were restrained to be similar using the SADI command. The heavy disorder, consisting primarily of solvents of crystallization, gave rise to the fair number of structure validation alerts, mostly level C.

Table 1.1. Crystal Data and Structure Refinement for **7**.

Identification code	07177	
Empirical formula	$C_{33}H_{37}NO_5$	
Formula weight	527.64	
Temperature	100(2) K	
Wavelength	0.71073 Å	
Crystal system	Monoclinic	
Space group	*P*2(1)/*n*	
Unit cell dimensions	$a = 15.177(3)$Å	$\alpha = 90°$
	$b = 8.8007(17)$ Å	$\beta = 97.664(3)°$
	$c = 21.417(4)$ Å	$\gamma = 90°$
Volume	2853.1(9) Å^3	
Z	4	
Density (calculated)	1.236	
Absorption coefficient	0.082	
F(000)	1128	
Crystal size	0.20 × 0.15 × 0.05 mm^3	
Θ range for data collection	1.55 to 29.13°	
Index ranges	$-20 \le h \le 20, -12 \le k \le 12, -29 \le \ell \le 29$	
Reflections collected	59756	
Independent reflections	7611 [$R_{int} = 0.0566$]	
Completeness to $\Theta = 29.13°$	100.0 %	
Absorption correction	SADABS	
Max. and min. transmission	0.996, 0.983	
Refinement method	Full–matrix least–squares on F^2	
Data / restraints / parameters	7611 / 424 / 370	
Goodness-of-fit on F^2	1.021	
Final R indices [$I > 2\sigma(I)$]	$R_1 = 0.0446$, $wR_2 = 0.1053$	
R indices (all data)	$R_1 = 0.0670$, $wR_2 = 0.1202$	
Largest diff. peak and hole	0.389 and – 0.228 e/Å^{-3}	

[a] GOF = $(\Sigma\, w(F_o^2 - F_c^2)^2/(n-p))^{1/2}$ where n is the number of data and p is the number of parameters refined. [b] $R1 = \Sigma||F_o| - |F_c||/\Sigma|F_o|$. [c] $wR2 = (\Sigma(w(F_o^2 - F_c^2)^2)/\Sigma(w(F_o^2)^2))^{1/2}$.

Table 1.2. Crystal Data and Structure Refinement for **8**.

Identification code	07160	
Empirical formula	$C_{41}H_{46}N_2O_5$	
Formula weight	646.8	
Temperature	100(2) K	
Wavelength	0.71073 Å	
Crystal system	Monoclinic	
Space group	$P2_1/c$	
Unit cell dimensions	a = 13.134(2)Å	α = 90°
	b = 15.114(3) Å	β = 104.532(3)°
	c = 18.249(3) Å	γ = 90°
Volume	3506.7(11)Å^3	
Z	4	
Density (calculated)	1.225	
Absorption coefficient	0.080	
F(000)	1384	
Crystal size	0.25 × 0.15 × 0.10 mm^3	
Θ range for data collection	1.77 to 28.28°	
Index ranges	$-17 \leq h \leq 17, -20 \leq k \leq 20, -24 \leq \ell \leq 24$	
Reflections collected	70918	
Independent reflections	8701 [R_{int} = 0.1223]	
Completeness to Θ = 28.28°	100.0 %	
Absorption correction	SADABS	
Max. and min. transmission	0.9920, 0.9803	
Refinement method	Full–matrix least–squares on F^2	
Data / restraints / parameters	8701 / 0 / 433	
Goodness-of-fit on F^2	1.012	
Final R indices [I > 2σ(I)]	R_1 = 0.0691, wR_2 = 0.1794	
R indices (all data)	R_1 = 0.1180, wR_2 = 0.2171	
Largest diff. peak and hole	0.406 and – 0.776 e/Å^{-3}	

[a] GOF = $(\Sigma\, w(F_o^2 - F_c^2)^2/(n-p))^{1/2}$ where n is the number of data and p is the number of parameters refined. [b] $R1 = \Sigma||F_o| - |F_c||/\Sigma|F_o|$. [c] $wR2 = (\Sigma(w(F_o^2 - F_c^2)^2)/\Sigma(w(F_o^2)^2))^{1/2}$.

Table 1.3. Crystal Data and Structure Refinement for **10**.

Identification code	07142	
Empirical formula	$C_{15}\ H_{22}CoN_6O_6$	
Formula weight	441.32	
Temperature	100(2) K	
Wavelength	0.71073 Å	
Crystal system	Monoclinic	
Space group	*C*2/*c*	
Unit cell dimensions	a = 17.621(2) Å	α = 90°
	b = 14.1850(17) Å	β = 101.043(2)°
	c = 7.6038(9) Å	γ = 90°
Volume	1865.4(4)Å^3	
Z	4	
Density (calculated)	1.571	
Absorption coefficient	0.967	
F(000)	916	
Crystal size	0.20 × 0.10 × 0.10 mm^3	
Θ range for data collection	1.86 to 27.87°	
Index ranges	$-23 \le h \le 23, -18 \le k \le 18, -10 \le \ell \le 10$	
Reflections collected	18036	
Independent reflections	2222 [R_{int} = 0.0254]	
Completeness to Θ = 27.87°	99.9 %	
Absorption correction	SADABS	
Max. and min. transmission	0.9095, 0.8301	
Refinement method	Full–matrix least–squares on F^2	
Data / restraints / parameters	2222 / 159 / 167	
Goodness-of-fit on F^2	1.158	
Final R indices [I > 2σ(I)]	R_1 = 0.0480, wR_2 = 0.1226	
R indices (all data)	R_1 = 0.0521, wR_2 = 0.1253	
Largest diff. peak and hole	0.589 and – 0.395 e/Å^{-3}	

[a] GOF = $(\Sigma\, w(F_o^2 - F_c^2)^2/(n-p))^{1/2}$ where n is the number of data and p is the number of parameters refined. [b] $R1 = \Sigma||F_o| - |F_c||/\Sigma|F_o|$. [c] $wR2 = (\Sigma(w(F_o^2 - F_c^2)^2)/\Sigma(w(F_o^2)^2))^{1/2}$.

Table 1.4. Crystal Data and Structure Refinement for **12.**

Identification code	08139	
Empirical formula	$C_{57.40}H_{87}Br_4N_8O_{5.40}Zn_2$	
Formula weight	1425.93	
Temperature	100(2) K	
Wavelength	0.71073 Å	
Crystal system	Triclinic	
Space group	*P-1*	
Unit cell dimensions	a = 14.4660(12) Å	α = 92.490(2)°
	b = 15.5347(13) Å	β = 93.795(2)°
	c = 15.8671(13) Å	γ = 110.9810(10)°
Volume	3313.4(5)Å^3	
Z	2	
Density (calculated)	1.429	
Absorption coefficient	3.185	
F(000)	1461	
Crystal size	0.10 × 0.10 × 0.10 mm^3	
Θ range for data collection	1.29 to 28.28°	
Index ranges	$-19 \le h \le 19$, $-20 \le k \le 20$, $-21 \le \ell \le 21$	
Reflections collected	69036	
Independent reflections	16451 [R_{int} = 0.0888]	
Completeness to Θ = 28.28°	99.9 %	
Absorption correction	SADABS	
Max. and min. transmission	0.7412, 0.7412	
Refinement method	Full–matrix least–squares on F^2	
Data / restraints / parameters	16451 / 700 / 747	
Goodness-of-fit on F^2	1.044	
Final R indices [I > 2σ(I)]	R_1 = 0.0766, wR_2 = 0.1927	
R indices (all data)	R_1 = 0.1449, wR_2 = 0.2280	
Largest diff. peak and hole	2.543 and – 1.303 e/Å^{-3}	

[a] GOF = $(\Sigma\, w(F_o^2 - F_c^2)^2/(n-p))^{1/2}$ where n is the number of data and p is the number of parameters refined. [b] $R1 = \Sigma||F_o| - |F_c||/\Sigma|F_o|$. [c] $wR2 = (\Sigma(w(F_o^2 - F_c^2)^2)/\Sigma(w(F_o^2)^2))^{1/2}$.

References

(1) Lewis, N. S.; Nocera, D. G. *Proc. Natl. Acad. Sci. U.S.A.* **2006**, *43*, 15729–15735.

(2) Hoffert, M. T.; Caldeira, K.; Jain, A. K.; Haites, E. F.; Harvey, L. D.; Potter, S. D.; Schlesinger, M. E.; Wigley, M. L.; Wuebbles, J. J. *Nature* **1998**, *395*, 881–884.

(3) Cook, T. R.; Dogutan, D. K.; Reece, S. Y.; Surendranath, Y.; Teets, T. S.; Nocera, D. G. *Chem. Rev.* **2010**, *110*, 6474–6502.

(4) Nocera, D. G. *Inorg. Chem.* **2009**, *48*, 10001–10017.

(5) Barber, J. *Chem. Soc. Rev.* **2009**, *38*, 185–196.

(6) Khaselev, O.; Turner, J. *Science* **1998**, *280*, 425–427.

(7) Kanan, M. W.; Nocera, D. G. *Science* **2008**, *321*, 1072–1075.

(8) Tard, C.; Pickett, C. J. *Chem. Rev.* **2009**, *109*, 2245–2274.

(9) Felton, G. A.; Mebi, C. A.; Petro, B. J.; Vannucci, A. K.; Evans, D. H.; Glass, R. S.; Lichtenberger, D. L. *J. Organomet. Chem.* **2009**, *694*, 2681–2699.

(10) Gloaguen, F.; Rauchfuss, T. B. *Chem. Soc. Rev.* **2009**, *38*, 100–108.

(11) Wilson, A. D.; Newell, R. H.; McNevin, M. J.; Muckerman, J. T.; Dubois, M. R.; Dubois, D. L. *J. Am. Chem. Soc.* **2006**, *128*, 358–366.

(12) Artero, V.; Fontecave, M. *Coord. Chem. Rev.* **2005**, *249*, 1518–1535.

(13) Wilson, A. D.; Shoemaker, R. K.; Miedaner, A.; Muckerman, J. T.; Dubois, D. L.; Dubois, M. R. *Proc. Natl. Acad. Sci. U.S.A.* **2007**, *104*, 6951–6956.

(14) Bigi, J. P.; Hana, T. E.; Harman, W. H.; Chang, A.; Chang, C. J. *Chem. Commun.* **2010**, 958–960.

(15) Hu, X. L.; Cossairt, B. M.; Brunschwig, B. S.; Lewis, N. S.; Peters, J. C. *Chem. Commun.* **2005**, 4723–4725.

(16) Hu, X. L.; Brunschwig, B. S.; Peters, J. C. *J. Am. Chem. Soc.* **2007**, *129*, 8988–8998.

(17) Baffert, C.; Artero, V.; Fontecave, M. *Inorg. Chem.* **2007**, *46*, 1817–1824.

(18) Razavet, M.; Artero, V.; Fontecave, M. *Inorg. Chem.* **2005**, *44*, 4786–4795.

(19) Jacques, P. –A.; Artero, V.; Pécaut, J.; Fontecave, M. *Proc. Natl. Acad. Sci. U.S.A.* **2009**, *106*, 20627–20632.

(20) Kellet, R. M.; Spiro, T. G. *Inorg. Chem.* **1985**, *24*, 2378–2382.

(21) Kellet, R. M.; Spiro, T. G. *Inorg. Chem.* **1985**, *24*, 2373–2377.

(22) Bhugun, I.; Lexa, D.; Saveant, J. –M. *J. Am. Chem. Soc.* **1996**, *118*, 3982–3983.

(23) Grass, V.; Lexa, D.; Saveant, J. –M. *J. Am. Chem. Soc.* **1997**, *119*, 7526–7532.

(24) Henry, R. M.; Shoemaker, R. K.; DuBois, D. L.; DuBois, M. R. *J. Am. Chem. Soc.* **2006**, *128*, 3002–3010.

(25) Curtis, C. J.; Miedaner, A.; Ciancanelli, R. F.; Ellis, W. W.; Noll, B. C.; DuBois, D. L.; DuBois, M. R. *Inorg. Chem.* **2003**, *42*, 216–227.

(26) Barton, B. E.; Olsen, M. T.; Rauchfuss, T. B. *J. Am. Chem. Soc.* **2008**, *130*, 16834–16835.

(27) Barton, B. E.; Rauchfuss, T. B. *J. Am. Chem. Soc.* **2010**, *132*, 14877–14885.

(28) Nicolet, Y.; de Lacey, A. L.; Vèrnede, X.; Fernandez, V. M.; Hatchikian, E. C.; Fontecilla–Camps, J. C. *J. Am. Chem. Soc.* **2001**, *123*, 1596–1601.

(29) McCormic, T. M.; Calitree, B. D.; Orchad, A.; Kraut, N. D.; Bright F. V.; Detty, M. R.; Eisenberg, R. *J. Am. Chem. Soc.* **2010**, *132*, 15480–15483.

(30) Dempsey, J. L.; Winkler, J. R.; Gray, H. B. *J. Am. Chem. Soc.* **2010**, *132*, 16774–16776.

(31) Rosenthal, J.; Nocera, D. G. *Prog. Inorg. Chem.* **2007**, *55*, 483–544.

(32) Rosenthal, J.; Nocera, D. G. *Acc. Chem. Res.* **2007**, *40*, 543–553.

(33) Liu, S.-Y.; Nocera, D. G. *J. Am. Chem. Soc.* **2005**, *127*, 5278–5279

(34) Yang, J. Y.; Nocera, D. G. *J. Am. Chem. Soc.* **2007**, *129*, 8192–8198

(35) Dogutan, D. K.; Stoian, S. A.; McGuire Jr., R.; Schwalbe, M.; Teets, T. S.; Nocera, D. G. *J. Am. Chem. Soc.* **2011**, *133*, 131–140

(36) Dogutan, D. K.; Bediako, D. K.; Teets, T. S.; Schwalbe, M.; Nocera, D. G. *Org. Lett.* **2010**, *12*, 1036–1039.

(37) McGuire Jr., R.; Dogutan, D. K.; Teets, T. S.; Suntivich, J.; Shao-Horn, Y.; Nocera, D. G. *Chem. Sci.* **2010**, *1*, 411–414.

(38) Lindsey, J. S.; Wagner, R. W. *J. Org. Chem.* **1989**, *54*, 828–836.

(39) Chang, C. J.; Yeh, C.–Y.; Nocera, D. G. *J. Org. Chem.* **2002**, *67*, 1403–1406.

(40) Laha, J. K.; Dhanalekshmi, S.; Taniguchi, M.; Ambroise, A.; Lindsey, J. S. *Org. Proc. Res. Dev.* **2003**, *7*, 799–812.

(41) Fourmond, V.; Jacques, P.-A. J.; Fontecave, M.; Artero, V. *Inorg. Chem.* **2010**, *49*, 10338–10347.

(42) Collman, J. P.; Ha, Y.; Wagenknecht, P. S.; Lopez, M. A.; Guilard, R. *J. Am. Chem. Soc.* **1993**, *115*, 9080–9088.

(43) Deng, Y.; Chang, C. J.; Nocera, D. G., *J. Am. Chem.Soc.* **2000**, *122*, 410–411.

(44) Karn, J. L.; Busch, D. H., *Nature* **1966**, *211*, 160–162.

(45) Tinnemans, A. H. A.; Koster, T. P. M.; Thewissen D. H. M. W.; Mackor, A. *Recl. Trav. Chim. Pays-Bas* **1984**, *103*, 288–295.

(46) Ishiyama, T.; Takagi, J.; Hartwig, J. F.; Miyaura, N. *Angew. Chem., Int. Ed.* **2002**, *4*, 3056–3058.

(47) Ishiyama, T.; Nobuta, Y.; Hartwig, J. F.; Miyaura, N. *Chem. Commun.* **2003**, 2924–2925.

(48) Long, K. M.; Busch, D. H. *Inorg. Chem.* **1970**, *3*, 505–512.

(49) Nicholson, R. S.; Shain, I. *Anal. Chem.* **1964**, *36*, 706–723.

(50) Polcyn, D. S.; Shain, I. *Anal.Chem.* **1966**, *38*, 376–382.

(51) Andrieux, C. P.; Blocman, C.; DumasBouchait, J. M.; Mhalla, F.; Saveant, J. M. *J. Electroanal. Chem.* **1980**, *113*, 19–40.

(52) Saveant, J. M.; Su, K. B. *J. Electroanal. Chem.* **1984**, *171*, 341–349.

(53) Zaidi, S. H. H.; Fico, R. M., Jr.; Lindsey, J. S. *Org. Proc. Res. Dev.* **2006**, *10*, 118–134.

(54) Wei, L. Y.; Padmaja, K.; Youngblood, W. J.; Lindsey, J. S.; Bocian, D. F. *J. Org. Chem.* **2004**, *69*, 1461–1469.

(55) Chang, C. J.; Chng, L. L.; Nocera, D. G. *J. Am. Chem. Soc.* **2003**, *125*, 1866–1876.

Chapter 2. HX Splitting Chemistry of Ni NHC Complexes

Portions of this work have been published:

(1) Lee, C. H.; Cook, R. T.; Nocera, D. G. *Inorg. Chem.* **2011**, *50*, 714–716. Reproduced with permission. Copyright 2011 American Chemical Society

2.1 Introduction

As discussed in previous chapter, drastic changes in energy supply from fossil fuels to carbon neutral energy sources are needed to meet the future energy demand while minimizing CO_2 emission from combustion of fossil fuels such as oil, natural gas and coal. The sun furnishes enough energy to adequately meet the enormous and ever increasing global energy appetite of future populations. Practical and large scale employment of solar energy, however, requires an effective means for its storage. The storage of solar energy in chemical bonds (e.g. H_2) is more attractive compared to other storage methods such as compressed air, flywheels, pumped water, super capacitors and batteries considering higher energy density in chemical bonds.[1]

As mentioned in the previous chapter, H_2 production from water splitting using electricity generated by sunlight through photovoltaics is one of the promising methods of storing solar energy in chemical bonds. This method is composed of two separate steps; generation of electricity from sunlight and then, water splitting with that electricity. Thus, the technology producing a fuel directly through chemical reactions driven by sunlight would be useful. Accordingly, significant research investment seeks to find efficient methods to photogenerate H_2 from appropriate substrates.[2–8] Whereas water-splitting to H_2/O_2 has received much attention as a potential means to store solar energy in chemical bonds, HX (X = Cl, Br) is also an attractive substrate for H_2 production. It can be reduced by metal ions through photoreduction, even if they are not electron rich enough for thermal reduction.[2,9–13] HX-splitting (X = Cl, Br) to hydrogen and halogen stores a comparable amount of energy to water-splitting (eq. 2.1.1–3) and it has an

$$H_2O \longrightarrow H_2 + 1/_2O_2 \qquad \triangle G = 239 \text{ kJ/mol} \quad (2.1.1)$$

$$2HCl \longrightarrow H_2 + Cl_2(g) \qquad \triangle G = 262 \text{ kJ/mol} \quad (2.1.2)$$

$$2HBr \longrightarrow H_2 + Br_2(l) \qquad \triangle G = 206 \text{ kJ/mol} \quad (2.1.3)$$

encompassing two electron transformation as compared to the more mechanistically challenging four electron process of water-splitting.[2,14,15] A possible catalytic cycle for HX splitting is depicted in Scheme 2.1. First, HX is oxidatively added to a metal center generating a metal hydrido halide complex. Then, the intermediate may react with another HX producing hydrogen

Scheme 2.1

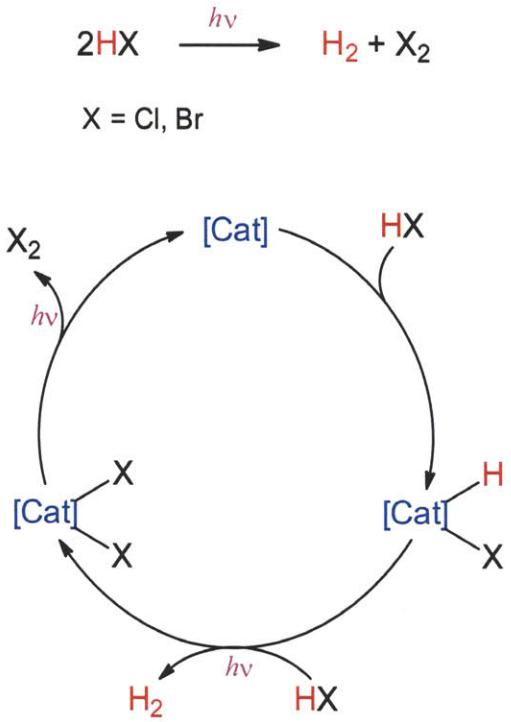

and a metal dihalide complex. To close the catalytic cycle, M–X bonds need to be activated, regenerating the reduced metal species and ideally forming X_2.[2,16] The hydrogen generation step may occur spontaneously in a given system. However, activation of strong M–X bonds requires an external driving force (e.g. photon) due to the thermodynamically uphill nature of the chemical process forming relatively weak halogen bonds. Moreover, even if X_2 is eliminated successfully from the metal center, the back reaction of oxidizing the metal center is thermodynamically favored.[15] Thus, usually the presence of halogen trap is required to drive the reaction. There have been reports of photocatalytic H_2 generation from HX metal complex adducts[17–19] as well as the efficient photoactivation of M—X bonds.[20–25] However, authentic energy storage is still rare.[22,23]

Our group reported photocatalytic H_2 production from HX splitting reaction mediated by dirhodium complex supported by bridging dfpma (dfpma = bis(difluorophosphino)methylamine) ligands (Figure 2.1. **A**).[17] The X_2 elimination step regenerating the reduced species only occurs in the presence of halogen traps and the quantum yield (0.6 %) was low with this system.

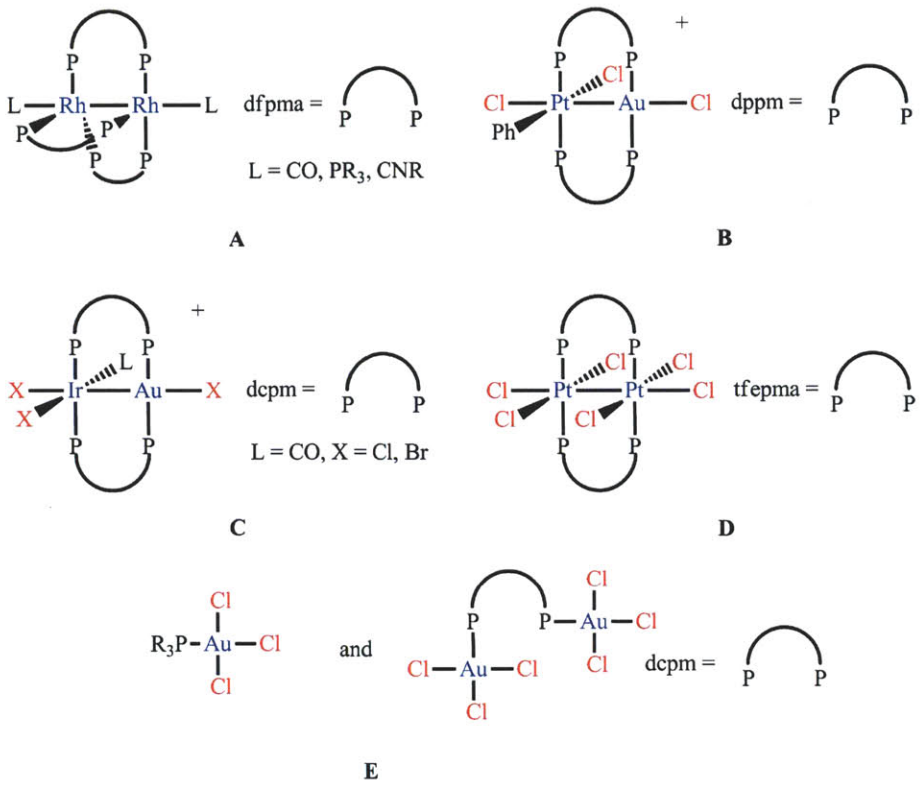

Figure 2.1. Examples of complexes for photoelimination of halogen.

Recently, halogen elimination of higher quantum efficiency (5.7 %) was achieved with a bimetallic core of platinum (III) and gold (II) supported by dppm (dppm = bis(diphenylphosphino)methane) (**B**) in the presence of 2,3-dimethly-1,3-butadiene as the halogen trap,[21] and a core of iridium (II) and gold (II) with bridging bisphosphines (e.g. dcpm = bis(dicyclohexylphosphino)methane) (**C**) exhibited a 10 % of quantum efficiency for halogen elimination in the presence of trap.[24] An even higher quantum yield of 38 % was observed on a diplatium (III) core with bridging tfepma (tfepma = $((CF_3CH_2O)_2P)_2NCH_3$) ligands (**D**) and the halogens even were eliminated in the absence of trap in solid state.[22] Mono- and bimetallic gold (III) complexes (**E**) coordinated by phosphines or bisphosphines also showed trap-free halogen photoelimination in solid state.[23]

2.2 HX Addition and Photochemical H_2 Elimination by Ni NHC Complexes

As discussed above, most stoichiometric and catalytic H_2/X_2 photoconversions are mediated by expensive transition elements on 2nd and 3rd row (Au, Ir, Rh and Pt). Thus, it is imperative to begin developing rational H_2 and X_2 photochemistry that is promoted by complexes of cheap first row metals.[5] We have explored HX splitting reactivity with Ni complexes and the photochemistry of the resulting Ni hydride complexes, and now report the photogeneration of H_2 from Ni(II) hydride complexes bearing *N*-heterocyclic carbene (NHC) ligands. The addition of HX to a Ni(0) complex furnishes $Ni(H)(X)(IMes)_2$ (IMes = 1,3-dimesitylimidazol-2-ylidene), which readily yields hydrogen upon photolysis. The treatment of $Ni(H)(Cl)(IMes)_2$ with HCl•dioxane gives rise to H_2 and $NiCl_2(IMes)_2$ (Scheme 2.2).

Scheme 2.2

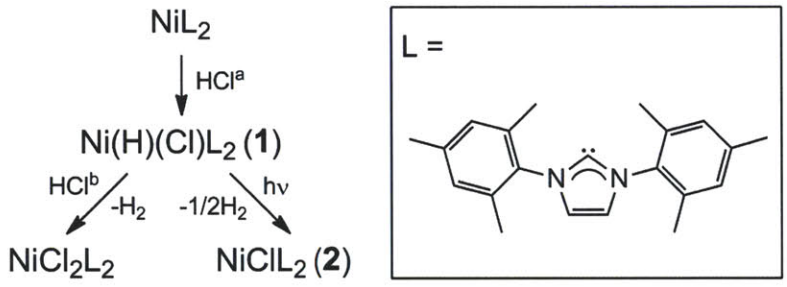

[a]2,6-lutidine•HCl, [b]HCl in 1,4-dioxane

Synthesis and Photochemistry

A facile oxidative addition chemistry of substrates such as organic halides and imidazolium salts to Ni(0) of $Ni(NHC)_2$[26–29] inspired us to explore the HX addition chemistry of $Ni(IMes)_2$. Treatment of $Ni(IMes)_2$ with 2 equiv of 4.0 M HCl dioxane solution gives rise to $NiCl_2(IMes)_2$ as a major product with the concomitant formation of H_2 along with $Ni(H)(Cl)(IMes)_2$ (**1**) and $NiCl(IMes)_2$ (**2**) as minor products. Hydride complex **1** may be obtained as the major product when $Ni(IMes)_2$ is treated only with 1 equiv of HCl. Nevertheless, we were unable to isolate **1** in pure form from this reaction mixture due to the co-crystallization of $NiCl_2(IMes)_2$ and **2**. **2** was independently obtained from the treatment of $Ni(IMes)_2$ with 4-

chlorobenzophenone in analogy to the synthesis of $NiCl(IPr)_2$ using $Ni(IPr)_2$ and aryl chlorides (IPr = 1,3-bis(2,6-diisopropylphenyl)imidazol-2-ylidene).[30] X-ray crystallography confirmed that **2** has a T-shaped geometry about the metal center (Figure 2.2, bottom).

The treatment of $Ni(IMes)_2$ with 2 eq. of 2,6-lutidine•HCl generates **1** in the absence of **2**,

$$Ni(IMes)_2 + 2Lut{\bullet}HX \rightarrow Ni(H)(X)(IMes)_2 \qquad (2.2)$$

(X = Cl, Br)

Analytically pure **1** in a crystalline form in *ca.* 70% yield is obtained upon subsequent

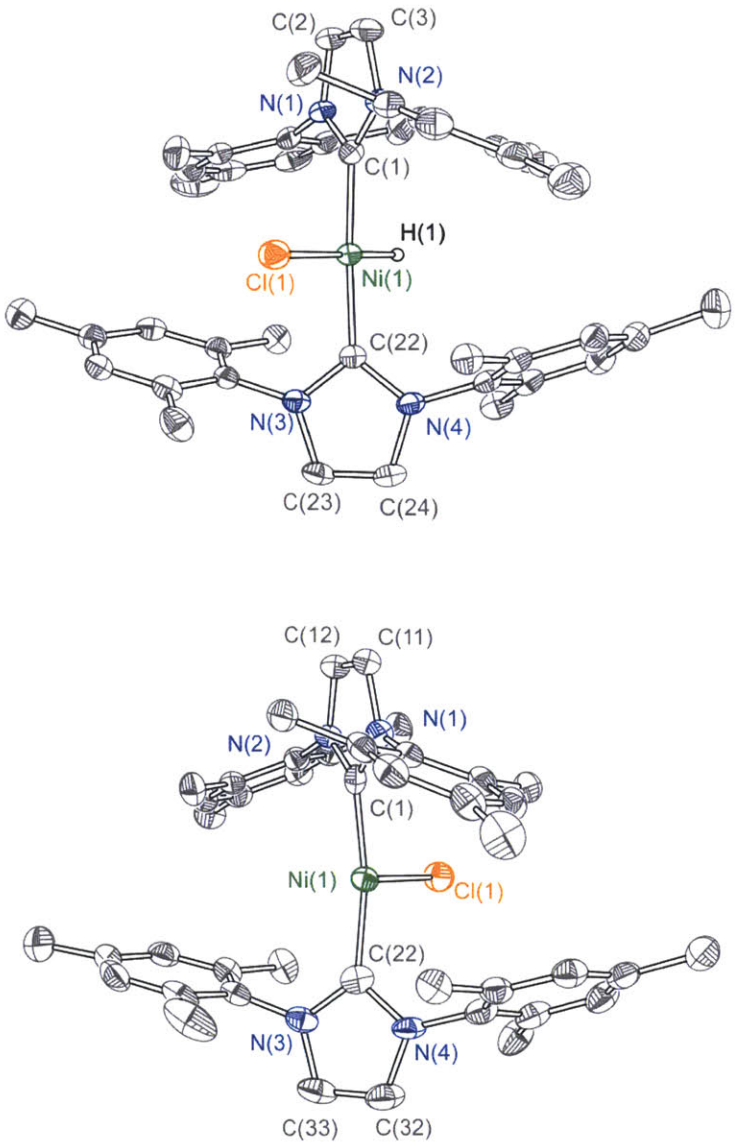

Figure 2.2. Thermal ellipsoid plots of **1** (top) and **2** (bottom) at the 50% probability level. Hydrogen atoms have been omitted for clarity.

recrystallization. If the stoichiometry of the 2,6-lutidine•HCl is reduced to 1 eq, in eq (2.2), **1** is obtained in a good yield but it is accompanied by the formation of $NiCl_2(IMes)_2$ and **2** as minor side products as determined by NMR. Also, if the reaction time is reduced to ~30 min with 2 eq. of 2,6-lutidine•HCl, formation of **2** and $NiCl_2(IMes)_2$ as minor side products was observed. The analogous bromide complex, Ni(H)(Br)$(IMes)_2$ (**3**), also is furnished by the reaction chemistry of eq. (2.2) along with paramagnetic and diamagnetic species that are consistent with $NiBr(IMes)_2$ and $NiBr_2(IMes)_2$, respectively. In contrast to **1**, a small amount of $NiBr_2(IMes)_2$, which could not be removed by recrystallization based on NMR analysis and X-ray structure, is obtained when $Ni(IMes)_2$ is treated with 2 eq. of 2,6-lutidine•HBr. However, no $NiBr(IMes)_2$ is formed.

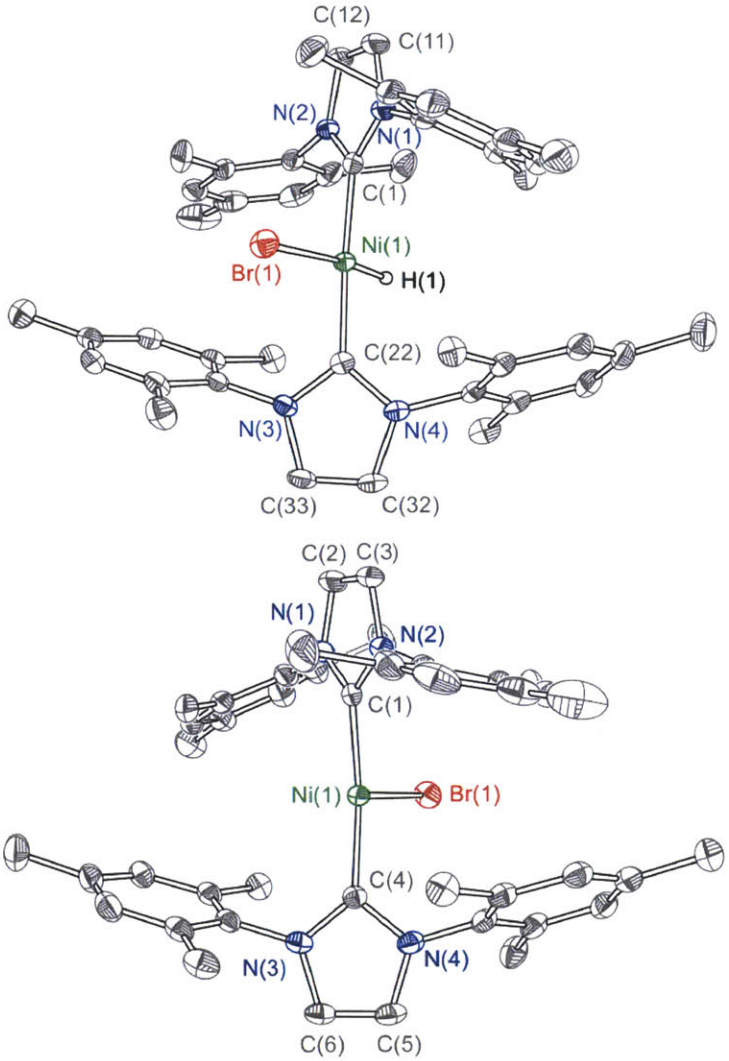

Figure 2.3. Thermal ellipsoid plots of **3** (top) and **4** (bottom) at the 50% probability level. Hydrogen atoms have been omitted for clarity. A bromide from disorder in the crystal is also omitted for clarity.

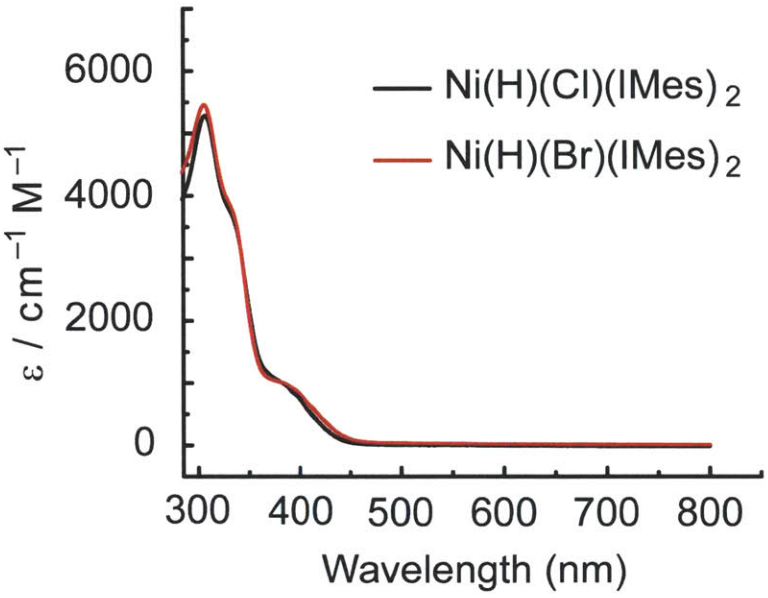

Figure 2.4. Comparison of UV-vis spectra of **1** (—) and **3** (—) in toluene.

The crystal structures of **1** and **3**, which are shown in Figures 2.2 (top) and 2.3 (top), respectively, reveal a square planar geometry about the Ni(II) center. The hydride was located crystallographically. The hydride signal appears in the ^{1}H NMR spectrum at –21.9 ppm for **1** and at –20.4 ppm for **3**. The UV-vis absorption spectrum of **1** in toluene is dominated by three features at λ_{max}/nm (ε / $10^3 M^{-1}cm^{-1}$) = 307 (5.3), 335 (sh, 3.6) and 390 nm (br sh, 0.9). The UV-vis absorption spectrum of **3** is similar to that of **1** (Figure 2.4) suggesting that the electronic transitions do not possess significant halide character.

Photolysis of **1** and **3** with λ_{exc} > 295 nm gives rise to H_2 and NiX(IMes)$_2$,

$$Ni(H)(X)(IMes)_2 \xrightarrow{\lambda > 295\ nm} Ni(X)(IMes)_2 + \tfrac{1}{2}H_2 \quad (2.3)$$

(X = Cl, Br)

at yields of *ca.* 50% and 70% (X = Cl and Br, respectively) as determined against an internal standard in the ^{1}H NMR spectrum. Intractable side products are formed in small quantities. The single crystal of NiBr(IMes)$_2$ (**4**) for X-ray crystallography was obtained from the reaction mixture (Figure 2.3, bottom). Notably, the yield of H_2 determined by GC was lower (*ca.* 33% for

X = Cl and 22% for X = Br) than that of $NiX(IMes)_2$, suggesting H_2-consuming side reactions. The presence of side products hindered kinetic studies to determine quantitatively the rate dependence with respect to Ni concentration as well as quantum yields, which could give the insight into the mechanism of H_2 production. In the case of the latter, the presence of side products caused sufficient perturbation of the absorption spectrum that quantitative assessment of the quantum yields could not be achieved. The side reactions may be decomposition associated with breakage of Ni ligand bonds other than Ni—H. No further reduction of $NiX(IMes)_2$ was observed under prolonged irradiation. We note that $NiCl_2(IMes)_2$ also does not undergo reduction upon irradiation. Addition of 1 equiv of an HCl dioxane solution to **1** generates H_2 and $NiCl_2(IMes)_2$ almost quantitatively.

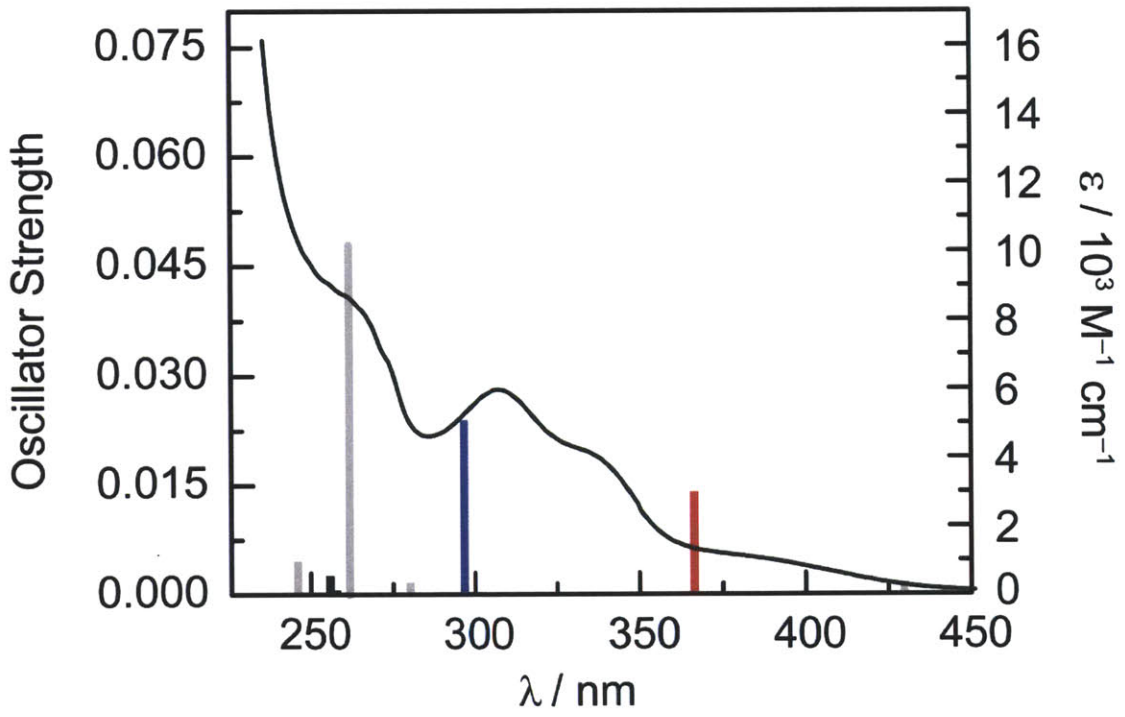

Figure 2.5. Comparison of UV-vis spectrum of **1** (—) in THF and calculated transitions (bars). The red and blue bars correspond to transitions that are color coded in Figure 2.6.

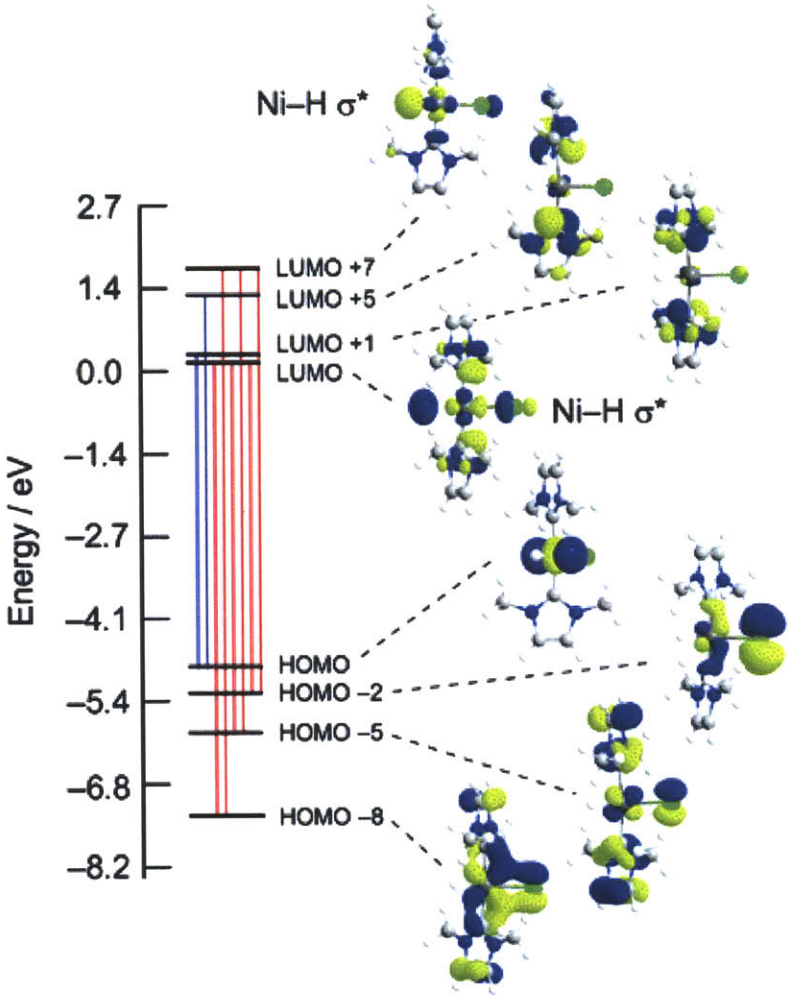

Figure 2.6. Energy diagram of the orbitals of the model complex involved in the most intense electronic transitions above 290 nm. Transitions indicated by blue and red lines correspond to the excitations calculated at 297 nm (blue) and 366 nm (red). The red bars of the MO picture correspond to the red transition of Figure 2.5 and likewise for blue.

A time dependent density functional theory calculation of the electronic structure of **1** was performed with the aim of gaining insight into the excited state parentage from which the photoreactivity of Ni(H)(X)(IMes)$_2$ complexes was derived. Computations were performed on a model complex of **1** in which the mesityl groups on the nitrogens of the imidazole rings were replaced by methyl groups (**1-CH$_3$**). The calculated transitions match well the energy and intensities of the observed transitions in the UV-vis spectra of **1** and **3** (Figure 2.5). Consistent with the observed photochemistry depicted in eq (2.3), the lowest energy transitions, which are

calculated to have a high oscillator strength, are involved with excited states that arise from the population of orbitals possessing appreciable Ni—H σ* character (Figure 2.6). LUMO + 7 and LUMO (lowest unoccupied molecular orbital) have hydride character of 4.2 and 4.5 %, respectively. Moreover, little halide character is observed in the lowest energy excited states; the highest contribution of halide character is 10.7 % for LUMO. This result is consistent with the similarity of the absorption spectra of **1** and **3**, and the lack of M—X bond activation photochemistry in these complexes. In addition, the excited states have a small but nonnegligible contribution of σ*(Ni–C) (LUMO + 7 and LUMO) and σ*(Ni–Cl) (LUMO) character. Contributions such as these may explain the formation of side products via excited-state decompositions owing to Ni-ligand bond disruption.

In summary, photolysis of the Ni(II) hydride complexes $Ni(H)(X)(IMes)_2$ gives rise to H_2 with the concomitant formation of reduced Ni(I) photoproduct $Ni(X)(IMes)_2$. Acid protonolysis of $Ni(H)(Cl)(IMes)_2$ also produces H_2 with the formation of $NiCl_2(IMes)_2$. Calculations reveal that the lowest energy electronic excitations of **1** and **3** involves the population of Ni–H σ* orbitals, which is consistent with disruption of Ni–H bond and the observation of H_2 photogeneration.

2.3 Photoactivation of Metal–Halogen bonds in a Ni(II) NHC Complex

As discussed above, we have explored HX-splitting reactivity with $Ni(IMes)_2$ (IMes = 1,3-dimesitylimidazol-2-ylidene) and the photoelimination of H_2 from the resulting Ni hydride complexes, $Ni^{II}(H)(X)(IMes)_2$. However, catalytic turnover is circumvented by the inability to photoactivate the Ni(I)–X bond of the photoproduct. The structurally related complex, $Ni^{II}Cl_2(IMes)_2$ did not exhibit M—X bond activation reactivity, either. These observations prompted us to begin exploring the Ni–X photochemistry of NHC complexes.

Halogen elimination from binuclear complexes of late transition metals is promoted from intermediates in which the eliminating halide ligands occupy bridging and terminal coordination sites.[31,32] We expected that such a similar structural motif for Ni NHC halide complexes might also facilitate halogen elimination. For this reason, we were intrigued by a potential photochemistry of the Ni(II) complex, $[Ni^{II}(\mu\text{-}Cl)Cl(IPr)]_2$ (Ipr = 1,3-bis(2,6-diisopropylphenyl)imidazol-2-ylidene) (**5**), which was previously prepared by Hillhouse and co-workers.[33]

Synthesis and Photochemistry

Crystals of **5** grown from dichloromethane/pentane solutions at −35 °C yield an X-ray diffraction structure, which shows a square planar geometry about the metal; the bond angles around nickel centre are 95−85° and 176°. Observed paramagnetism of solutions of the complex led Hillhouse and co-workers to propose the possibility of a tetrahedral distortion for the complex in solution.[34] Our studies described here support this contention. The X-ray crystal structure shown in Figure 2.7 was obtained for crystals of **5** grown from toluene/hexanes solution at −40 °C. The coordination environment about the Ni(II) centre is tetrahedral; the bond angles around nickel centre are 108, 110, 108, 115, 92 and 123°. If crystals of **5** obtained from toluene/hexanes solution are recrystallized from dichloromethane/pentane solution at −20 °C, then Ni(II) in a square planar environment is observed predominantly (Figure 2.8); a slight disorder in the crystal structure is accounted for the presence of tetrahedral Ni(II) (13%). These observations suggest that the barrier for interconversion between two geometries is small and crystal packing is sufficient to induce a tetrahedral or square planar geometry about the metal centre. Assuming the dimeric structure in toluene solution, the population of tetrahedral geometry in solution estimated from magnetic susceptibilities of solution and solid was *ca.* 90%.

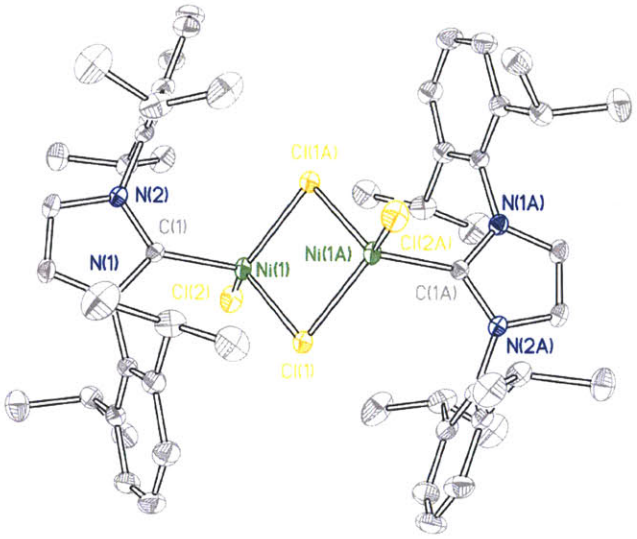

Figure 2.7. X-ray crystal structure of **5** from a single crystal grown in toluene/hexanes. Thermal ellipsoids are shown in 50 % probability. Hydrogen atoms are omitted for clarity. Selected bond angles (deg) : C(1)–Ni(1)–Cl(2) 107.87(3), C(1)–Ni(1)–Cl(1) 109.90(3), C(1)–Ni(1)–Cl(1A) 107.83(3), Cl(1)–Ni(1)–Cl(2) 115.067(13), C1(1)–Ni(1)–Cl(1A) 92.336(11), C1(2)–Ni(1)–Cl(1A) 122.767(13).

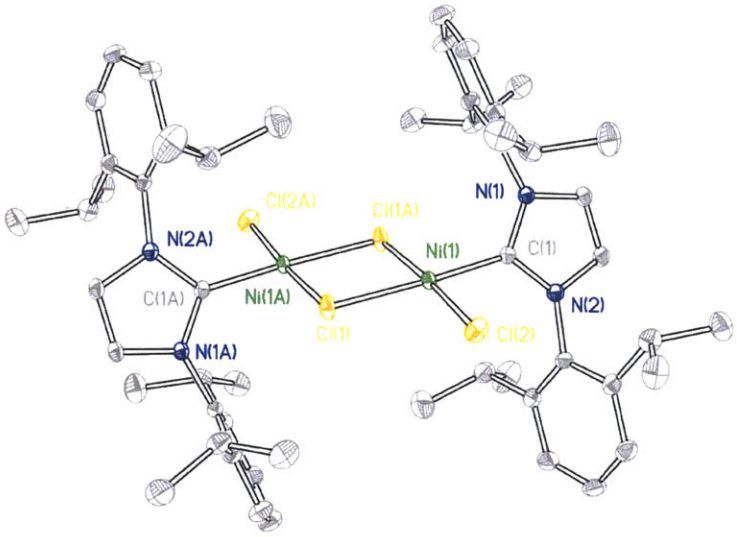

Figure 2.8. X-ray crystal structure of **5** from a single crystal grown in dichloromethane/pentane. Thermal ellipsoids are shown in 50 % probability. Hydrogen atoms, solvent and chloride atoms from a disorder due to tetrahedral distortion are omitted for clarity. Selected bond angles (deg) : C(1)–Ni(1)–Cl(2) 93.28(6), C(1)–Ni(1)–Cl(1) 175.54(6), C(1)–Ni(1)–Cl(1A) 89.94(6), Cl(1)–Ni(1)–Cl(2) 91.17(2), C1(1)–Ni(1)–Cl(1A) 85.62(2), C1(2)–Ni(1)–Cl(1A) 175.93(2).

The photolysis of **5** in benzene or toluene with > 295 nm light gave $[Ni^{I}(\mu\text{-Cl})(IPr)]_2$[35] in *ca.* 27% yield as determined against an internal standard by NMR spectroscopy (Figure 2.11). Further reduction of $[Ni^{I}(\mu\text{-Cl})(IPr)]_2$ to $[Ni^{0}(IPr)]_2$ was not observed. The overall photochemical process is shown in Scheme 2.3. The accurate determination of quantum yields for the photolysis reaction was hindered by formation of insoluble precipitation along with intractable side products. Conventional halogen traps such as 2,3-dimethly-1,3-butadiene could not be used because they reacted directly with the photolysis product yielding compound decomposing under photolysis condition.

To better understand the nature of observed photochemistry of **5**, we examined the electronic structure of the complex by density functional theory (DFT) and time-dependent DFT (TD-DFT) calculations on related model complexes. The diisopropylphenyl substituents on nitrogen atoms of the carbene ligand were replaced with methyl groups for the purposes of these calculations. Initial structural inputs from the crystal structures of both the tetrahedral and square planar geometries were used for the calculations. However, the minimum energy gas-phase structure (**5-S**) was computed to be square planar, regardless of an initial square planar or tetrahedral input. This indicates that solvent and steric bulkiness of ligands play a role in stabilization of tetrahedral geometry,[34,36] and the possibility of monomerization of a dimer in

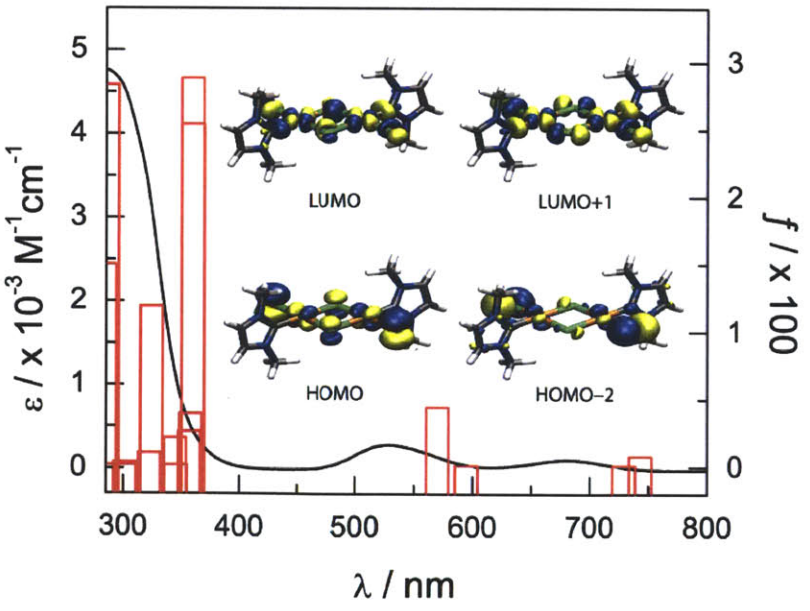

Figure 2.9. UV-vis spectrum of **5** (—) in toluene, calculated transitions (red bars) of **5-S**, and selected molecular orbitals involved in calculated transitions.

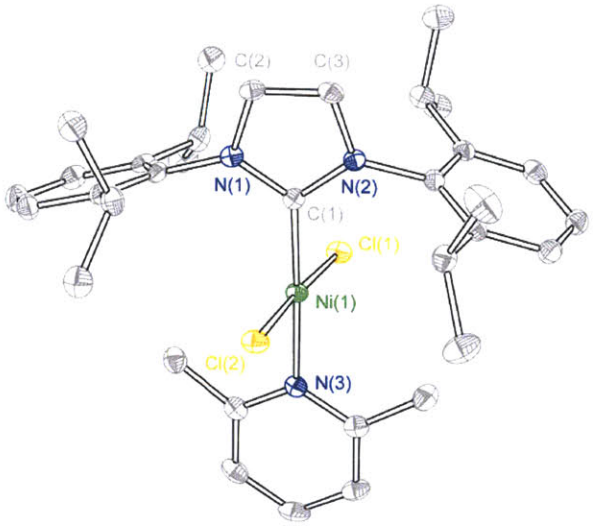

Figure 2.10. X-ray crystal structure of **6**. Thermal ellipsoids are shown at 50 % probability level. Hydrogen atoms are omitted for clarity.

solution also cannot be ruled out. The calculated transition energies for **5-S** matched rather well with the observed electronic absorption spectra of **5** (Figure 2.9), suggesting that the major paramagnetic species in solution may possess similar absorption patterns to **5-S**. The calculated absorption features are composed of a combination of transitions involving promotion of an electron from occupied molecular orbitals (MOs) of significant chloride character into the lowest unoccupied molecular orbitals (LUMO and LUMO+1) that possess appreciable σ*(Ni–Cl) character. Population of such orbitals is expected to weaken the nickel–halide bond. These results are consistent with the observed photochemistry of **5**.

We next explored whether an HX reaction chemistry could provide entry into the Ni(II) halide complexes (Scheme 2.3). The treatment of $[Ni^0(IPr)]_2$ with HCl•dioxane solution gave rise to $[Ni^I(\mu\text{-Cl})(IPr)]_2$ in *ca.* 60 % as determined by NMR spectroscopy and a corresponding amount of H_2 (*ca.* ~58 %) as determined by GC measurement. The further treatment of $[Ni^I(\mu\text{-Cl})(IPr)]_2$ with HCl•dioxane solution did not yield a tractable reaction chemistry. When 2,6-lutidine•HCl was used as a HCl source, the reaction gave rise to $Ni^{II}Cl_2(IPr)$(2,6-lutidine) (**6**) in *ca.* 37 %, as determined by NMR spectroscopy; H_2 was not observed as a product of this reaction. Complex **6** was independently prepared by treating **5** with 2,6-lutidine (77 %) and the compound was structurally characterized (Figure 2.10). The crystal structure shows square planar geometry in which 2,6-lutidine is located in trans position to the IPr ligand. An HX chemistry to yield H_2

thus appears limited to low valent Ni(0) as depicted in Scheme 2.3 whereas an X_2 photoelimination chemistry is confined to Ni(II). In summary, our results show that the chemistry of Ni(I) NHC is critical to elaborating catalytic HX splitting. Species to develop the further refinement of the system is needed for H_2 chemistry from Ni(I) or photocycle for HX splitting. However, $[Ni^I(\mu\text{-Cl})(IPr)]_2$ lacks Ni—Cl photoactivation reactivity and is stable under photolysis condition.

Scheme 2.3

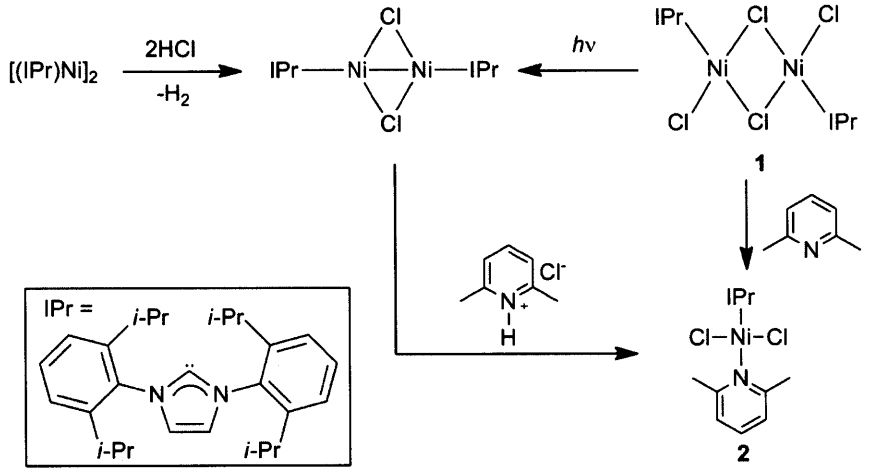

In conclustion, the photolysis of **5** resulted in activation of Ni–Cl bonds yielding reduced species $[Ni^I(\mu\text{-Cl})(IPr)]_2$ and the calculations for the complex with square planar geometry of the possible two geometries indicates that the photoreactivity originates from population of electrons into σ^* (Ni–Cl) orbitals.

2.4. Experimental Section

2.4.1 HX Addition and Photochemical H_2 Elimination by Ni NHC Complexes

All synthetic manipulations were performed using standard Schlenk techniques under a nitrogen atmosphere, or in a glovebox under an atmosphere of nitrogen. Reactions were carried out in oven-dried glassware cooled under vacuum. Elemental analysis was performed by Midwest Microlab, LLC, Indianapolis, IN. Toluene, THF and hexanes were purified by passing them under argon pressure through packed columns of neutral alumina. Anhydrous benzene was purchased from Aldrich and stored in a glovebox over molecular sieves. NMR solvents were obtained from Cambridge Isotope Laboratories. C_6D_6 was degassed, and stored in a glovebox over molecular sieves.

^1H NMR spectra were recorded on Varian 300 MHz and 500 MHz instruments, with shifts reported relative to the residual solvent peak. UV-vis spectra were recorded on a Varian Cary 5000 spectrophotometer and spectra were referenced against the appropriate solvent. GC measurements were performed with an Agilent 7890A GC.

$(IMes)_2Ni$ [37] and 2,6-lutidine•HBr [38] were synthesized as described by published procedures. 2,6-lutidine•HCl was prepared by treatment of 2,6-lutidine with 1.0 M HCl diethyl ether solution under anhydrous conditions. 4.0 M HCl 1,4-dioxane solution (Aldrich), 2,6-lutidine (Aldrich), 1.0 M HCl diethyl ether solution (Aldrich), 1,4-dimethoxybenzene (Aldrich) and 4-chlorobenzophenone (Aldrich) were used as received.

Syntheses

Preparation of $Ni(H)(Cl)(IMes)_2$ (1)

In a glovebox, $Ni(IMes)_2$ (0.0500 g, 0.0749 mmol) and 2,6-lutidine•HCl (0.022 g, 0.150 mmol) were added to a vial equipped with a Teflon-coated magnetic stirbar. THF (5 mL) was added and the mixture was stirred for 50 min. The mixture was filtered through glass fiber and dried *in vacuo*. The resulting solid was dispersed in toluene and the mixture was filtered through glass fiber. Hexanes were added to the resulting solution, which were cooled in a vial to –40 °C for 1 day. If substantial amount of crystals were not seen, the mixture was dried and the recrystallization process described above, including filtering the toluene solution, was repeated.

The supernatant was decanted to remove small particles and the resulting yellow crystals were washed with hexanes. This process was repeated several times. The resulting crystals were dried *in vacuo* to give 0.037 g (70 %) of **1**. ^{1}H NMR (C_6D_6, 300 MHz): δ 6.84 (s, 8 H, *meta*-CH), 6.03 (s, 4 H, NCH), 2.37 (s, 12 H, *para*-CC$\underline{H}_3$), 2.07 (s, 24 H, *ortho*-CC$\underline{H}_3$), –21.9 (s, 1 H, NiH). λ_{max} /nm (ε / $10^3 M^{-1} cm^{-1}$) in toluene: 307 (5.3), 335 (sh, 3.6), 390 (br sh, 0.9). λ_{max} /nm (ε / $10^3 M^{-1} cm^{-1}$) in THF: 307 (6.0), 335 (sh, 4.1), 390 (br sh, 1.0). Anal. Calcd. $C_{42}H_{49}N_4ClNi \cdot 0.5C_6H_{14}$: C, 72.34; H, 7.55; N, 7.50. Found: C, 72.68; H, 7.46; N, 7.45. The 0.5 equiv of C_6H_{14} contained in samples for elemental analysis was verified by ^{1}H NMR.

Preparation of NiCl(IMes)$_2$ (2)

In a glovebox, Ni(IMes)$_2$ (0.100 g, 0.150 mmol) and 4-chlorobenzophenone (0.036 g, 0.165 mmol) were added to a vial equipped with a Teflon-coated magnetic stirbar. Toluene was added and the mixture was stirred for 5 h. The mixture was filtered through glass fiber and hexanes were layered on the solution. The resulting solution was cooled at –40 °C for 1 day. The mixture was filtered through glass fiber to remove dark powder and the resulting solution was cooled at –40 °C for an additional 3 days. The supernatant was decanted and the resulting lumps were washed with hexanes. This process was repeated several times. After drying *in vacuo*, the resulting dried lumps were dispersed in toluene and hexanes were added. The resulting solution in a vial was cooled at –40 °C for 3 days. The supernatant was decanted to remove small particles and the resulting crystalline materials were washed with hexanes. This process was repeated several times. After drying *in vacuo*, the resulting crystalline materials were dispersed in toluene and hexanes were added. The resulting solution in a vial was cooled at –40 °C for 2 days. The supernatant was decanted to remove small particles and the resulting orange crystals were washed with hexanes. This process was repeated several times to furnish 0.028 g (27 %) of crystalline **2**. The crystals contained small amounts of impurities including ~6% $NiCl_2(IMes)_2$, as determined by ^{1}H NMR. ^{1}H NMR (C_6D_6, 500 MHz): δ 11.18 (br, 4 H, NCH), 8.43 (br, 8 H, *meta*-CH), 3.31 (s, 12 H, *para*-CC$\underline{H}_3$), 1.66 (br, 24 H, *ortho*-CC$\underline{H}_3$). λ_{max} /nm (ε / $10^3 M^{-1} cm^{-1}$) in toluene: 349 (6.8).

Preparation of Ni(H)(Br)Cl(IMes)$_2$ (3)

In a glovebox, Ni(IMes)$_2$ (0.100 g, 0.0150 mmol) and 2,6-lutidine•HBr (0.056 g, 0.300 mmol) were added to a vial equipped with a Teflon-coated magnetic stirbar. THF (5 mL) was added and the mixture was stirred for 50 min. The mixture was filtered through glass fiber and

dried *in vacuo*. The resulting solid was dispersed in toluene and the mixture was filtered through glass fiber. The solution was dried again and the residue was redispersed in toluene. The mixture was filtered and hexanes were layered onto it. The resulting solution in the vial was cooled at –40 °C for 4 days. The supernatant was decanted to remove small particles and the resulting yellow crystals were washed with hexanes. This process was repeated several times. The resulting crystals were dried *in vacuo* to give 0.060 g (54%) of **3**. The crystals contained ~5% of $NiBr_2(IMes)_2$ as determined by ^1H NMR and crystallography. ^1H NMR (C_6D_6, 300 MHz): δ 6.82 (s, 8 H, *meta*-CH), 6.02 (s, 4 H, NCH), 2.36 (s, 12 H, *para*-CC$\underline{H}_3$), 2.10 (s, 24 H, *ortho*-CC$\underline{H}_3$), –20.4 (s, 1 H, NiH). λ_{max} /nm (ε / $10^3 M^{-1} cm^{-1}$) in toluene: 306 (5.5), 335 (sh, 3.7), 390 (br sh, 0.9).

Photochemistry

Photochemical reactions were performed at 10 °C using a 1000 W high-pressure Hg/Xe arc lamp (Oriel) for 1 day for **1** and 2.5 h for **3**. The beam was passed through a water-jacketed filter holder containing appropriate long pass filters, an iris and collimating lens. Samples for all photolysis experiments were prepared in a nitrogen-filled glovebox in NMR tubes or Schlenk flasks. After photolysis of **1** and **3**, the headspace gases of the flask were analyzed by GC. After removing volatile materials, 1,4-dimethoxybenzene and C_6D_6 were added to resulting solid and the yields of the products were determined by NMR. The headspace gas was also analyzed by GC for the addition reactions of HCl to **1** and $Ni(IMes)_2$.

X-ray Crystallography

Experiments were performed on single crystals of **1** – **4**. The single crystals of **1** and **2** were grown at –40 °C from toluene/hexanes solution. The single crystals of **3** were grown at –40 °C by layering hexanes on concentrated toluene solution of the compound. The single crystals of **4** were grown at room temperature by evaporation of C_6D_6 from reaction mixture after photolysis experiment. The crystals were removed from the supernatant and transferred onto a microscope slide coated with Paratone N oil. Crystals were affixed to a glass fiber or a cryoloop using the oil, frozen in a nitrogen stream, and optically centered. Graphite monochromators were employed for wavelength selection of the Mo Kα radiation (λ = 0.71073 Å) for **1**, **3** and **4**, and Cu Kα radiation (λ = 1.54178 Å) for **2**. The structures were solved by direct methods (SHELXS)[39] and refined against *F*2 on all data by full matrix least squares with SHELXL-97.[40] All non-hydrogen atoms were refined anisotropically. Hydrogen atoms were placed at idealized positions and

refined using a riding model with the exception of hydrides, which were located crystallographically from the difference maps during refinements.

Computational Methods

All calculations were performed using the Gaussian03 (G03) program package,[41] with the Becke three-parameter hybrid exchange and the Lee–Yang–Parr correlation functionals (B3LYP).[42–44] The 6-31G* basis set was used for H, C and N,[45] along with LANL2DZ energy-consistent pseudopotentials for Ni.[46,47] All geometry optimizations were performed in C_1 symmetry with subsequent vibrational frequency analysis to confirm that each stationary point was a minimum on the potential energy surface. The percentage of Ni, H or halide character in the occupied (canonical) molecular orbitals (MOs) and virtual orbitals discussed were calculated from a full population analysis, using eq. (2.4),

$$\%\ \text{Orbital Character}_{(\text{Ni,H,Cl})} = \frac{\sum \phi^2_{(Ni,H,Cl)}}{\sum \phi^2_{(all)}} \times 100\% \qquad (2.4)$$

where $\sum \phi_i$ (i = Ni, H, Cl or all) is the sum of the squares of the eigenvalues associated with the atomic orbital (AO) of interest and all of the AOs in a particular MO, respectively. The vertical singlet transition energies of the complexes were computed at the time-dependent density functional theory (TD-DFT) level within G03 using the ground state optimized structure.

Table 2.1. Crystal Data and Structure Refinement for **1**.

Identification code	10047	
Empirical formula	$C_{42}H_{49}N_4ClNi$	
Formula weight	704.01	
Temperature	100(2) K	
Wavelength	0.71073 Å	
Crystal system	Orthorhombic	
Space group	*Pbca*	
Unit cell dimensions	a = 17.067(3) Å	α = 90°
	b = 18.815(3) Å	β = 90°
	c = 23.195(4) Å	γ = 90°
Volume	7448(2) Å^3	
Z	8	
Density (calculated)	1.256	
Absorption coefficient	0.627	
F(000)	2992	
Crystal size	0.20 × 0.05 × 0.05 mm^3	
Θ range for data collection	1.76 to 27.48°	
Index ranges	$-22 \le h \le 22$, $-24 \le k \le 24$, $-30 \le \ell \le 30$	
Reflections collected	137616	
Independent reflections	8541 [R_{int} = 0.1393]	
Completeness to Θ = 27.48°	100.0%	
Absorption correction	SADABS	
Max. and min. transmission	0.8848, 0.9693	
Refinement method	Full–matrix least–squares on F^2	
Data / restraints / parameters	8541 / 0 / 437	
Goodness-of-fit on F^2	1.023	
Final R indices [I > 2σ(I)]	R_1 = 0.0581, wR_2 = 0.1405	
R indices (all data)	R_1 = 0.0999, wR_2 = 0.1664	
Largest diff. peak and hole	0.612 and –0.584 e/Å^{-3}	

[a] GOF = $(\Sigma\, w(F_o^2 - F_c^2)^2/(n-p))^{1/2}$ where n is the number of data and p is the number of parameters refined. [b] $R1 = \Sigma||F_o| - |F_c||/\Sigma|F_o|$. [c] $wR2 = (\Sigma(w(F_o^2 - F_c^2)^2)/\Sigma(w(F_o^2)^2))^{1/2}$.

Table 2.2. Crystal Data and Structure Refinement for **2**.

Identification code	d810043	
Empirical formula	$C_{42}H_{48}N_4ClNi$	
Formula weight	703.00	
Temperature	100(2) K	
Wavelength	1.54178 Å	
Crystal system	Orthorhombic	
Space group	*Pbca*	
Unit cell dimensions	a = 17.0558(10) Å	α = 90°
	b = 18.7976(12) Å	β = 90°
	c = 23.1314(14) Å	γ = 90°
Volume	7416.1(8) Å^3	
Z	8	
Density (calculated)	1.259	
Absorption coefficient	1.672	
F(000)	2984	
Crystal size	0.30 × 0.15 × 0.10 mm^3	
Θ range for data collection	3.82 to 66.59°	
Index ranges	$-20 \le h \le 20$, $-22 \le k \le 22$, $-27 \le \ell \le 26$	
Reflections collected	134974	
Independent reflections	6550 [R_{int} = 0.1525]	
Completeness to Θ = 66.59°	100.0 %	
Absorption correction	SADABS	
Max. and min. transmission	0.6339, 0.8506	
Refinement method	Full–matrix least–squares on F^2	
Data / restraints / parameters	6550 / 0 / 433	
Goodness-of-fit on F^2	1.125	
Final R indices [I > 2σ(I)]	R_1 = 0.0687, wR_2 = 0.2114	
R indices (all data)	R_1 = 0.0946, wR_2 = 0.2711	
Largest diff. peak and hole	0.764 and – 1.256 e/Å^{-3}	

[a] GOF = $(\Sigma\, w(F_o^2 - F_c^2)^2/(n-p))^{1/2}$ where n is the number of data and p is the number of parameters refined. [b] $R1 = \Sigma||F_o| - |F_c||/\Sigma|F_o|$. [c] $wR2 = (\Sigma(w(F_o^2 - F_c^2)^2)/\Sigma(w(F_o^2)^2))^{1/2}$.

Table 2.3. Crystal Data and Structure Refinement for **3**.

Identification code	10152	
Empirical formula	$C_{42}H_{48.96}N_4Br_{1.04}Ni$	
Formula weight	751.60	
Temperature	100(2) K	
Wavelength	0.71073 Å	
Crystal system	Orthorhombic	
Space group	*Pbca*	
Unit cell dimensions	a = 17.1678(11) Å	α = 90°
	b = 18.7108(12) Å	β = 90°
	c = 23.3170(15) Å	γ = 90°
Volume	7490.0(8) Å^3	
Z	8	
Density (calculated)	1.327	
Absorption coefficient	1.662	
F(000)	3146	
Crystal size	0.40 × 0.40 × 0.10 mm^3	
Θ range for data collection	1.75 to 28.29°	
Index ranges	$-22 \le h \le 22$, $-24 \le k \le 24$, $-30 \le \ell \le 30$	
Reflections collected	149027	
Independent reflections	9290 [R_{int} = 0.0816]	
Completeness to Θ = 28.29°	99.9 %	
Absorption correction	SADABS	
Max. and min. transmission	0.5636, 0.8548	
Refinement method	Full–matrix least–squares on F^2	
Data / restraints / parameters	9290 / 0 / 447	
Goodness-of-fit on F^2	1.048	
Final R indices [I > 2σ(I)]	R_1 = 0.0437, wR_2 = 0.1092	
R indices (all data)	R_1 = 0.0703, wR_2 = 0.1253	
Largest diff. peak and hole	0.631 and – 0.683 e/Å^{-3}	

[a] GOF = $(\Sigma\, w(F_o^2 - F_c^2)^2/(n-p))^{1/2}$ where n is the number of data and p is the number of parameters refined. [b] $R1 = \Sigma||F_o| - |F_c||/\Sigma|F_o|$. [c] $wR2 = (\Sigma(w(F_o^2 - F_c^2)^2)/\Sigma(w(F_o^2)^2))^{1/2}$.

Table 2.4. Crystal Data and Structure Refinement for **4**.

Identification code	10203	
Empirical formula	$NiBrN_4C_{42}H_{48}$	
Formula weight	747.46	
Temperature	100(2) K	
Wavelength	0.71073 Å	
Crystal system	Orthorhombic	
Space group	*Pbca*	
Unit cell dimensions	a = 17.2448(16) Å	α = 90°
	b = 18.7973(18) Å	β = 90°
	c = 23.302(2) Å	γ = 90°
Volume	7553.4(12) $Å^3$	
Z	8	
Density (calculated)	1.315	
Absorption coefficient	1.606	
F(000)	3128	
Crystal size	0.40 × 0.40 × 0.40 mm^3	
Θ range for data collection	1.75 to 30.03°	
Index ranges	$-24 \le h \le 24$, $-26 \le k \le 26$, $-32 \le \ell \le 32$	
Reflections collected	169036	
Independent reflections	11060 [R_{int} = 0.0516]	
Completeness to Θ = 30.03°	100.0 %	
Absorption correction	SADABS	
Max. and min. transmission	0.5660, 0.5660	
Refinement method	Full–matrix least–squares on F^2	
Data / restraints / parameters	11060 / 16 / 455	
Goodness-of-fit on F^2	1.036	
Final R indices [I > 2σ(I)]	R_1 = 0.0351, wR_2 = 0.0869	
R indices (all data)	R_1 = 0.0487, wR_2 = 0.0948	
Largest diff. peak and hole	0.951 and –0.367 e/$Å^{-3}$	

[a] GOF = $(\Sigma\, w(F_o^2 - F_c^2)^2/(n-p))^{1/2}$ where n is the number of data and p is the number of parameters refined. [b] $R1 = \Sigma||F_o| - |F_c||/\Sigma|F_o|$. [c] $wR2 = (\Sigma(w(F_o^2 - F_c^2)^2)/\Sigma(w(F_o^2)^2))^{1/2}$.

Table 2.5. Cartesian coordinates of calculated optimized geometry for **1–CH_3**.

Atomic	Coordinates (Angstroms)		
Type	X	Y	Z
Ni	0.000081	-0.003168	-0.134781
Cl	-0.001000	-0.020608	2.197255
N	-2.702293	-0.966254	-0.819296
N	-2.794292	0.917922	0.207009
N	2.799882	-0.915521	0.195389
N	2.697220	0.979389	-0.809965
C	-1.911867	-0.009659	-0.255529
C	-4.048234	-0.647695	-0.700185
C	-4.104189	0.545912	-0.057950
C	-2.404415	2.152941	0.880170
C	-2.194359	-2.193008	-1.415046
C	1.912182	0.012463	-0.256235
C	4.107585	-0.533840	-0.066534
C	4.044879	0.666499	-0.695452
C	2.182611	2.209892	-1.392140
C	2.417215	-2.160279	0.854493
H	-0.000377	0.006169	-1.595649
H	-4.831372	-1.290896	-1.069178
H	-4.946610	1.154079	0.231342
H	-3.224921	2.480756	1.522293
H	-2.184455	2.938346	0.149903
H	-1.524308	1.945809	1.491006
H	-2.769782	-2.432666	-2.313513
H	-2.262108	-3.027188	-0.709587
H	-1.149864	-2.026890	-1.680765

H	4.953443	-1.140653	0.215509
H	4.824335	1.317890	-1.057822
H	2.248944	3.037318	-0.678628
H	1.138075	2.042003	-1.656534
H	2.754556	2.460766	-2.289757
H	3.235813	-2.485760	1.500267
H	2.210581	-2.941316	0.115662
H	1.530722	-1.966818	1.460487

2.4.2 Photoactivation of Metal–Halogen bonds in a Ni(II) NHC Complex

All synthetic manipulations were performed using standard Schlenk techniques under a nitrogen atmosphere, or in a glovebox under an atmosphere of nitrogen. Reactions were carried out in oven-dried glassware cooled under vacuum. Elemental analysis was performed by Midwest Microlab, LLC, Indianapolis, IN. Toluene, THF, Et_2O and hexanes were purified by passing them under argon pressure through packed columns of neutral alumina. NMR solvents were obtained from Cambridge Isotope Laboratories. C_6D_6 was degassed, and stored in a glovebox over molecular sieves.

^1H NMR spectra were recorded on Varian 300 MHz instruments, with shifts reported relative to the residual solvent peak. UV-vis spectra were recorded on a Varian Cary 5000 spectrophotometer and Spectral Instruments 400 series diode array spectrometer. Spectra were referenced against the appropriate solvent. GC measurements were performed with an Agilent 7890A GC.

$[Ni(IPr)]_2$ (See chapter 3 experimental section) and $[Ni(\mu\text{-}Cl)(IPr)]_2$[35] were synthesized as described by published procedures. 2,6-lutidine•HCl was prepared by treatment of 2,6-lutidine with 1.0 M HCl diethyl ether solution under anhydrous conditions. 4.0 M HCl 1,4-dioxane solution (Aldrich), 2,6-lutidine (Aldrich) and 1,4-dimethoxybenzene (Aldrich) were used as received.

Syntheses

Preparation of $[Ni(\mu\text{-}Cl)Cl(IPr)]_2$ (5)

The crude product was prepared as described by published procedure.[33] The crude product was recrystallized in toluene solution layered with hexanes at –40 °C for 3 days. The supernatant was decanted and the resulting purple crystals were washed with hexanes. This process was repeated several times to remove the powder. The recrystallization was repeated several times until not much powder was observed. ^1H NMR (C_6D_6, 300 MHz): δ 5.96 (br), 5.75 (br), 4.49 (br), −1.55 (br). Anal. Calcd. $C_{54}H_{72}N_4Cl_4Ni_2$: C, 62.58; H, 7.00; N, 5.41. Found: C, 62.61; H, 6.99; N, 5.47. λ_{max} /nm (ε / $10^3 M^{-1} cm^{-1}$) in toluene: 286 (4.8), 529 (0.3), 679 (0.1).

Preparation of $NiCl_2$(IPr)(2,6−lutidine) (6)

In a glovebox, **5** (0.030 g, 0.0289 mmol) were added to a vial equipped with a Teflon-coated magnetic stirbar. Toluene was added and the mixture was stirred until all of compound was dissolved. 2,6-lutidine (0.0062 g, 0.0579 mmol) was added. Hexanes were layered on the resulting pinkish solution and the solution was cooled at –40 °C overnight. The mixture was filtered through glass fiber to remove white precipitation and the resulting solution was cooled at –40 °C. The process was repeated until significant amount of white precipitation or crystals were not observed. The resulting pinkish solution was dried to prepare more concentrated toluene solution. Hexanes were added to the resulting pinkish solution and the solution was cooled at –40 °C for 4 days. The supernatant was decanted to remove small particles and the resulting pinkish red crystals were washed with hexanes. This process was repeated several times to remove small particles. The resulting crystals were dried *in vacuo* to give 0.028 g (77%) of **6**. ^{1}H NMR (C_6D_6, 300 MHz): δ 7.55-7.44 (m, 6 H, CH), 6.61 (s, 4 H, NCH), 6.38 (t, J = 7.8 Hz, 1 H, CH), 6.00 (d, J = 7.9 Hz, 2 H, CH), 3.51 (s, 6H, CCH_3), 3.32 (sept, J = 6.9 Hz, 4 H, $-C\underline{H}(CH_3)_2$), 1.63 (d, J = 6.6 Hz, 12 H, $-CH(C\underline{H}_3)_2$), 1.06 (d, J = 7.0 Hz, 12 H, $-CH(C\underline{H}_3)_2$). Anal. Calcd. $C_{34}H_{45}N_3Cl_2Ni$: C, 65.30; H, 7.25; N, 6.72. Found: C, 64.84; H, 7.24; N, 6.76.

Photolysis of 5

Photochemical reactions were performed at 10 °C using a 1000 W high-pressure Hg/Xe arc lamp (Oriel) until purple solution turned greenish yellow solution with precipitation. The beam was passed through a water-jacketed filter holder containing appropriate long pass filters, an iris and collimating lens. Samples for all photolysis experiments were prepared in a nitrogen-

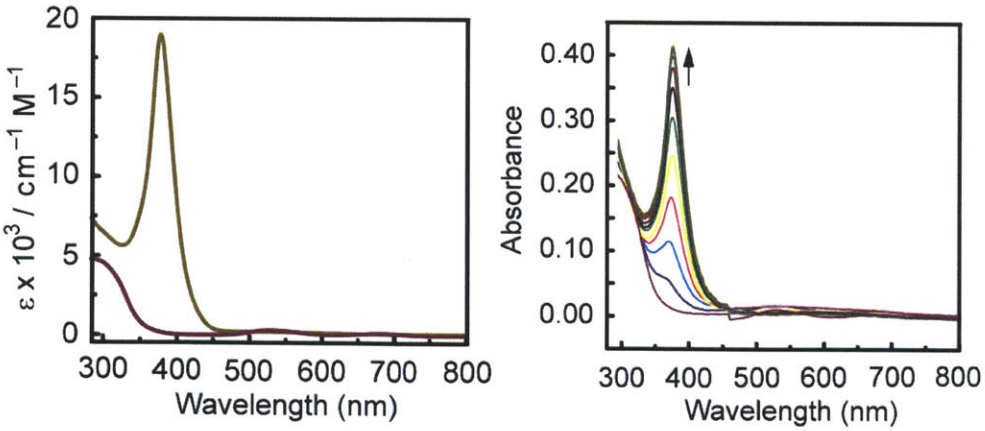

Figure 2.11. UV-vis spectra of $[Ni(\mu\text{-}Cl)(IPr)]_2$ in benzene (—) and **5** in toluene (—) (left). Photolysis of **5** in toluene with > 295 nm light (right).

filled glovebox in NMR tubes or Schlenk flasks. After removing volatile materials, 1,4-dimethoxybenzene and C_6D_6 were added to resulting solid and the yields of the products were determined by NMR.

Treatment of $[Ni(IPr)]_2$ with HCl·dioxane.

In a glovebox, $[Ni(IPr)]_2$ (0.030 g, 0.0335 mmol) were added to a vial equipped with a Teflon-coated magnetic stirbar. Toluene was added. Sometimes, a small amount of insoluble materials was present. In that case, the mixture was filtered. The solution was transferred to a Schlenk flask and was sealed with septa. 4.0 M HCl·dioxane solution (16.8 μL, 0.0672 mmol HCl) was added via syringe. The mixture was stirred for ~ 1 hour. The headspace gas was analyzed by GC. After removing volatile materials, 1,4-dimethoxybenzene and C_6D_6 were added to resulting solid and the yields of the products were determined by NMR.

Treatment of $[Ni(\mu\text{-}Cl)(IPr)]_2$ with 2,6-lutidine·HCl.

In a glovebox, $[Ni(\mu\text{-}Cl)(IPr)]_2$ (0.030 g, 0.031 mmol) and 2,6-lutidine·HCl (0.0089 g, 0.062 mmol) were added to a round bottom flask equipped with a Teflon-coated magnetic stirbar. THF was added and the mixture was stirred for ~ 2 hours. After removing volatile materials, 1,4-dimethoxybenzene and C_6D_6 were added to resulting solid and the yields of the products were determined by NMR.

X-ray Crystallographic Details

Experiments were performed on single crystals of **5**, **5**·CH_2Cl_2 and **6**. The single crystals of **5** and **6** were grown at –40 °C from toluene/hexanes solution and the single crystal of **5**·CH_2Cl_2 was grown at –20 °C by slow diffusion of pentane into dichloromethane solution. The crystals were removed from the supernatant and transferred onto a microscope slide coated with Paratone N oil. Crystals were affixed to a glass fiber or a cryoloop using the oil, frozen in a nitrogen stream, and optically centered. Graphite monochromators were employed for wavelength selection of the Mo Kα radiation (λ = 0.71073 Å). The structures were solved by direct methods (SHELXS)[39] and refined against *F*2 on all data by full matrix least squares with SHELXL-97.[40] All non-hydrogen atoms were refined anisotropically. Hydrogen atoms were placed at idealized positions and refined using a riding model.

Computational Methods

All calculations were performed using the Gaussian03 (G03) program package,[41] with the Becke three-parameter hybrid exchange and the Lee–Yang–Parr correlation functionals (B3LYP).[43–44] The 6-31G* basis set was used for H, C and N,[45] along with LANL2DZ energy-consistent pseudopotentials for Ni.[46,47] All geometry optimizations were performed in C_1 or C_i symmetry with subsequent vibrational frequency analysis to confirm that each stationary point was a minimum on the potential energy surface. The percentage of Ni or halide character in the occupied (canonical) molecular orbitals (MOs) and virtual orbitals discussed were calculated from a full population analysis, using eq. (2.5),

$$\%\ \text{Orbital Character}_{(\text{Ni,Cl})} = \frac{\sum \phi^2_{(Ni,Cl)}}{\sum \phi^2_{(all)}} \times 100\% \qquad (2.5)$$

where $\sum \phi_i$ (i = Ni, Cl or all) is the sum of the squares of the eigenvalues associated with the atomic orbital (AO) of interest and all of the AOs in a particular MO, respectively. The vertical singlet transition energies of the complexes were computed at the time-dependent density functional theory (TD-DFT) level within G03 using the ground state optimized structure.

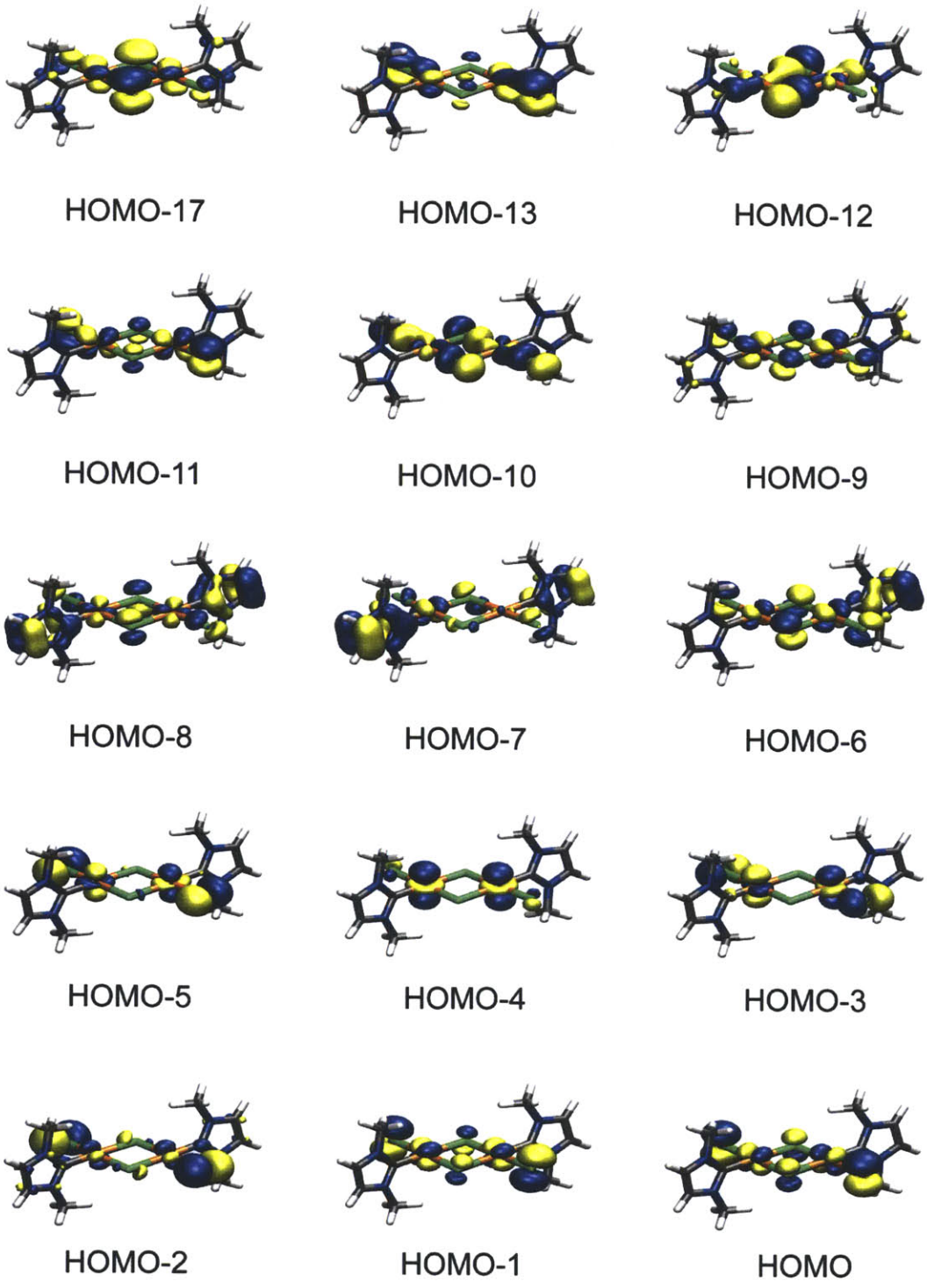

Figure 2.12. The list of occupied orbitals of **5–S** involved in calculated transitions between 360.39–301.40nm.

Table 2.6. Crystal Data and Structure Refinement for **5**.

Identification code	10019	
Empirical formula	$C_{54}H_{72}N_4Cl_4Ni_2$	
Formula weight	1036.38	
Temperature	100(2) K	
Wavelength	0.71073 Å	
Crystal system	Monoclinic	
Space group	*P2(1)/n*	
Unit cell dimensions	a = 12.4363(8) Å	α = 90°
	b = 13.7770(8) Å	β = 94.5330(10)°
	c = 16.4633(10) Å	γ = 90°
Volume	2811.9(3) Å^3	
Z	2	
Density (calculated)	1.224	
Absorption coefficient	0.896	
F(000)	1096	
Crystal size	0.20 × 0.15 × 0.10 mm^3	
Θ range for data collection	1.93 to 29.13°	
Index ranges	$-15 \le h \le 17$, $-18 \le k \le 18$, $-22 \le \ell \le 22$	
Reflections collected	59460	
Independent reflections	7557 [R_{int} = 0.0260]	
Completeness to Θ = 29.13°	99.9%	
Absorption correction	SADABS	
Max. and min. transmission	0.8411, 0.9157	
Refinement method	Full–matrix least–squares on F^2	
Data / restraints / parameters	7557 / 0 / 297	
Goodness-of-fit on F^2	1.017	
Final R indices [I > 2σ(I)]	R_1 = 0.0242, wR_2 = 0.0605	
R indices (all data)	R_1 = 0.0284, wR_2 = 0.0631	
Largest diff. peak and hole	0.393 and –0.234 e/Å^{-3}	

[a] GOF = $(\Sigma\, w(F_o^2 - F_c^2)^2/(n-p))^{1/2}$ where n is the number of data and p is the number of parameters refined. [b] $R1 = \Sigma||F_o| - |F_c||/\Sigma|F_o|$. [c] $wR2 = (\Sigma(w(F_o^2 - F_c^2)^2)/\Sigma(w(F_o^2)^2))^{1/2}$.

Table 2.7. Crystal Data and Structure Refinement for **5·CH_2Cl_2**.

Identification code	10297	
Empirical formula	$C_{56}H_{76}N_4Cl_8Ni_2$	
Formula weight	1206.23	
Temperature	100(2) K	
Wavelength	0.71073 Å	
Crystal system	Orthorombic	
Space group	*Pbca*	
Unit cell dimensions	a = 14.1246(8) Å	α = 90°
	b = 18.6899(11) Å	β = 90°
	c = 22.9177(13) Å	γ = 90°
Volume	6050.0(6) $Å^3$	
Z	4	
Density (calculated)	1.324	
Absorption coefficient	1.014	
F(000)	2528	
Crystal size	0.30 × 0.30 × 0.15 mm^3	
Θ range for data collection	1.78 to 28.51°	
Index ranges	$-18 \le h \le 18$, $-25 \le k \le 25$, $-30 \le \ell \le 30$	
Reflections collected	121899	
Independent reflections	7670 [R_{int} = 0.0544]	
Completeness to Θ = 28.51°	100.0%	
Absorption correction	SADABS	
Max. and min. transmission	0.8628, 0.7507	
Refinement method	Full–matrix least–squares on F^2	
Data / restraints / parameters	7670 / 2 / 334	
Goodness-of-fit on F^2	1.048	
Final R indices [I > 2σ(I)]	R_1 = 0.0377, wR_2 = 0.0888	
R indices (all data)	R_1 = 0.0468, wR_2 = 0.0953	
Largest diff. peak and hole	1.405 and –0.922 e/$Å^{-3}$	

[a] GOF = $(\Sigma\, w(F_o^2 - F_c^2)^2/(n-p))^{1/2}$ where n is the number of data and p is the number of parameters refined. [b] $R1 = \Sigma||F_o| - |F_c||/\Sigma|F_o|$. [c] $wR2 = (\Sigma(w(F_o^2 - F_c^2)^2)/\Sigma(w(F_o^2)^2))^{1/2}$.

Table 2.8. Crystal Data and Structure Refinement for **6**.

Identification code	10230	
Empirical formula	$C_{34}H_{45}N_3Cl_2Ni$	
Formula weight	625.34	
Temperature	100(2) K	
Wavelength	0.71073 Å	
Crystal system	Monoclinic	
Space group	*C2/c*	
Unit cell dimensions	a = 34.143(4) Å	α = 90°
	b = 15.1633(19) Å	β = 106.720(2)°
	c = 15.8525(17) Å	γ = 90°
Volume	6372.7(14) Å^3	
Z	8	
Density (calculated)	1.304	
Absorption coefficient	0.804	
F(000)	2656	
Crystal size	0.45 × 0.20 × 0.10 mm^3	
Θ range for data collection	1.25 to 25.35°	
Index ranges	$-41 \le h \le 41$, $-18 \le k \le 18$, $-15 \le \ell \le 15$	
Reflections collected	52647	
Independent reflections	5835 [R_{int} = 0.0696]	
Completeness to Θ = 25.35°	100.0 %	
Absorption correction	SADABS	
Max. and min. transmission	0.7137, 0.9239	
Refinement method	Full–matrix least–squares on F^2	
Data / restraints / parameters	5835 / 0 / 371	
Goodness-of-fit on F^2	1.032	
Final R indices [I > 2σ(I)]	R_1 = 0.0316, wR_2 = 0.0686	
R indices (all data)	R_1 = 0.0480, wR_2 = 0.0766	
Largest diff. peak and hole	0.347 and – 0.279 e/Å^{-3}	

[a] GOF = $(\Sigma\, w(F_o^2 - F_c^2)^2/(n-p))^{1/2}$ where n is the number of data and p is the number of parameters refined. [b] $R1 = \Sigma||F_o| - |F_c||/\Sigma|F_o|$. [c] $wR2 = (\Sigma(w(F_o^2 - F_c^2)^2)/\Sigma(w(F_o^2)^2))^{1/2}$.

Table 2.7. Cartesian coordinates of calculated optimized geometry for **5–S**.

Atomic	Coordinates (Angstroms)		
Type	X	Y	Z
Ni	1.556786	-0.563174	0.225436
Ni	-1.555377	0.544362	-0.267427
Cl	2.529362	-2.360988	1.063840
Cl	-2.531347	2.386750	-0.998314
Cl	-0.608919	-1.378876	0.503555
Cl	0.610255	1.321673	-0.636298
C	3.279242	0.155663	-0.021021
C	-3.278666	-0.149320	0.037207
N	3.892449	1.078521	0.753876
N	-3.950232	-1.025503	-0.743139
N	4.158032	-0.141765	-1.004101
N	-4.100969	0.125222	1.074261
C	5.161729	1.354007	0.264806
C	-5.200680	-1.293493	-0.203701
H	5.820807	2.060919	0.743841
H	-5.897968	-1.966939	-0.676766
C	5.326546	0.588715	-0.844807
C	-5.292987	-0.572149	0.943111
H	6.154232	0.504003	-1.531294
H	-6.084068	-0.498719	1.672732
C	-3.763716	1.038350	2.163938
H	-3.035511	0.574736	2.835185
H	-3.347125	1.952759	1.737197
H	-4.674275	1.272904	2.718930
C	-3.449758	-1.544929	-2.013155

H	-3.646207	-0.831849	-2.818927
H	-2.375433	-1.712750	-1.926213
H	-3.947079	-2.493130	-2.228651
C	3.896574	-1.107398	-2.069177
H	3.456568	-2.002909	-1.626429
H	3.212463	-0.681659	-2.808583
H	4.842718	-1.362306	-2.550890
C	3.317778	1.637979	1.974630
H	2.254447	1.820804	1.813565
H	3.449551	0.942591	2.808509
H	3.817133	2.582931	2.198986

References

(1) Cook, T. R.; Dogutan, D. K.; Reece, S. Y.; Surendranath, Y.; Teets, T. S.; Nocera, D. G. *Chem. Rev.* **2010**, *110*, 6474–6502.

(2) Esswein, A. J.; Nocera, D. G. *Chem. Rev.* **2007**, *107*, 4022–4047.

(3) Goldsmith, J. I.; Hudson, W. R.; Lowry, M. S.; Anderson, T. H.; Bernhard, S. *J. Am. Chem. Soc.* **2005**, *127*, 7502–7510.

(4) Arachchige, S. M.; Brown, J. R.; Chang, E.; Jain, A.; Zigler, D. F.; Rangan, K.; Brewer, K. J. *Inorg. Chem.* **2009**, *48*, 1989–2000.

(5) Lazarides, T.; McCormick, T.; Du, P.; Luo, G.; Lindley, B.; Eisenberg, R. *J. Am. Chem. Soc.* **2009**, *131*, 9192–9194.

(6) Gartner, F.; Sundararaju, B.; Surkus, A. E.; Boddien, A.; Loges, B.; Junge, H.; Dixneuf, P. H.; Beller, M. *Angew. Chem. Int. Ed.* **2009**, *48*, 9962–9965.

(7) Tschierlei, S.; Karnahl, M.; Presselt, M.; Dietzek, B.; Guthmuller, J. Gonzalez, L.; Schmitt, M.; Rau, S. Popp, J. *Angew. Chem. Int. Ed.* **2010**, *49*, 3981–3984.

(8) Lilac, A.; Alivisatos, A. P. *J. Phys. Chem. Lett.* **2010**, *1*, 1051–1054.

(9) Ryason, P. R. *Sol. Energy* **1977**, *19*, 445–448.

(10) Collinson, E.; Dainton, F. S.; Malati, M. A. *Trans. Faraday Soc.* **1959**, *55*, 2096–2106.

(11) Heidt, L. J.; Mullin, M. G.; Martin, W. B., Jr.; Beatty, M. J. *J. Phys. Chem.* **1962**, *66*, 336–341.

(12) Heidt, L. J.; McMillan, A. F. *J. Am. Chem. Soc.* **1954**, *76*, 2135–2139.

(13) Stevenson, K. L.; Kaehr, D. M.; Davis, D. D.; Davis, C. R. *Inorg. Chem.* **1980**, *19*, 781–783.

(14) Lewis, N. S.; Nocera, D. G. *Proc. Natl. Acad. Sci. U.S.A.* **2006**, *103*, 15729–15735.

(15) Nocera, D. G. *Inorg. Chem.* **2009**, *48*, 10001–1017.

(16) Dempsey, J. L. ; Essewein, A. J. ; Manke, D. R. ; Rosenthal., J.; Soper, J. D.; Nocera, D. G. *Inorg. Chem.* **2005**, *44*, 6879–6892.

(17) Heyduk, A. F.; Nocera, D. G. *Science* **2001**, *293*, 1639–1641.

(18) Odom, A. L.; Heyduk, A. F.; Nocera, D. G. *Inorg. Chim. Acta* **2000**, *297*, 330–337.

(19) Esswein, A. J.; Veige, A. S.; Nocera, D. G. *J. Am. Chem. Soc.* **2005**, *127*, 16641–16651.

(20) Dempsey, J. L. ; Essewein, A. J.; Manke, D. R.; Rosenthal, J.; Soper, J. D.; Nocera, D. G. *Inorg. Chem.* **2005**, *44*, 6879–6892.

(21) Cook, T. R.; Esswein, A. J.; Nocera, D. G. *J. Am. Chem. Soc.* **2007**, *129*, 10094–10095.

(22) Cook, T. R.; Surendranath, Y.; Nocera, D. G. *J. Am. Chem. Soc.* **2009**, *131*, 28–29.

(23) Teets, T. T.; Nocera, D. G. *J. Am. Chem. Soc.* **2009**, *131*, 7411–7420.

(24) Teets, T. T.; Lutterman, D. A.; Nocera, D. G. *Inorg. Chem.* **2009**, *49*, 3035–3043.

(25) Trogler, W. C.; Erwin, D. K.; Geoffroy, G. L.; Gray, H. B. *J. Am. Chem. Soc.* **1978**, *100*, 1160–1163.

(26) Mcquinness, D. S.; Cavell, K. J. *Organometallics* **1999**, *18*, 1596–1605.

(27) Clement, N. D.; Cavell, K. J.; Jones, C.; Elsevier, C. J. *Angew. Chem. Int. Ed.* **2004**, *43*, 1277–1279.

(28) Schaub, T.; Backes, M.; Plietzsch, O.; Radius, U. *Dalton Trans.* **2009**, 7071–7079.

(29) Schaub, T.; Backes, M.; Radius, U. *Eur. J. Inorg. Chem.* **2008**, 2680–2690.

(30) Miyazaki, S.; Koga, Y.; Matsumoto, T.; Matsubara K. *Chem. Commun.* **2010**, 1932–1934.

(31) Gray, T. G.; Veige, A. S.; Nocera, D. G. *J. Am. Chem. Soc.* **2004**, *126*, 9760–9768.

(32) Pistorio, B. J.; Nocera, D. G. *Chem. Commun.* **1999**, 1831–1838.

(33) Laskowski, C. A.; Hillhouse, G. L. *Inorg. Chem.* **2009**, *48*, 6114–6120.

(34) La Mar, G. N.; Sherman, E. O. *J. Am. Chem. Soc.* **1970**, *92*, 2691–2699.

(35) Dible, B. R.; Sigman, M. S.; Arif, A. M. *Inorg. Chem.* **2005**, *44*, 3774–3776.

(36) Hayter, R. G.; Humiec, F. S. *Inorg. Chem.* **1965**, *4*, 1701–1706.

(37) Arduengo, A. J.; Gamper, S. F.; Calabrese, J. C.; Davidson, F. *J. Am. Chem. Soc.* **1994**, *116*, 4391-4394.

(38) Cioffi, E. A.; Bailey, W. F. *Tetrahedron Lett.* **1998**, *39*, 2679–2680.

(39) Sheldrick, G. M. *Acta Crystallogr. Sect. A* **1990**, *46*, 467.

(40) Sheldrick, G. M. *SHELXL 97*; Universität Göttingen: Göttingen, Germany, 1997

(41) Frisch, M. J. et al. Gassian 03, revision C.02; Gaussian: Wallingford, CT, 2004.

(42) Becke, A. D. *J. Chem. Phys.* **1993**, *98*, 5648–5652.

(43) Becke, A. D. *Phys. Rev. A: Gen. Phys.* **1988**, *38*, 3098–3100.

(44) Lee, C.; Yang, W.; Parr, R. G. *Phys. Rev. B: Condens. Matter Mater. Phys.* **1988**, *37*, 785–789.

(45) Hehre, W. J.; Radom, L.; Schleyer, P. v. R.; Pople, J. A. *Ab Initio Molecular Orbital Theory*; John Wiley: New York, 1986.

(46) Wedig, U.; Dolg, M.; Stoll, H. *Quantum Chemistry: The Challenge of Transition Metals and Coordination Chemistry*; Springer: Dordrecht, The Netherlands, 1986.

(47) Andrea, D.; Haeussermann, U.; Dolg, M.; Stoll, H. Preuss, H. *Theor. Chim. Acta* **1990**, *77*, 123–141.

Chapter 3. CO_2 activation by Ni(0) NHC Complexes

Portions of this work have been published:

(1) Lee, C. H.; Laitar, D. S.; Mueller, P.; Sadighi, J. P. *J. Am. Chem. Soc.* **2007**, *129*, 13802−13803. Reproduced with permission. Copyright 2007 American Chemical Society

3.1 Introduction

As discussed in previous chapters, H_2 is promising medium for the storage of solar energy and solar energy can be stored in the chemical bond of H_2, which results in high energy density per weight.[1] However, in terms of volumetric energy density, H_2 itself is not very attractive because it is a gas at room temperature. Thus, the technology to store H_2 efficiently in small volume space is an imperative for utilization of H_2 as routine energy source.

Nature has the technology to store H_2 in forms of organic molecules by combining it with CO_2. In the process of photosynthesis, the plant splits water and then releases O_2 while converting CO_2 to hydrocarbons by hydrogenating it with protons and electrons generated during water splitting, instead of releasing molecular H_2.[2] Actually, fossil fuels or biomass which we are consuming now were made this way and we are burning those to utilize solar energy stored in H_2, which is fixed on CO_2 as a form of organic molecules. Many hydrocarbons (e.g. oil) have much higher volumetric energy densities than H_2, mainly because they are liquid. For example, alcohols (e.g. methanol and ethanol) have been proposed as promising candidates for alternative fuels due to their high octane ratings and volumetric energy densities. Hence, production of liquid hydrocarbon fuels from H_2 and CO_2 could solve the problems associated with H_2 storage.[3,4] CO_2 released from combustion of those fuels will be recycled into regeneration of fuels through hydrogenation of CO_2 with H_2.

Accordingly, significant research efforts are being invested in chemistry utilizing CO_2 as a carrier of H_2 by production of liquid fuels from CO_2.[4,5] In conjunction with current concerns about global climate changes due to accumulation of atmospheric CO_2, development of the methods utilizing nontoxic and cheap CO_2 as a C1 feedstock for organic syntheses are also becoming important.[5–9] Not only direct syntheses of liquid fuels from CO_2 but also indirect methods producing fuels from a chemical species derived from CO_2 could be adopted for production of liquid fuels as H_2 carriers. If there is an efficient way of producing CO from CO_2, CO could be combined with H_2 in order to produce hydrocarbon fuels through the Fischer–Tropsch process.[3] Also, CO could be used as a source of H_2 through water gas shift reaction.[10]

The challenge in utilization of CO_2 as a H_2 carrier or C1 feed stock is the activation of thermodynamically stable C=O bonds in CO_2 (bond strength: 187 kcal/mole). The coordination of CO_2 to metal complexes could be a way of weakening such a strong bond. Thus, transition

metal complexes can offer a wide range of strategies for CO_2 fixation and activation.[5–9] Since

Chart 3.1

Mononuclear

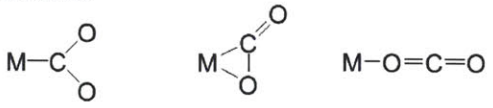

Polynuclear

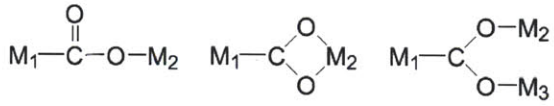

$Ni(PCy_3)_2(\eta^2\text{-}CO_2)$ (Cy : cyclohexyl), the first structurally characterized CO_2 complex, was reported, [11] several complexes with different binding modes of CO_2 ligands including $Rh(diars)_2(\eta^1\text{-}CO_2)(Cl)$ [12] (diars : *o*-phenylenebis(dimethylarsine)) and $[((^{ad}ArO)_3tacn)U(\eta^1\text{-}OCO)]$ [13] ($(^{ad}ArOH)_3tacn$: 1,4,7-tris(3-admantyl-5-*tert*-butyl-2-hydroxylbenzyl)1,4,7-triazacyclclononane) have been prepared (Chart 3.1).[14–24] However, new entries into CO_2 binding modes are still open to inquiry since they are expected to show new interesting chemistry.

In a few examples, the reactions of metal complexes with CO_2 result in the reduction of CO_2 to CO.[25–34] Meyer et al. showed an uranium(III) complex deoxygenated CO_2 yielding CO and a μ-oxo bridged complex (Figure 3.1. **A**).[25] The formation of tungsten oxo carbonyl species

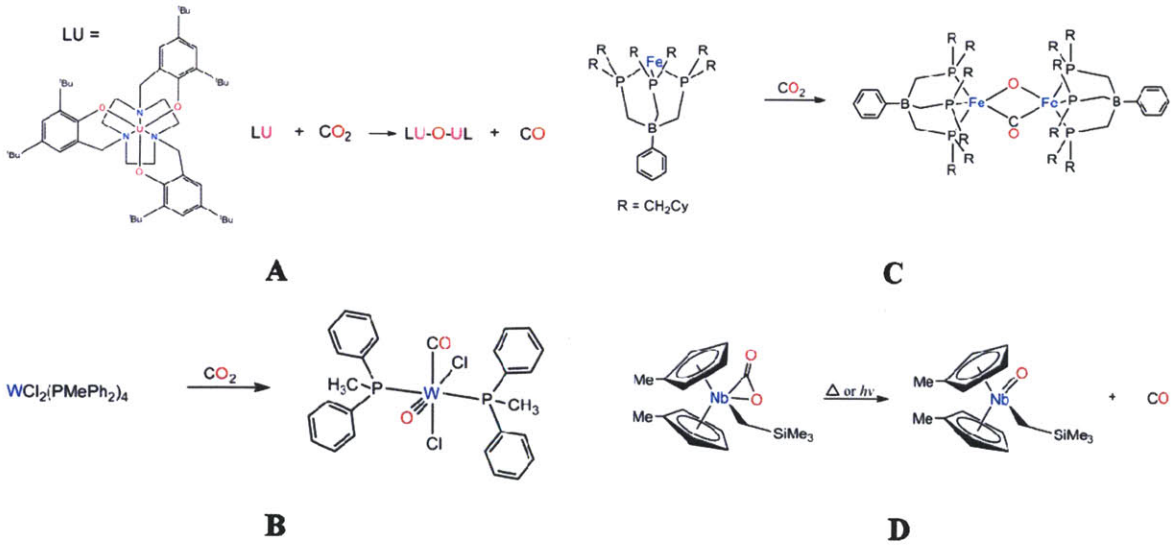

Figure 3.1. Examples of CO_2 activation resulting in CO and metal oxo species by metal complexes.

from CO_2 activation was reported by the Mayer group (**B**),[28] and Peters et al. reported the production of Fe(μ-O)(μ-CO)Fe core by activating CO_2 with an Fe(I) complex (**C**).[29] The thermal or photochemical activation of coordinated CO_2 to CO was reported by Nicholas et al (**D**).[33] The reduction of CO_2 to CO by metal complexes is an interesting process because breaking the C=O bond in CO_2 is energetically demanding. Often CO_2 is reduced to CO at a metal center with the concomitant formation of strong metal-oxygen bonds to compensate for overcoming the high enthalpy of the O=CO bond.

The formation of strong and stable metal oxo bond would hinder catalytic turnover in a possible catalytic cycle and the formation of reactive metal oxo species could result in production of undesirable chemical species through immediate further reaction.[27,34] Thus, to close a catalytic cycle after activating CO_2, the metal oxo species must be converted to desirable chemical species (e.g. generation of reduced metal species and oxygen)[10] or a pathway avoiding formation of metal oxo species is needed. There have been reports about overcoming this challenge. The Sadighi group reported homogenous catalytic deoxygenation of CO_2 to CO (Scheme 3.1A).[35] In this report, they utilized formation of strong B–O bonds to regenerate the catalyst, which follows CO_2 activation. The Cummins group developed a method using binding of CO_2 to a ligand. They reported binding of CO_2 to terminal nitride and a reaction cycle for reduction of the bound CO_2 to CO (Scheme 3.1B).[36] They also showed functionalization of CO_2 following binding of CO_2 to terminal oxo of a titanium complex.[37]

Scheme 3.1A.

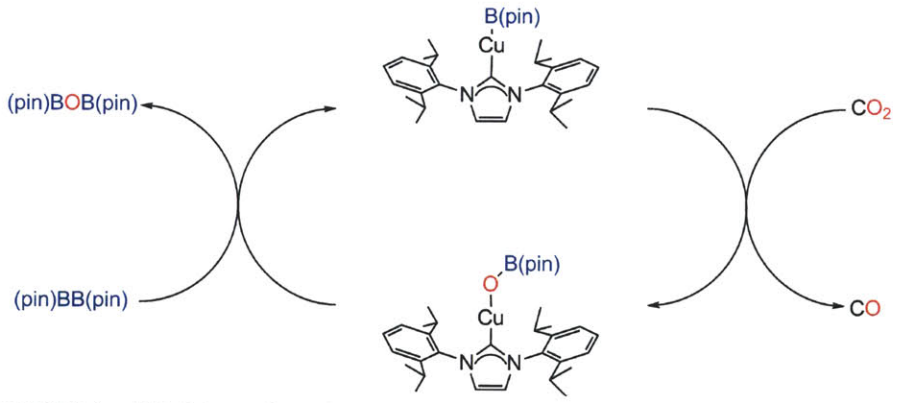

(Pin)BB(Pin) = Bis(pinacolato)diboron

Scheme 3.1B.

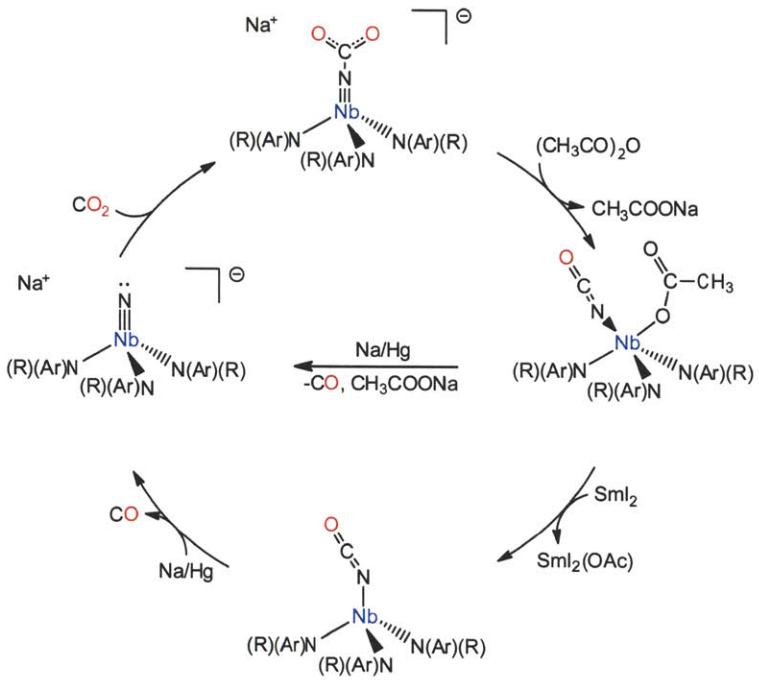

Ar = 3,5-$C_6H_3Me_2$, R = *t*-Bu

3.2 Generation of a Doubly Bridging CO_2 Ligand and Deoxygenation of CO_2 by an (NHC)Ni(0) Complex

In nature, catalytic CO_2 reduction is performed by the enzyme acetyl-CoA synthase/CO dehydrogenase (ACS-CODH)[38,39] with the Ni site of the C-cluster in the CODH subunit believed to play a crucial role in CO_2 reduction.[40,41] The anticipation of the importance of Ni in fixing CO_2 at synthetic active sites is borne out in Kubiak et al.'s resourceful use of dinuclear and trinuclear nickel complexes to reduce CO_2,[42–44] and Louie et al.'s catalytic fixation of CO_2 in organic substrates by $(NHC)_2Ni(0)$ (N-heterocyclic carbene) precatalysts that were generated in situ.[45,46] We now report the reduction of CO_2 by a (NHC)Ni(0) complex give rise to a heretofore unknown coordination mode for CO_2, μ-η^2,η^2-CO_2, at a dinickel core.

Synthesis and Characterization

The reaction of $[(IPr)Ni(\mu\text{-}Cl)]_2$ [47] (IPr = 1,3-bis(2,6-diisopropylphenyl)imidazol-2-ylidene) with NaO*t*-Bu in benzene followed by the addition of an excess of bis(pinacolato)diboron caused the solution to change from yellow to brown to reddish brown. A ^1H NMR spectrum of the reacted solution indicated the clean formation of the new nickel complex **1** (Scheme 3.2). When a crystalline solid of **1** is dissolved in C_6D_6, the ^1H NMR spectrum shows two resonances for NHC backbone protons. However, over the course of a week, the ^1H NMR changes and a single resonance appears for the backbone protons (Figure 3.2B). We propose that dimer **1a** slowly dissociates in benzene solution, likely forming the monomer, $(IPr)Ni(\eta^6\text{-}C_6D_6)$ (**1b**). We note that this symmetric pattern for the backbone protons is observed upon synthesis of **1**, suggesting that a monomer is produced as the initial reaction product, which then dimerizes upon isolation of the product as a solid.

Scheme 3.2

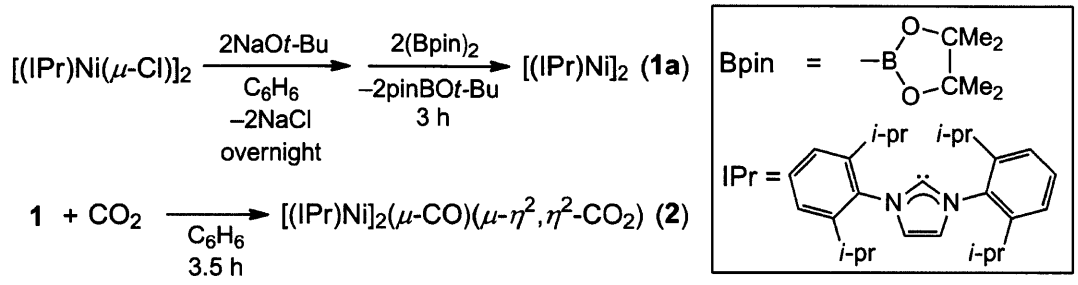

[a] The putative by-product was not isolated.

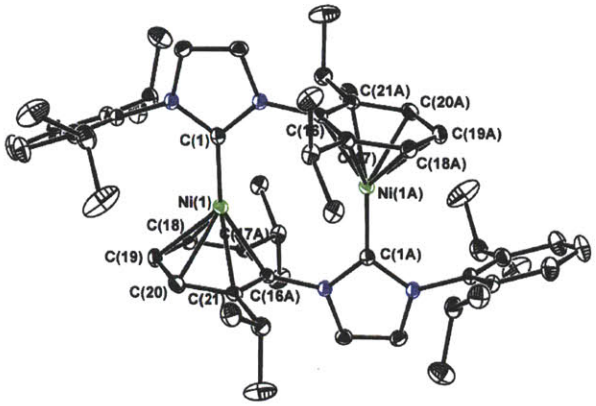

Figure 3.2A. The molecular structure of **1a** showing thermal ellipsoids at 50% probability. The solvent molecules are omitted for clarity.

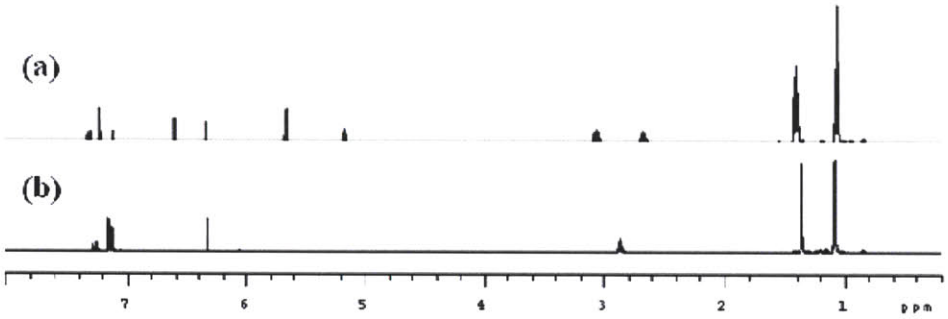

Figure 3.2B. (a) ^{1}H NMR spectrum of **1a** in C_6D_6. (b) ^{1}H NMR spectrum of **1a** after one week at 45 °C.

Reaction of $[(IPr)Ni(\mu\text{-}Cl)]_2$ with $Li(HBEt_3)$ or with NaO*t*-Bu followed by $HSi(OEt)_3$ also formed the same product. No deuterium resonance is observed in the ^{2}H NMR spectrum of the product when $Li(DBEt_3)$ was used. Single crystals of **1a** that were subject to X-ray analysis were grown by slow diffusion of 2,2-dimethylbutane into the THF solution of the reaction mixture. The dimeric nature of **1a** is confirmed by the crystal structure shown in Figure 3.2A. Each nickel center of the bimetallic core interacts in an η^6 fashion with a 2,6-diisopropyl phenyl group of the NHC ligand. The reaction of $Li(HBEt_3)$ with $[(IPr)Ni(\mu\text{-}Cl)]_2$ to form **1** is unexpected inasmuch as phosphine complexes of Ni(II) furnish dihydride complexes such as $[(dippe)NiH]_2$ (dippe = $(i\text{-}Pr_2PCH_2)_2$) using similar reaction conditions.[48]

Complex **1** is an ideal synthon for the coordinatively unsaturated (IPr)Ni moiety since the relatively weakly coordinated arene rings are readily displaced. CO_2 (1 atm) reacts readily with **1** to form a single product as judged by ^{1}H NMR spectroscopy (48% isolated yield) (Scheme 3.2).

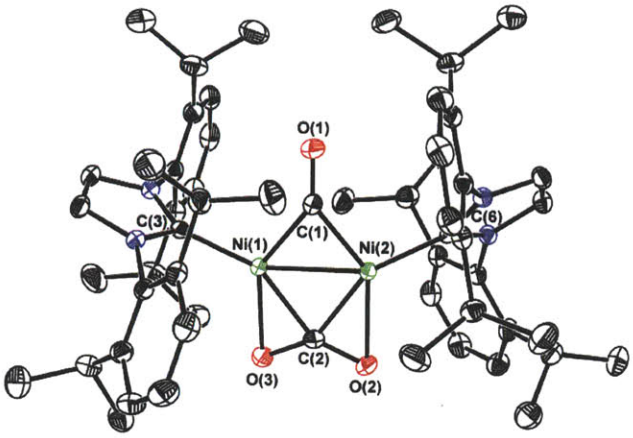

Figure 3.3. The molecular structure of **2** showing thermal ellipsoids at 50% probability.

Single crystals of the product, suitable for X-ray crystallography, were grown from a solution of the crude reaction product in hexanes. The X-ray structure of the product, $[(IPr)Ni]_2(\mu\text{-}CO)(\mu\text{-}\eta^2,\eta^2\text{-}CO_2)$ (**2**), is shown in Figure 3.3. The most remarkable feature of the crystal structure is a CO_2 bridging two Ni atoms. The CO_2 ligand is bent at 133.43(15)° and the C–O bond lengths are 1.2552(19) Å and 1.257(2) Å, which are longer than the C–O bond length (1.16 Å) of free CO_2. A similar binding mode has been observed for other heterocumulenes such as isocyanates and carbodiimides, but a symmetric double-bridging binding mode for CO_2 appears to be unprecedented as determined from a search of the Cambridge Crystallographic Database. All other known dinuclear CO_2 complexes coordinate the CO_2 carbon atom to only one metal center.[6,9,22–24]

Two signals are isotopically enriched in the ^{13}C NMR spectrum of **2** prepared using $^{13}CO_2$ (Figure 3.4A). The carbon atoms for the signals are weakly coupled to each other ($J = 3.5$ Hz) and they are assigned to $\mu\text{-}\eta^2,\eta^2\text{-}CO_2$ (δ 172.6) and μ-CO (δ 246.4 ppm). When complex **2**, prepared using CO_2 with natural isotopic abundance, is treated with $^{13}CO_2$ (1 atm), the signal at δ 172.6 ppm increases in intensity. This is consistent with exchange of the CO_2 ligand of **2** with free CO_2. Complex **2** exhibits intense CO stretching bands at 1773, 1630 and 1205 cm^{-1}; these absorptions shift to 1731, 1586 and 1183 cm^{-1} upon $^{13}CO_2$ isotopic substitution (Figure 3.4B).

CO_2 reduction is evident from the presence the bridging CO in **2**. Notwithstanding, the crystal structure of **2** does not account for the fate of the oxygen atom delivered from CO_2 on its

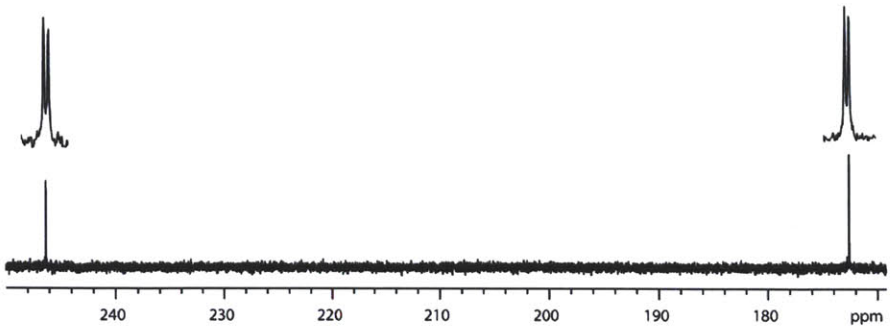

Figure 3.4A. ^{13}C NMR spectrum of **2** prepared using $^{13}CO_2$ showing resonances of μ-CO and μ-η^2,η^2-CO_2. Insets show the splitting of each resonance.

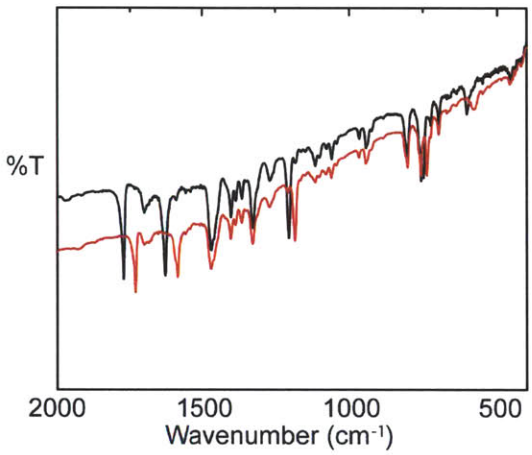

Figure 3.4B. IR spectra of **2** (black) and **2** prepared using $^{13}CO_2$ (red) showing shift of bands corresponding to μ-CO and μ-η^2,η^2-CO_2.

reduction. Though **2** was the only product observed by NMR spectroscopy and no free, oxidized or carboxylated carbene ligands were formed, the yield of the product was 66% by ^1H NMR relative to an internal standard. Thus, the formation of an NMR-silent paramagnetic nickel complex accounting for the missing oxygen is assumed, though such a complex could not be cleanly isolated from the solid residue of recrystallized samples of **2**. An IR spectrum of the residue showed strong peaks at 1618, 1595 and 1561 cm^{-1}. These peaks shift to 1576, 1560 and 1515 cm^{-1} upon isotopic substitution using $^{13}CO_2$. We propose that complex **1** effectively disproportionates CO_2 to form **2** and a nickel(II) carbonate complex, which is consistent with the well-known metal-mediated disproportionation of CO_2 to CO and CO_3^{2-}.[11,15,30–32,34]

The outcome for CO_2 activation reported here may be extended to other nickel(0) complexes. We find that the biscarbene complex $(IMes)_2Ni(0)$,[49] also reacts with CO_2 to form an analogous complex, $[(IMes)Ni]_2(\mu\text{-}CO)(\mu\text{-}\eta^2,\eta^2\text{-}CO_2)$ (**3**) (IMes = 1,3-dimesitylimidazol-2-ylidene) with concomitant formation of $IMesCO_2$. The complex **3** shares similar spectral and structural characteristics with **2** (Figure 3.5). The ^{13}C NMR spectrum of ^{13}C-labeled product shows resonances at 175.5 and 249.2 ppm for carbon atoms coupled to each other (J = 3.5 Hz). This complex exhibits intense IR signals at 1767, 1610 and 1202 cm^{-1} which shift to 1721, 1579 and 1182 cm^{-1} upon $^{13}CO_2$ isotopic substitution. The crystal structure of **3** shows μ-CO and μ-η^2,η^2-CO_2 and all bonding parameters around metal coordination sphere are similar to those of **2** (Figure 3.6, C(44)–O(5) 1.258(3) Å, C(44)–O(6) 1.254(2) Å, O(5)–C(44)–O(6) 132.9(2) °).

CO_2 has been observed to bind to a mononuclear metal site in the three different modes shown in Chart 3.1.[11–20] Since the report of the first structurally characterized CO_2 complex in a

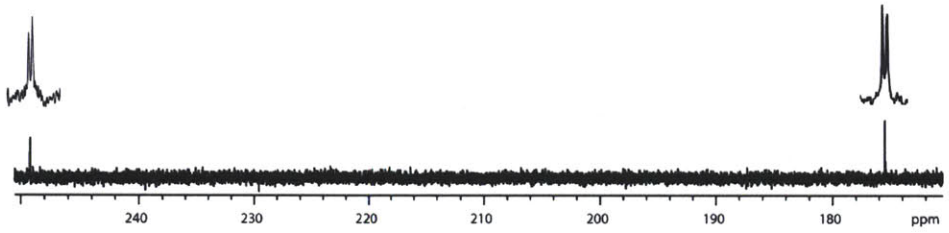

Figure 3.5A. ^{13}C NMR spectrum of **3** prepared using $^{13}CO_2$ showing resonances of μ-CO and μ-η^2,η^2-CO_2. Insets show the splitting of each resonance.

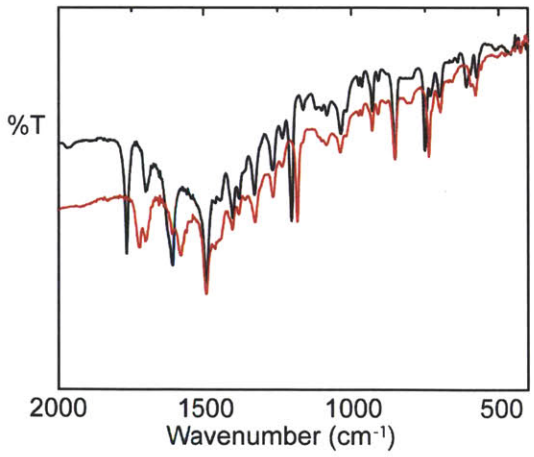

Figure 3.5B. IR spectra of **3** (black) and **3** prepared using $^{13}CO_2$ (red) showing shift of bands corresponding to μ-CO and μ-η^2,η^2-CO_2.

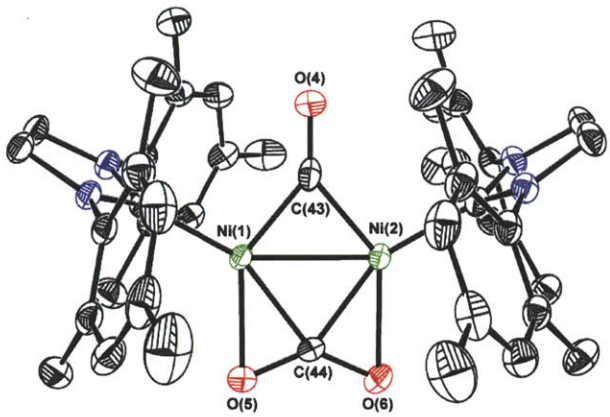

Figure 3.6. The molecular structure of **3** showing thermal ellipsoids at 50% probability.

η^2-CO_2 binding mode in $Ni(PCy_3)_2(\eta^2\text{-}CO_2)$[11] (Cy = cyclohexyl), CO_2 has been observed to assume η^1-CO_2 and η^1-OCO coordination geometries as well.[12,13,17,18] At polynuclear metal centers, the three additional binding modes,[6,9,21–24] shown in Chart 3.1 have been observed. We now report a new mode for CO_2 binding to a metal, the μ-η^2,η^2-CO_2 coordination geometry shown in Figure 3.3 and 3.6. Noting that the activation of small molecules is pre-disposed by the nature of its mode of binding to the metal center, the new binding mode reported here for CO_2 may present new strategies for the CO_2 activation.

3.3 Experimental Section

General Methods

All synthetic manipulations were carried out using standard Schlenk techniques under an argon atmosphere, or in an Innovative Technologies glovebox under an atmosphere of purified nitrogen. Reactions were carried out in oven- or flame-dried glassware cooled under vacuum. Elemental analyses were performed by Desert Analytics, Tucson, AZ. Anhydrous tetrahydrofuran and hexane were purchased from Aldrich in 18-L Pure-Pac™ solvent delivery kegs and sparged vigorously with argon for 40 minutes prior to first use. The solvents were further purified by passing them under argon pressure through two packed columns of neutral alumina and for tetrahydrofuran, a third column packed with activated 4 Å molecular sieves. Benzene, pentane, 2,2-dimethylbutane and hexamethyldisiloxane were purchased from Aldrich and stored in a glovebox over 4 Å molecular sieves. 2,2-dimethylbutane and hexamethyldisiloxane were degassed by three freeze-pump-thaw cycles prior to being stored in a glovebox.

IR spectra were recorded on a Nicolet Impact 410 spectrometer as CsI pellets. NMR solvents were obtained from Cambridge Isotope Laboratories. C_6D_6 was dried over sodium benzophenone ketyl. The solvent was degassed by three freeze-pump-thaw cycles, and vacuum-transferred prior to use. ^1H NMR and ^{13}C NMR spectra were recorded on a Varian 500 MHz instrument, with shifts reported relative to the residual solvent peak.

$[(IPr)Ni(\mu\text{-}Cl)]_2$[47] and $(IMes)_2Ni$[49] were synthesized as described in the published procedure. 1.0 M lithium triethylborohydride in THF (Aldrich), bis(pinacolato)diboron (Frontier Scientific) and sodium *tert*-butoxide (Aldrich) were used as received.

Syntheses

Preparation of [(1,3-bis(2,6-diisopropylphenyl)imidazol-2-ylidene)Ni]$_2$ (1).

Method A. In a glovebox, $[(IPr)Ni(\mu\text{-}Cl)]_2$ (0.200 g, 0.207 mmol) and sodium *tert*-butoxide (0.040 g, 0.416 mmol) were added to a vial equipped with a Teflon-coated magnetic stirbar. Benzene (10 mL) was added and the mixture was stirred overnight. Bis(pinacolato)diboron (0.100 g, 0.395 mmol) was added to the resulting greenish brown solution, and the mixture was stirred for 3 hours. The resulting reddish brown solution was

filtered through Celite on a fritted glass funnel and dried *in vacuo*. The resulting brown solid was dispersed in hexamethyldisiloxane (2 mL) and transferred into a vial. The resulting suspension in the vial was cooled at –40 °C for 3 days. If substantial amount of crystals or precipitation is not seen, the mixture has to be dried and re-dispersed in hexamethyldisiloxane. The brown solid was collected on a fritted glass funnel and washed with cold hexamethyldisiloxane 5 times. The product was dried *in vacuo* giving 0.052 g (28 %) of **1a**.

Method B. In a glovebox, [(IPr)Ni(μ-Cl)]$_2$ (0.200 g, 0.207 mmol) was added to a vial equipped with a Teflon-coated magnetic stirbar. Benzene (10 mL) was added and lithium triethylborohydride in THF solution (0.410 mL, 0.410 mmol) was added via syringe. The mixture was stirred for 3 hours. The resulting reddish brown solution was filtered through Celite on a fritted glass funnel and dried *in vacuo*. A reddish brown solid was collected, dispersed in pentane (3 mL) and transferred into a vial. The suspension was cooled at –40 °C for 2 days. The brown solid was collected on a fritted glass funnel and washed with cold pentane 5 times. The product was dried *in vacuo* giving 0.095 g (51 %) of **1a**. ^{1}H NMR (C_6D_6)[50]: δ 7.36 (t, J = 7.7 Hz, 2 H, *para*-CH), 7.26 (d, J = 7.5 Hz, 4 H, *meta*-CH), 6.65 (d, J = 1.8 Hz, 2 H, NCH), 6.38 (d, J = 1.8 Hz, 2 H, NCH), 5.71 (d, J = 6.4 Hz, 4 H, *meta*-CH), 5.22 (t, J = 6.3 Hz, 2 H, *para*-CH), 3.11 (sept., J = 6.8 Hz, 4 H, C$\underline{\text{H}}$(CH$_3$)$_2$), 2.72 (sept., J = 6.8 Hz, 4 H, C$\underline{\text{H}}$(CH$_3$)$_2$), 1.44 (m, 24 H, CH(C$\underline{\text{H}}_3$)$_2$), 1.10 (m, 24 H, CH(C$\underline{\text{H}}_3$)$_2$). ^{13}C NMR (C_6D_6): δ 198.0, 147.2, 140.2, 128.9, 123.8, 121.9, 120.4, 108.8, 106.0, 93.1, 86.8, 28.9, 28.1, 25.6, 25.2, 23.9, 23.8. IR (CsI, cm^{-1}): 3069, 2960, 2868, 1467, 1423, 1384, 1363, 1327, 1280, 1234, 1182, 1121, 1087, 1062, 955, 928, 800, 782, 760, 715, 669. Anal. Calcd. $C_{54}H_{72}N_4Ni_2$: C, 72.50; H, 8.11; N, 6.26. Found: C, 72.39; H, 8.04; N, 6.17.

Complex **1a** is obtained from monomer (**1b**) in the reaction mixture. Solids of **1a** convert to **1b** by dissolving in benzene (Figure 3.2B). ^{1}H NMR (C_6D_6): δ 7.30 (t, J = 7.7 Hz, 2 H, *para*-CH), 7.19 (d, J = 7.6 Hz, 4 H, *meta*-CH), 6.37 (s, 2 H, NCH), 2.90 (sept., J = 6.9 Hz, 4 H, C$\underline{\text{H}}$(CH$_3$)$_2$), 1.40 (d, J = 6.9 Hz, 12 H, CH(C$\underline{\text{H}}_3$)$_2$), 1.12 (d, J = 7.0Hz, 12 H, CH(C$\underline{\text{H}}_3$)$_2$). ^{13}C NMR (C_6D_6): δ 195.5 (NCNi), 147.0 (*ortho*-C), 139.5 (*ipso*-C), 129.1 (*para*-C), 123.8(*meta*-C), 119.8 (NCH), 29.0 (C$\underline{\text{H}}$(CH$_3$)$_2$), 24.9 (CH(C$\underline{\text{H}}_3$)$_2$), 23.9 (CH(C$\underline{\text{H}}_3$)$_2$).

Preparation of [(1,3-bis(2,6-diisopropylphenyl)imidazol-2-ylidene)Ni]$_2$(μ-CO)(μ-η^2,η^2-CO$_2$) (2).

Method A. In a glovebox, [(IPr)Ni(μ-Cl)]$_2$ (0.200 g, 0.207 mmol) and sodium *tert*-butoxide (0.040 g, 0.416 mmol) were added to a vial equipped with a Teflon-coated magnetic stirbar. Benzene (10 mL) was added and the mixture was stirred overnight. Bis(pinacolato)diboron (0.100 g, 0.395 mmol) was added to the resulting greenish brown solution, and the mixture was stirred for 3 hours. The resulting reddish brown solution was filtered through Celite on a fritted glass funnel and dried *in vacuo*. The resulting brown solid was re-dissolved in benzene (5 mL) and transferred into a sealable Schlenk flask. The solution was degassed by one freeze-pump-thaw cycle and backfilled with CO_2 (1 atm). The flask was sealed after 30 minutes stirring, and the solution was stirred for 3 hours. The solution was dried *in vacuo* and the resulting solid was recrystallized in benzene (1 mL) / hexane (10 mL) at –40 °C for 3 days. The supernatant was decanted to remove small particles and the resulting orange red crystals were washed with cold pentane. This process was repeated until the supernatant became a clear orange solution. The resulting crystals were dried *in vacuo* giving 0.097 g (48 %) of **2**.

Method B. In a glovebox, [(IPr)Ni(μ-Cl)]$_2$ (0.200 g, 0.207 mmol) was added to a vial equipped with a Teflon-coated magnetic stirbar. Benzene (10 mL) was added and lithium triethylborohydride in THF solution (0.410 mL, 0.410 mmol) was added via syringe. The mixture was stirred for 3 hours. The resulting reddish brown solution was filtered through Celite on a fritted glass funnel and dried *in vacuo*. The reddish brown solid that was collected was re-dissolved in benzene (10 mL) and transferred into a sealable Schlenk flask. The solution was degassed by one freeze-pump-thaw cycle and backfilled with CO_2 (1 atm). The flask was sealed after 30 minutes stirring, and the solution was stirred for 3 hours. The solution was dried *in vacuo* and the resulting solid was recrystallized in benzene (1 mL) / hexane (10 mL) at –40 °C for 3 days. The supernatant was decanted to remove small particles and the resulting orange red crystals were washed with cold pentane. This process was repeated until the supernatant became a clear orange solution. The resulting crystals were dried *in vacuo* giving 0.064 g (32 %) of **2**. ^{1}H NMR (C_6D_6): δ 7.24 (t, J = 7.7 Hz, 4 H, *para*-CH), 7.13 (d, J = 7.8 Hz, 8 H, *meta*-CH), 6.46 (s, 4 H, NCH), 2.87 (sept., J = 6.9Hz, 8 H, C$\underline{H}$(CH$_3$)$_2$), 1.32 (d, J = 6.7 Hz, 24 H, CH(C$\underline{H}_3$)$_2$), 1.06 (d, J = 7.0 Hz, 24 H, CH(C$\underline{H}_3$)$_2$). ^{13}C NMR (C_6D_6): δ 246.4 (μ-CO), 195.0 (NCNi), 172.6 (μ-η^2,η^2-CO_2), 146.6 (*ortho*-C), 136.6 (*ipso*-C), 129.9 (*para*-C), 124.2 (*meta*-C), 123.3 (NCH), 29.1 (C$\underline{H}$(CH$_3$)$_2$), 26.0 (CH(C$\underline{H}_3$)$_2$), 24.0 (CH(C$\underline{H}_3$)$_2$). IR (CsI, cm^{-1}): 2963, 2869, 1773, 1702, 1630,

1468, 1401, 1385, 1364, 1327, 1269, 1205, 1115, 1060, 966, 943, 802, 756, 748, 696, 602. Anal. Calcd. $C_{56}H_{72}N_4O_3Ni_2$: C, 69.58; H, 7.51; N, 5.80. Found: C, 69.57; H, 7.32; N, 5.62

Preparation of [(1,3-dimesitylimidazol-2-ylidene)Ni]$_2$(μ-CO)(μ-η^2,η^2-CO$_2$) (3).

In a glovebox, $(IMes)_2Ni$ (0.200 g, 0.300 mmol) was added to a sealable Schlenk flask equipped with a Teflon-coated magnetic stirbar and dissolved in benzene (10 mL). The solution was degassed by one freeze-pump-thaw cycle and backfilled with CO_2 (1 atm). The solution turned red immediately. The solution was stirred for 3 days. The mixture turned orange slowly forming precipitation. The resulting solution was filtered on a fritted glass funnel and dried *in vacuo*. The resulting solid was recrystallized in benzene (2 mL) / hexane (6 mL) at –40 °C for 3 days. The supernatant was decanted to remove small particles and the resulting orange red crystals were washed with cold pentane. This process was repeated until the supernatant became a clear orange solution. The resulting crystals were dried *in vacuo* giving 0.047 g (39 %) of **3**. ^{1}H NMR (C_6D_6): δ 6.71 (s, 8H, *meta*-CH), 6.11 (s, 4 H, NCH), 2.22 (s, 12H, *para*-CC$\underline{H}_3$), 2.05 (s, 24 H, *ortho*-CC$\underline{H}_3$). ^{13}C NMR (C_6D_6): δ 249.2 (μ-CO), 194.0 (NCNi), 175.5 (μ-η^2,η^2-CO$_2$), 138.0 (*ipso*-C), 137.0 (*para*-C), 136.2 (*ortho*-C), 129.4 (*meta*-C), 121.8 (NCH), 21.7 (*para*-C$\underline{C}H_3$), 18.2 (*ortho*-C$\underline{C}H_3$). IR (CsI, cm^{-1}): 2922, 1767, 1702, 1610, 1489, 1400, 1327, 1267, 1202, 1035, 928, 850, 750, 702, 609, 575. Anal. Calcd. $C_{44}H_{48}N_4O_3Ni_2$: C, 66.20; H, 6.06; N, 7.02. Found: C, 66.02; H, 6.37; N, 6.95

X-ray Diffraction Studies: Experiments were performed on single crystals of **1a, 2** and **3**. The single crystals of **1a** were grown at –40 °C by slow diffusion of 2,2-dimethylbutane into a THF solution of the reaction mixture prepared through method **B**. The target molecule co-crystallizes with one molecule of THF and 2,2-dimethylbutane. The single crystals of **2** were grown at –40 °C from hexane solution of the reaction mixture prepared through method **A**. The single crystals of **3** were grown at –40 °C from benzene / hexane solution of the reaction mixture. The crystals were removed from the supernatant and transferred onto a microscope slide coated with Paratone N oil. Crystals were affixed to a glass fiber or a cryoloop using the oil, frozen in a nitrogen stream, and optically centered. The data were collected on a Siemens three-circle platform goniometer equipped with a Bruker Smart Apex CCD detector with graphite-monochromated Mo Kα radiation (λ = 0.71073 Å), using both phi and omega scans at –173 °C. The structures were solved by direct methods (SHELXS)[51] and refined against $F2$ on all data by

full matrix least squares with SHELXL-97. [52] All non-hydrogen atoms were refined anisotropically. Hydrogen atoms were placed at idealized positions and refined using a riding model. The ratio between the two components of the disordered 2,2-dimethylbutane in a single crystal of **1a** was refined freely and converged at 0.687(6). The disorder was refined with the help of displacement parameters as well as rigid bond restraints for anisotropic displacement parameters.

Table 3.1. Crystal Data and Structure Refinement for **1**.

Identification code	06021	
Empirical formula	$C_{74}H_{116}N_4Ni_2O_2$	
Formula weight	1211.13	
Temperature	100(2) K	
Wavelength	0.71073 Å	
Crystal system	Triclinic	
Space group	*P-1*	
Unit cell dimensions	a = 10.704(6) Å	α = 102.176(15)°
	b = 12.403(8) Å	β = 91.346(19)°
	c = 14.597(9) Å	γ = 112.839(12)°
Volume	1734.0(18)Å^3	
Z	1	
Density (calculated)	1.160	
Absorption coefficient	0.589	
F(000)	660	
Crystal size	0.10 × 0.10 × 0.10 mm^3	
Θ range for data collection	2.04 to 28.25°	
Index ranges	$-14 \le h \le 14$, $-16 \le k \le 16$, $-19 \le \ell \le 19$	
Reflections collected	35482	
Independent reflections	8555 [R_{int} = 0.0431]	
Completeness to Θ = 28.25°	99.7%	
Absorption correction	Semi-empirical from equivalents	
Max. and min. transmission	0.922, 0.950	
Refinement method	Full–matrix least–squares on F^2	
Data / restraints / parameters	8555 / 32 / 405	
Goodness-of-fit on F^2	1.027	
Final R indices [I > 2σ(I)]	R_1 = 0.0413, wR_2 = 0.1003	
R indices (all data)	R_1 = 0.0549, wR_2 = 0.1074	
Largest diff. peak and hole	0.696 and –0.376 e/Å^{-3}	

[a] GOF = $(\Sigma\, w(F_o^2 - F_c^2)^2/(n-p))^{1/2}$ where n is the number of data and p is the number of parameters refined. [b] $R1 = \Sigma||F_o| - |F_c||/\Sigma|F_o|$. [c] $wR2 = (\Sigma(w(F_o^2 - F_c^2)^2)/\Sigma(w(F_o^2)^2))^{1/2}$.

Table 3.2. Crystal Data and Structure Refinement for **2**.

Identification code	06235	
Empirical formula	$C_{56}H_{72}N_4Ni_2O_3$	
Formula weight	966.60	
Temperature	100(2) K	
Wavelength	0.71073 Å	
Crystal system	Monoclinic	
Space group	*P*2(1)/*c*	
Unit cell dimensions	a = 13.154(3) Å	α = 90°
	b = 14.404(3) Å	β = 92.470(3)°
	c = 27.869(5) Å	γ = 90°
Volume	5275.6(17)Å^3	
Z	4	
Density (calculated)	1.217	
Absorption coefficient	0.759	
F(000)	2064	
Crystal size	0.15 × 0.15 × 0.10 mm^3	
Θ range for data collection	2.03 to 28.70°	
Index ranges	$-17 \le h \le 17, -19 \le k \le 19, -37 \le \ell \le 37$	
Reflections collected	108988	
Independent reflections	13643 [R_{int} = 0.0560]	
Completeness to Θ = 28.70°	100.0%	
Absorption correction	Semi-empirical from equivalents	
Max. and min. transmission	0. 8947, 0. 9280	
Refinement method	Full–matrix least–squares on F^2	
Data / restraints / parameters	13643 / 0 / 602	
Goodness-of-fit on F^2	1.017	
Final R indices [I > 2σ(I)]	R_1 = 0. 0330, wR_2 = 0. 0708	
R indices (all data)	R_1 = 0. 0531, wR_2 = 0. 0789	
Largest diff. peak and hole	0. 428 and –0. 266 e/Å^{-3}	

[a] GOF = $(\Sigma\, w(F_o^2 - F_c^2)^2/(n-p))^{1/2}$ where n is the number of data and p is the number of parameters refined. [b] $R1 = \Sigma||F_o| - |F_c||/\Sigma|F_o|$. [c] $wR2 = (\Sigma(w(F_o^2 - F_c^2)^2)/\Sigma(w(F_o^2)^2))^{1/2}$.

Table 3.3. Crystal Data and Structure Refinement for **3**.

Identification code	06147	
Empirical formula	$C_{44}H_{48}N_4Ni_2O_3$	
Formula weight	798.28	
Temperature	100(2) K	
Wavelength	0.71073 Å	
Crystal system	Monoclinic	
Space group	*C2/c*	
Unit cell dimensions	a = 28.1093(17) Å	α = 90°
	b = 17.2503(11) Å	β = 124.6070(10)°
	c = 20.5848(12) Å	γ = 90°
Volume	8215.4(9)Å^3	
Z	8	
Density (calculated)	1.291	
Absorption coefficient	0.959	
F(000)	3360	
Crystal size	0.40 × 0.06 × 0.05 mm^3	
Θ range for data collection	1.47 to 28.28°	
Index ranges	$-37 \le h \le 37$, $-22 \le k \le 22$, $-27 \le \ell \le 27$	
Reflections collected	83316	
Independent reflections	10194 [R_{int} = 0.0641]	
Completeness to Θ = 28.28°	100.0%	
Absorption correction	Semi-empirical from equivalents	
Max. and min. transmission	0. 7002, 0. 9536	
Refinement method	Full–matrix least–squares on F^2	
Data / restraints / parameters	10194 / 0 / 490	
Goodness-of-fit on F^2	1.030	
Final R indices [I > 2σ(I)]	R_1 = 0. 0404, wR_2 = 0.0886	
R indices (all data)	R_1 = 0.0638, wR_2 = 0.0987	
Largest diff. peak and hole	0.944 and – 0.303 e/Å^{-3}	

[a] GOF = $(\Sigma\, w(F_o^2 - F_c^2)^2/(n-p))^{1/2}$ where n is the number of data and p is the number of parameters refined. [b] $R1 = \Sigma||F_o| - |F_c||/\Sigma|F_o|$. [c] $wR2 = (\Sigma(w(F_o^2 - F_c^2)^2)/\Sigma(w(F_o^2)^2))^{1/2}$.

References

(1) Nocera, D. G. *Inorg. Chem.* **2009**, *48*, 10001–1017.

(2) Barber, J. *Chem. Soc. Rev.* **2009**, *38*, 185–196.

(3) Esswein, A. J.; Nocera, D. G. *Chem. Rev.* **2007**, *107*, 4022–4047.

(4) Cook, T. R.; Dogutan, D. K.; Reece, S. Y.; Surendranath, Y.; Teets, T. S.; Nocera, D. G. *Chem. Rev.* **2010**, *110*, 6474–6502.

(5) Arakawa, H.; Aresta, M.; Armor, J. N.; Barteau, M. A.; Beckman, E. J.; Bell, A. T.; Bercaw, J. E.; Creutz, C.; Dinjus, E.; Dixon, D. A.; Domen, K.; DuBois, D. L.; Eckert, J.; Fujita, E.; Gibson, D. H.; Goddard, W. A.; Goodman, D. W.; Keller, J.; Kubas, G. J.; Kung, H. H.; Lyons, J. E.; Manzer, L. E.; Marks, T. J.; Morokuma, K.; Nicholas, K. M.; Periana, R.; Que, L.; Rostrup-Nielson, J.; Sachtler, W. M. H.; Schmidt, L. D.; Sen, A.; Somorjai, G. A.; Stair, P. C.; Stults, B. R.; Tumas, W. *Chem. Rev.* **2001**, *101*, 953–996.

(6) Yin, X. L.; Moss, J. R. *Coord. Chem. Rev.* **1999**, *181*, 27–59.

(7) Braunstein, P.; Matt, D.; Nobel, D. *Chem. Rev.* **1988**, *88*, 747–764.

(8) Leitner, W. *Angew. Chem., Int. Ed. Engl.* **1995**, *34*, 2207–2221.

(9) Leitner, W. *Coord. Chem. Rev.* **1996**, *153*, 257–284.

(10) Lewis, N. S.; Nocera, D. G. *Proc. Natl. Acad. Sci. U.S.A.* **2006**, *43*, 15729–15735.

(11) Aresta, M.; Nobile, C. F.; Albano, V. G.; Forni, E.; Manassero, M. *J. Chem. Soc. Chem. Commun.* **1975**, 636–637.

(12) Calabrese, J. C.; Herskovitz, T.; Kinney, J. B. *J. Am. Chem. Soc.* **1983**, *105*, 5914–5915.

(13) Castro-Rodriguez, I; Nakai, H.; Zakharov, L. N.; Rheingold, A. L.; Meyer, K. *Science* **2004**, *305*, 1757–1759.

(14) Karsch, H. H. *Chem. Ber.* **1977**, *110*, 2213–2221.

(15) Bristow, G. S.; Hitchcock, P. B.; Lappert, M. F. *J. Chem. Soc. Chem. Commun.* **1981**, 1145–1146.

(16) Gambarotta, S.; Floriani, C.; Chiesi-Villa, A.; Guastini, C. *J. Am. Chem. Soc.* **1985**, *107*, 2985–2986.

(17) Gambarotta, S.; Arena, F.; Floriani, C.; Zanazzi, P. F. *J. Am. Chem. Soc.* **1982**, *104*, 5082–5092.

(18) Tanaka, H.; Nagao, H.; Peng, S.; Tanaka, K. *Organometallics* **1992**, *11*, 1450–1451.

(19) Alvarez, R.; Carmona, E.; Marin, J. M; Poveda, M. L.; Gutiérrez-Puebla, E.; Monge, A. *J. Am. Chem. Soc.* **1986**, *108*, 2286–2294.

(20) Komiya, S.; Akita, M.; Kasuga, N.; Hirano, M; Fukuoka, A. *J. Chem. Soc. Chem. Commun.* **1994**, 1115–1116.

(21) Lundquist, E. G.; Huffman, J. C.; Caulton, K. G. *J. Am. Chem. Soc.* **1986**, *108*, 8309–8310.

(22) Gibson, D. H.; Ye, M.; Richardson, J. F. *J. Am. Chem. Soc.* **1992**, *114*, 9716–9717.

(23) Gibson, D. H.; Mehta, J. M.; Ye, M. Richardson, J. F.; Mashuta, M. S. *Organometallics* **1994**, *13*, 1070–1072.

(24) Gibson, D. H. *Chem. Rev.* **1996**, *96*, 2063–2096 and references in there.

(25) Castro-Rodriguez, I.; Meyer, K. *J. Am. Chem. Soc.* **2005**, *127*, 11242–11243.

(26) Procopio, L. J.; Carroll, P. J.; Berry, D. H. *Organometallics* **1993**, *12*, 3087–3093.

(27) Ziegler, W.; Nicholas, K. M. *J. Organomet. Chem.* **1992**, *423*, C35–C37.

(28) Bryan, J. C.; Geib, S. J.; Rheingold, A. L.; Mayer, J. M. *J. Am. Chem. Soc.* **1987**, *109*, 2826–2828.

(29) Lu, C. C.; Saouma, C. T.; Day, M. W.; Peters, J. C. *J. Am. Chem. Soc.* **2007**, *129*, 4–5.

(30) Fachinetti, G.; Floriani, C.; Chiesi-Villa, A.; Guastini C. *J. Am. Chem. Soc.* **1979**, *101*, 1767–1775.

(31) Belmore, K. A.; Vanderpool, R. A.; Tsai, J.; Khan, M. A.; Nicholas, K. M. *J. Am. Chem. Soc.* **1988**, *110*, 2004–2005.

(32) Bogdanovic, B.; Leitner, W.; Six, C.; Wilczok, U.; Wittmann, K. *Angew. Chem., Int. Ed. Engl.* **1997**, *36*, 502–504.

(33) Fu, P.–F.; Khan, M. A.; Nicholas, K. M. *Organometallics* **1991**, *10*, 382–384.

(34) Bianchini, C.; Mealli, C; Meli, A.; Sabat, M. *Inorg. Chem.* **1984**, *23*, 2731–2732.

(35) Laitar, D. S.; Sadighi, J. P.; Mueller, P. *J. Am. Chem. Soc.* **2005**, *127*, 17196–17197.

(36) Silvia, J. S.; Cummins, C. C. *J. Am. Chem. Soc.* **2010**, *132*, 2169–2171.

(37) Silvia, J. S.; Cummins, C. C. *Chem. Sci.* **2011**, *2*, 1474–1479.

(38) Doukov, T. I.; Iverson, T. M.; Seravalli, J.; Ragsdale, S. W.; Drennan, C. L. *Science* **2002**, *298*, 567–572.

(39) Dobbek, H.; Svetlitchnyi, V.; Gremer, L.; Huber, R.; Meyer, O. *Science* **2001**, *293*, 1281–1285.

(40) Ragsdale, S. W.; Kumar, M. *Chem. Rev.* **1996**, *96*, 2515–2539.

(41) Lindahl P. A. *Biochemistry* **2002**, *41*, 2097–2105.

(42) Símon-Manso E.; Kubiak, C. P. *Organometallics* **2005**, *24*, 96–102.

(43) Morgenstern, D. A.; Wittrig, R. E.; Fanwick, P. E.; Kubiak, C. P. *J. Am. Chem. Soc.* **1993**, *115*, 6470–6471.

(44) Ratliff, K. S.; Lentz, R. E.; Kubiak, C. P. *Organometallics* **1992**, *11*, 1986–1988.

(45) Tekavec, T. N.; Arif, A. M.; Louie, J. *Tetrahedron* **2004**, *60*, 7431–7437.

(46) Louie, J.; Gibby, J. E.; Farnworth, M. V.; Tekavec, T. N. *J. Am. Chem. Soc.* **2002**, *124*, 15188−15189.

(47) Dible, B. R.; Sigman, M. S.; Arif, A. M. *Inorg. Chem.* **2005**, *44*, 3774−3776.

(48) Vicic, D. A.; Jones, W. D. *J. Am. Chem. Soc.* **1997**, *119*, 10855−10856.

(49) Arduengo, A. J.; Gamper, S. F.; Calabrese, J. C.; Davidson, F. J. *Am. Chem. Soc.* **1994**, *116*, 4391−4394.

(50) The splitting of resonances at δ 6.65, 6.38, 5.71, 5.22, 3.11and 2.72 ppm is not obvious sometimes, even though the samples with those broad signals are converted to monomer cleanly.

(51) Sheldrick, G. M. *Acta Crystallogr. Sect. A* **1990**, *46*, 467.

(52) Sheldrick, G. M. *SHELXL 97*; Universität Göttingen: Göttingen, Germany, 1997